Title
Seeking the Structural Basis of Tau Seeding

Author
Zeng, Zhikai

Publication Date
2022

Peer reviewed|Thesis/dissertation

University of California
Santa Barbara

Seeking the Structural Basis of Tau Seeding

A dissertation submitted in partial satisfaction
of the requirements for the degree

Doctor of Philosophy
in
Chemistry

by

Zhikai Zeng

Committee in charge:

Professor Songi Han, Chair
Professor Frederick Dahlquist
Professor Michael Bowers
Professor Stuart Feinstein

June 2022

The Dissertation of Zhikai Zeng is approved.

Professor Frederick Dahlquist

Professor Michael Bowers

Professor Stuart Feinstein

Professor Songi Han, Committee Chair

June 2022

Seeking the Structural Basis of Tau Seeding

by

Zhikai Zeng

Acknowledgements

I would like to express my sincere gratitude to my Ph.D. advisor, Prof. Songi Han, for her guidance, understanding, wisdom, patience, enthusiasm, and encouragement. She is an amazing scientist as well as an advisor, who guided me through each step of my research projects, including hypotheses, experimental designs, data collection, and analysis as well as writing. I am and always will be in awe of her extensive view in tau and how our lab can contribute to tauopathies' therapeutic development. She has taught me skills that are critical for my future careers, such as critical thinking, writing skills, effective presentations and communications, project management, etc. I am also very grateful for her support in my career development and the opportunities she gave me to explore and solve problems in the industry with the scientific skills I learned from research in internships. These helped me tremendously to decide what I want to pursue in the future.

To my committee, Prof. Rick Dahlquist, Prof. Mike Bowers, and Prof. Stu Feinstein, I am extremely grateful for your suggestions throughout my Ph.D. To the staff at the Chemistry and Biochemistry Department, thank you - especially to India Madden, Rosemary Rivas, Heather Gardner, Trevor Bellefeuille, and Cabe Fletcher.

I would like to thank all my colleagues in the Han Lab. Especially, I would like to thank Dr. Yann Fichou (now Prof. Fichou), whom I had shared an office with for 4 years. He helped me in the fundamental understanding of tau and DEER theory, data analysis, and many fruitful discussions. I greatly appreciate Michael Vigers, Dr. Yanxian Lin, and Dr. Neil Eschmann for the help in experiments and discussions on data and papers. I would like to thank Karen Tsay, Dr. Timothy Keller, and Dr. Thomas Casey for the help in setting up DEER experiments. Karen also helped me greatly with DEER data analysis and discussion. I would like to thank Vishnu Vjayan and Austin Dubose

for their help in experiments and discussions in my final year of Ph.D. I also want to thank undergraduate researchers who I have enjoyed working with and who have helped me greatly in experiments, including Kevin Nguyen, Athena Quddus, and Alexa Albert. I would like to thank researchers who contributed directly or indirectly to my projects or career development, including Dr. Kendrick Nguyen, Dr. Jennifer Rauch, Dr. Andrew Longhini, and Dr. Karen Bogart.

Finally, I would like to give my special thanks to my friends and family for all the love and support over the years. I am very grateful to my parents, Yan Zeng and Zhaofei Jiang, for their unconditional support. I would like to thank my husband, Hadley Souther, and his family for their love and support. I would love to thank all my friends who have given me great companions and so many fun times during my Ph.D. (listed in no specific order): Li Li, Miranda Li, KC Chen, Sheng-Ping Liang, Kan Tagami, Jennifer Chen, Aly Schippers, Julianne Truong, Anetka Jelo, Selena Staun, Sean Lee, and many others. Lastly, I would like to thank my dogs, Luffy and Freya, for being the best puppies and for their emotional support.

Curriculum Vitæ

Zhikai Zeng

Education

09/2016-06/2022	Ph.D. in Chemistry (Expected), University of California, Santa Barbara.
09/2012-06/2016	B.S. in Polymer Science and Engineering, South China University of Technology, Guangzhou, Guangdong, China

Research Experience

Graduate Student Researcher

Prof. Songi Han, University of California, Santa Barbara, CA

• High-level analytical skills with experience in processing large scientific datasets, resulting in the development and optimization of 2 high-throughput methodologies and 1 protein propagation model

• Top-notch problem-solving skills and creativity with expertise in biophysics and molecular biology, and proven ability to meet tight deadlines by working in a fast-paced environment as evidenced by 3 publications

• Excellent teamwork and collaboration ability demonstrated by managing multifaceted bio-physical chemistry research projects, resulting in the development of 3 interdisciplinary collaborations.

• Strong organization and project management skills as reflected by handling 3 projects simultaneously, planning and executing advanced experiments, maintaining documentation and supervising 5 undergraduate researchers in multiple projects

Project Leader, undergraduate researcher

Prof. Lan Liu, Prof. Qsinghua Xu, South China University of Technology, China

• Outstanding adaptability as demonstrated by conducting 4 projects in 2 research groups as undergraduate research assistant and project leader and contributing significantly to 4 publications.

• Effective communication skills as reflected by leading an interdisciplinary collaboration with the Business Management Department to develop an integrated strategy and business plan for a new tire firm.

• Strong leadership skills and conflict-resolving skills as established by leading a group of 5 undergraduates to win first place in the National Training Program of Innovation and Entrepreneurship.

• Good presentation skills as demonstrated by presenting research findings to a room of 200-300 people from academia and industry.

Publications

1. Fichou, Y., Lin, Y., Rauch, J. N., Vigers, M., **Zeng, Z.**, Srivastava, M., Keller, T. J., Freed, J. H., Kosik, K. S., and Han, S. (2018). Cofactors are essential constituents of stable and seeding-active tau fibrils. Proceedings of the National Academy of Sciences of the United States of America, 115(52), 13234–13239.

2. Lin, Y., Fichou, Y., **Zeng, Z.**,, Hu, N. Y., and Han, S. (2020). Electrostatically Driven Complex Coacervation and Amyloid Aggregation of Tau Are Independent Processes with Overlapping Conditions. ACS Chemical Neuroscience, 11(4), 615–627.

Manuscripts in Preparation

1. **Zeng, Z.**, Fichou, Y., Vigers, M., and Han, S. (2022). The Journal of Physical Chemistry B, under review.

2. **Zeng, Z.**, Tsay, K., Vigers, M., Woerman, A., and Han, S. (2022). Proceedings of the National Academy of Sciences of the United States of America, in preparation.

Posters and Presentations

1. Zhikai Zeng, Yann Fichou, and Songi Han. "Impact of Sonication Treatment of Tau Seeds on Seeding." Tau Consortium, 2019 Febuary. Poster

2. Lin, Yanxian, Kate Zeng, Yann Fichou, Yuge Hu, and Songi Han. "Impact of Complex Coacervation on Tau Amyloid Aggregation." In American Physical Society Meeting Abstracts, 2019.

Abstract

Seeking the Structural Basis of Tau Seeding

by

Zhikai Zeng

Tau is an intrinsically disordered protein found in neurons that binds and stabilizes microtubules. Under pathological conditions, tau aggregates into amyloid fibrils and this process is central to several neurodegenerative diseases, collectively known as tauopathies. It has been proposed that tau pathology occurs in a "prion-like" mechanism, where pathological tau conformers (termed "seeds" or "strains") recruit native monomeric tau to form amyloid aggregates by templated seeding. Recently, a high-resolution clue that distinct tau strains underpin different tauopathies came to light: tau fibrils isolated from tauopathies were found to have distinct core structures by cryo-electron microscopy. These fibril core structures are unique to and homogeneous within one disease, but typically different between different tauopathies. This dissertation is aimed to answer two key questions, which remain unclear in the current state of knowledge: (1) what are the defining properties or conditions that determine the shape of a fibril (e.g. physico-chemical conditions, tau state such as mutations, fragmentation, and/or the presence of cofactors)? (2) What structural properties of the fibril are replicated and propagated in seeding, if at all? This work will guide you through a tour to establish the experimental conditions that enable *in vitro* tau seeding and use these conditions to gain a molecular understanding of tau structures in seeded fibrils.

Contents

List of Figures

Chapter 1

Introduction

The tau protein is an intrinsically disordered protein (IDP) in its unbound state and becomes partially structured when bound to microtubules [1]. Under pathological conditions, tau dissociates from microtubules and forms aggregated inclusions that are directly implicated in various neurodegenerative diseases, collectively known as tauopathies [2, 3]. Pathological tau inclusions are insoluble amyloid fibrils with cross-β secondary structure, formed by the stacking of monomeric tau to assemble fibrils in a process referred to as aggregation [4]. It was recently confirmed by cryogenic electron microscopy (cryo-EM) that tau protein adopts a variety of atomic structures (that we henceforth refer to as tau "shapes") when incorporated in fibrils. The cryo-EM structures of post-mortem human brain-derived tau fibrils, thus far of Alzheimer's disease (AD) [5, 6], Pick's disease (PiD) [7], corticobasal degeneration (CBD) [8, 9], chronic traumatic encephalopathy (CTE) [10], progressive supranuclear palsy (PSP) [11, 12], argyrophilic grain disease (AGD) [12] and globular glial tauopathy (GGT) [12] reveal that a core segment of tau is precisely folded into a distinct shape, unique within each tauopathy disease category, that stacks in identical replicates into long (up to micrometer) fibrils. It seems that the defining differences between tauopathy phenotypes lie at the atomic structural detail of the fibril structure.

The findings by cryo-EM are consistent with the hypothesis that fibril shapes are the determinant of the selectivity of conformation-dependent antibodies, such as GT-7, GT-38, and 18F12 that can distinguish AD-tau from pathological tau of other tauopathies [13, 14]. However, it has never been directly verified at high resolution whether the basis of the recognition by these antibodies of tau lies in the fibril shapes, and if so, which fibril motif, and/or post-translational modifications (PTMs) and specific tau fragments. For instance, immunotherapy (such as using the monoclonal antibody UCB0107's mouse version, antibody D [15]) relies on the hypothesis that seeded aggregation of tau aggregates will faithfully propagate a given fibril shape with the affinity to the antibody.

Hence, verifying and understanding the mechanisms of tau fibril shape formation and propagation is crucial for therapeutic development.

During the development of the work described in this dissertation, we and others found that tau aggregates from different sources can induce aggregation of monomeric tau *in vitro* and *in vivo* [16, 17, 18, 19, 20, 21, 22, 23, 24, 25, 26, 27]. These misfolded tau species that are capable of recruiting and inducing aggregation of tau monomers are known as tau "seeds". *In vitro* seeded aggregation is often facilitated by the addition of polyanionic cofactors and reducing agent, and/or sonication treatment of the seeds, even though the effect of these conditions on seeding is poorly understood. Our group understands that it is impossible to recreate the exact biological conditions needed to generate the disease-relevant end structures of tau fibrils, not only because of the complexity of the biological milieu but also because of the timescale of tau fibril formation occurs over decades during aging. However, we aim to recreate artificial conditions for tau aggregation that results in the formation of converged fibrils with similar folds as the disease fibrils. Once such conditions are found, these offer promising tools for further development of therapeutic strategies for tauopathies. Furthermore, despite the prevailing hypothesis that seeding generates daughter fibrils with similar structures that preserve the structure of the parent fibrils, direct experimental validation is lacking, and what exact structural features are transmitted and preserved is not known. Therefore, this dissertation is aimed to investigate the experimental conditions that enable tau seeding and verify the templated seeding mechanism at high resolution. Specifically, this work focuses on two key, fundamental questions: (1) what are the defining properties or conditions that determine the shape of a fibril (e.g. tau state such as the disulfide bonding, fragmentation, and the presence of cofactors)? (2) What structural properties of the fibril are replicated and propagated in seeded aggregation of tau, if at all?

Disulfide bonds formed between two thiol groups from cysteine residues were proposed

to play a role in tau aggregation and may be important for fibril shape formation [28, 29, 30]. Although it has been reported that intramolecular disulfide bonds impede tau aggregation [31, 28], the view of intermolecular disulfide bonding's role in tau aggregation remains controversial. Some studies showed that intermolecular disulfide bonds facilitate tau aggregation [31, 32, 33], while another suggest otherwise [34]. Interestingly, recent evidence suggests that disulfide cross-linked tau dimers induce tau seeded aggregation and transmission in HEK293 biosensor cells and primary neuron culture [35], indicating the importance of tau disulfide bond formation in tau pathogenesis. Besides, reducing agents are commonly used in various *in vitro* studies to avoid disulfide bond formation; NFTs are found to induce seeded aggregation of recombinant tau in the presence of DTT [17, 36]. The precise mechanisms underlying these observations remain unclear. Chapter 2 of this dissertation is set out to explore the role of disulfide bonding in tau aggregation. The outcome of this study found that incubation under reducing conditions or mutation of cysteine to another uncharged residue leads to increased aggregation. Both intermolecular and intramolecular disulfide bonds hinder tau aggregation, and disulfide bonds are not the driving force for tau aggregation. The results of this chapter also rationalize the use of cysteine-less protein as a monomeric substrate in the following chapters.

In addition to the role of disulfide bonds in aggregation, we are also interested in the effect of polyanionic cofactors (e.g. heparin) on tau aggregation and seeding. Cryo-EM found unknown non-tau densities within CTE folds [10], CBD folds [8], and PSP folds [11], suggesting that cofactors may be involved in tau aggregation in these tauopathies. As for *in vitro* studies, heparin-induced fibrils are widely used as seed to induce tau aggregation *in vitro* and *in vivo* [37, 38, 39, 40, 41]. Heparin is also present in seeding reaction buffer in some studies [42, 43, 44, 45, 46]. One hypothesis is that the initiation of tau aggregation in human and animal models is driven by pathogenic cofactors, which

are also needed to assist the soluble tau monomers to interact with the seeds *in vitro*. However, whether the cofactors serve as reactants that incorporate into the product fibrils or only act as catalysts that can be removed without breaking the fibrils has not been elucidated. Therefore, chapter 3 of this dissertation discusses the role of cofactors in aggregation. The results in this chapter demonstrated that cofactors, specifically heparin and RNA, bind to tau proteins, and are incorporated into tau fibrils at specific stoichiometry and that cofactors are essential for *in vitro* seeding. The results of this chapter thus suggest that in neurons under pathological conditions, tau aggregation can be facilitated by interactions with polyanionic cofactors, which may, in turn, determine the shape of the fibril.

Besides the use of reducing agents and cofactors in seeding, the seed (e.g. heparin-induced fibrils) is often subjected to sonication before the treatment of cells or recombinant monomer [37, 38, 39, 40, 41]. It was recently proposed that monomeric tau release from heparin-induced fibrils by sonication maintains aggregate-templated conformations that provide high seeding capacities [39]. Sonication may result in fibril breakage into a mixture of short fibrils, and some studies hypothesized that short fibrils provide more open fibril ends as templates and thus seeding is enhanced [45, 47, 48]. In contrast, some studies suggested that the propagation and spreading of sonicated fibrils could be due to soluble tau aggregates and oligomers [38], or monomers [39] formed during sonication. Therefore, the effect of sonication on tau fibrils and the nature of the infectious seeding agent remains controversial. Here, chapter 4 is aimed to understand the effect of sonication on tau fibrils and the nature of tau seeds. Results of this chapter showed that sonication induces artificial fragmentation in heparin-induced tau fibrils and the fibril fragments are seeding competent to trigger further amyloid formation both *in vitro* and in cells. Mass spectrometry results showed that upon sonication, tau fibrils are more protected compared with monomers, but the fragmentation cleavage sites are random.

Since it is not clear which fragment is responsible for the seeding activity observed, we argue that sonication, especially long-time sonication should be used to process fibrils with caution.

As we established the experimental conditions that are crucial for *in vitro* seeding and affect fibril shape formation, we set foot to explore what tau fibril structural properties are replicated and propagated in seeding. Although *in vivo* and *in vivo* data provide strong circumstantial evidence that seeding with patient-derived materials can propagate disease structures [16, 17, 18, 19, 20, 21, 22, 24, 49, 50, 23, 51], molecular-level structural characterization is needed to show what motifs and shapes are propagating in seeding and what environmental conditions are required for faithful structural replications. In chapter 5, we used two types of seeds, generated in HEK293T cell lines engineered to express specific tau variants, upon seeding with post-mortem CBD and PSP human tissue materials. We made the selection because these cell-derived seeds are more disease-relevant than heparin-induced fibrils; human materials passaging through and amplified by HEK293T cells have been shown to maintain tauopathies strain properties [27, 49, 50], whereas heparin-induced tau fibrils are different from disease folds [5, 6, 7, 10, 8, 11, 12, 9] and are more heterogeneous [26, 52]. In this project, we successfully achieved robust *in vitro* seeding activity by inducing aggregation of recombinant tau monomer with CBD and PSP cell-derived seeds without added cofactors, sonication treatment of the seeds, or the use of a reducing agent. To investigate the structure of seed-induced fibrils at high resolution, electron paramagnetic resonance (EPR) based double electron-electron resonance (DEER) distance measurements coupled with site-directed spin-labeling (SDSL) were used. DEER is a powerful biophysical technique used to assess long-range distances of 1.5–8 nm between two amino acid residues of interest. Compared to NMR or cryo-EM, DEER distance measurements provide a fast and flexible solution to characterize partial features of tau conformational ensembles irrespective of structural heterogeneity in

the sample. By employing DEER distance measurements, we found that CBD and PSP seed-induced fibrils have distinct conformations compared with heparin-induced fibrils, and a subpopulation resembles CBD and PSP disease folds. These results indicated that by controlling the experimental conditions and by using a shape-defined seed, we could converge the tau aggregation pathway towards distinct fibril shapes.

1.1 Tau Protein

Tau is a microtubule-binding protein (also known as microtubule-associated protein, MAP) that is encoded by the MAPT gene on human chromosome 17q21. There are six major isoforms in the human brain [53] (Fig. 1.1). Alternative splicing of exons 2 and 3 produces tau isoforms with no (0N, without exons 2 and 3), one (1N, without exon 3), or two (2N, with exons 2 and 3) amino-terminal inserts, whereas alternative splicing of exon 10 produces isoforms with either three (3R, without exon 10) or four (4R, with exon 10) microtubule-binding regions. This generates proteins that in humans are between 352 and 441 amino acids in length.

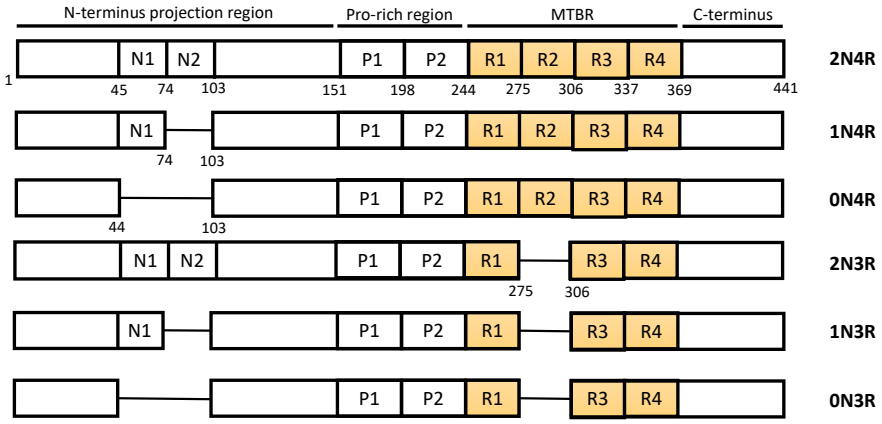

Figure 1.1: Six isoforms of tau protein.

The expression of tau isoforms is developmentally regulated. Whereas the fetal human brain expresses only 0N3R tau, in the adult brain all six isoforms are present, with a 1:1 ratio of the 3R and 4R isoforms. Splicing of exon 10 has received particular attention because an altered 3R:4R ratio can cause tauopathy (which will be discussed in the next subsection).

MAP2 and MAP4 are additional members of the MAP family; however, whereas MAP4 is expressed in many tissues, MAP2 and tau are predominantly localized to neurons. Early in development, tau is distributed throughout the neuron, and with maturation, it becomes enriched in the axon [54]. This differs from MAP2, which is excluded from axons. A pathological role has been identified for tau in the dendritic compartment [55, 56], but under physiological conditions, the role of Tau in this compartment is less understood. The localization of Tau to other organelles, such as nuclei, has also been reported [57, 58, 59]. Invertebrate species such as the roundworm Caenorhabditis Elegans have only one functional ortholog, Ptl-1 (protein with tau-like repeats-1) [60, 61], that is required for the structural integrity of neurons [62].

Tau can be divided into four functional domains: the N-terminal projection domain, a proline-rich region, the microtubule-binding domain, and the C-terminal region (Fig. 1.1). Within the microtubule-binding domain are repeats that bind to the heterodimers of α- and β-tubulin that in a polymerized form constitute the microtubules, thereby facilitating motor-driven axonal transport [63]. Microtubule binding and assembly are enhanced by the proline-rich region that contains seven PXXP motifs, of which a subset interacts with the SH3 domain of a number of signaling molecules, including the tyrosine kinase Fyn [58, 64]. Fyn also interacts with Tau via its SH2 domain when Tau is phosphorylated at residue Y18 [58, 65]. The short C-terminal region likely has a role in inhibiting tau polymerization [66, 67]. Insight into the roles of the distinct tau isoforms and their functional domains has been provided by determining the tau interactome and

the pathways through which these proteins are involved, suggesting a role for 2N Tau in disease [68]. Considering its multiple interactions and localization, tau is best described as a scaffolding protein.

Tau undergoes a remarkable degree of post-translational modification (PTMs) even under physiological conditions, including N- and O-glycosylation, ubiquitination, truncation, glycation, and oxidation, amounting to 63 unique PTMs that have been reported in wild-type mice [69]. The most widely studied PTM is phosphorylation, owing to the fact that the longest isoform of human tau contains 80 serine and threonine residues and 5 tyrosine residues, all of which can potentially be phosphorylated. An increase in tau phosphorylation reduces its affinity for microtubules. PTMs are highly augmented in the tauopathies, causing tau to accumulate in the cytoplasm and aggregate [70]. Hyperphosphorylation of tau destabilizes tau–microtubule interactions, leading to microtubule instability and transport defects. Hyperphosphorylation also contribute to tau aggregation [71]. Acetylation of tau at specific lysine residues has also been proposed to contribute to the aggregation and accumulation of the protein [72, 73].

1.2 Tauopathies

Tauopathies are a group of clinically, morphologically, and biochemically heterogeneous diseases that are characterized by the deposition of tau aggregates. The primary tauopathies are a subgroup of frontotemporal lobar degeneration (FTLD), an umbrella term for neurodegenerative diseases characterized by neuronal and glial tau inclusions with predominant atrophy of the frontal and temporal lobes. FTLD includes Pick's disease (PiD), PSP, corticobasal degeneration (CBD), globular glial tauopathy (GGT), and argyrophilic grain disease (AGD). In contrast, AD is a secondary tauopathy that is characterized by Tau pathology in combination with extracellular amyloid plaques. The

following section is an overview of these tauopathies.

1.2.1 Frontotemporal lobar degeneration with tau inclusions

FTLD is a group of diseases characterized by the degeneration of the cortex of the frontal and temporal lobes, which commonly affects people under the age of 65. FTLD with tau immunoreactive inclusions (FTLD-tau) accounts for approximately 40% of all FTLD cases [74]. Pathologically, FTLD-tau is characterized by the widespread deposition of tau in morphologically diverse intracellular inclusions, and these are associated with severe neuronal loss in the frontal and temporal lobes, and superficial laminar spongiosis in the cortex, and gliosis of the gray and white matter.

In FTLD, tau amyloid pathology is deposited in both neuron and glial cells. The majority of glial tau pathology occurs in oligodendrocytes and astrocytes, and in some instances, tau is seen in microglia [75, 76]. The morphology of the inclusions separates FTLD-tau into the major subtypes of PiD, PSP, CBD, GGT, and AGD. These FTLD-tau subtypes are clinically and pathologically heterogeneous with regard to the distribution, type, and biochemistry of their Tau pathology, their uniting feature being that Tau abnormally aggregates and forms filamentous deposits in the brain [77]. Here, a few diseases are discussed. They are classified by the isoform of tau pathology (3R or 4R).

3R Tauopathies: Pick's disease. PiD, first described by Arnold Pick, is characterized by severe atrophy of the frontal, temporal, and parietal lobes [78]. The major pathological hallmarks of PiD are significant neuronal loss, gliosis, and argyrophilic, round, intraneuronal inclusions called Pick bodies [79]. Pick bodies are composed of filamentous 3R Tau and characterized by straight filaments that are 15–18 nm in diameter and twisted ribbons that are 20–22 nm wide; these assemblies are argyrophilic with some silver stains but consistently negative with the Gallyas silver stain [80, 81, 82]. They are

found predominantly in the hippocampus and frontal and temporal cortices [83]. To a lesser extent, glial tau pathology is observed in ramified astrocytes and as round, Pick body–like inclusions in both oligodendroglia and astrocytes [84, 85]. Interestingly, PiD is the only tauopathy to be predominantly associated with 3R Tau inclusions.

4R Tauopathies. In contrast to 3R tauopathies, inclusions of 4R Tau are more commonly observed and are the main pathological hallmark of a number of diseases, including PSP, CBD, GGT and AGD.

Progressive supranuclear palsy. PSP is characterized pathologically by Tau inclusions in the pons, the subthalamic nucleus, and the substantia nigra [86]. Neuronal Tau pathology is predominantly observed in subcortical structures and consists of NFTs and globular inclusions that do not fit the characterization of Pick bodies as they are composed of 4R Tau and are reactive with Gallyas silver stain [87]. Tufted astrocytes—Tau-positive inclusions characterized by densely packed fibrils that form tufts in the proximal processes surrounding astrocytic nuclei—are the pathological signature of PSP, and are detectable by Gallyas staining [88]. Coiled bodies—intracytoplasmic inclusions that surround the nucleus in oligodendrocytes—are also common and uniquely found in the cerebellar medulla in PSP [89, 90].

Corticobasal degeneration. Cerebral atrophy in CBD is diverse, particularly compared with atrophy in PSP, with neuronal loss and gliosis occurring primarily in the frontoparietal cortex but also extending to the frontal and superior temporal lobes. In contrast to the diversity of cerebral pathology, the distribution of pathology in the subcortical areas is uniform, with the most prominent site of subcortical degeneration being the substantia nigra, where moderate to severe neuronal loss and gliosis are always seen. In addition to neuronal loss, CBD also has several characteristic neuronal and glial pathologies. Ballooned neurons are predominantly found in the cortical and limbic regions and are immunoreactive for phosphorylated neurofilaments and αB-crystallin rather than for

Tau [91, 92]. Furthermore, although NFTs are rare in CBD, pretangles are commonly observed in the cerebral cortex and subcortical nuclei [93]. CBD is distinguished from PSP by the presence of astrocytic plaques, particularly in the cerebral cortex [94]. Coiled bodies are widely distributed in degenerating areas in oligodendrocytes, and argyrophilic threads—Tau-positive threadlike structures in the processes of astrocytes and oligodendrocytes—are observed in white and gray matter and are more severe in CBD than in PSP [95].

1.2.2 Alzheimer's Disease

AD is considered a secondary tauopathy due to the formation of NFTs in the presence of extracellular amyloid plaques that are composed predominately of the amyloid-β (Aβ) peptide in a fibrillar form. In contrast to FTLD-tau, AD primarily affects people over the age of 75 and presents as dementia rather than a change in behavior [96]. Furthermore, in AD, Tau aggregates in the form of NFTs and neuropil threads that are composed of both 3R and 4R Tau and are observed only in neurons. Tau-containing neurites within amyloid plaques are termed neuritic plaques and are also composed of 3R and 4R Tau. Sporadic AD is the most common etiology, but a small percentage of patients (¡1%) have autosomal dominant inherited AD caused by pathogenic mutations in the genes encoding the amyloid precursor protein (APP), presenilin-1 (PS1), or presenilin-2 (PS2). Tau pathology in AD begins in the transentorhinal cortex and then spreads to the hippocampus and neocortex, giving rise to six progressive Braak stages [97].

1.3 Tauopathy-specific protein fibril shapes in tau fibrils

Besides differences in the isoform composition and tau pathology morphologies, recent cryo-EM studies discovered that the core segment of tau derived from post-mortem brains is precisely folded into distinct tauopaties, and stacks in identical replicates into long fibrils. Specifically, distinct fibril shapes has been found in AD [5, 6], PiD [7], CBD [8, 9], CTE [10], PSP [11, 12], AGD [12], and GGT [12].

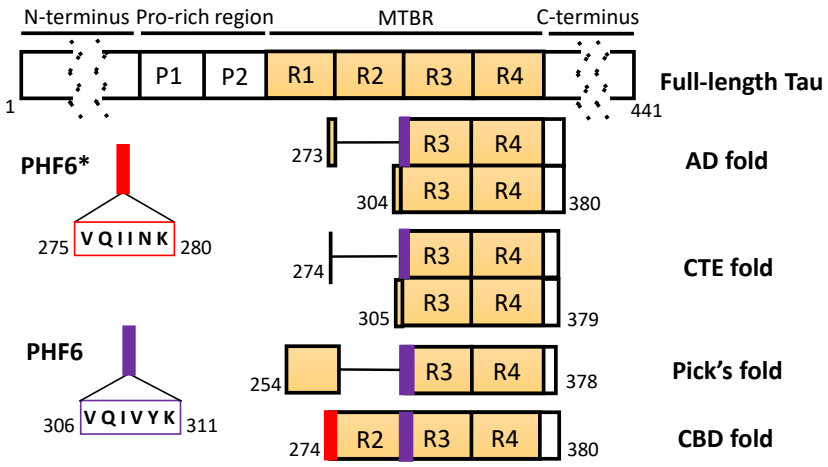

Figure 1.2: Schematics of the full-length tau and the fibril core constructs of four disease folds[5, 6, 7, 10, 8, 11, 12, 9], showing the major domains and location of the disease folds. The full-length tau here is the longest human tau isoform with 441 residues, containing N-terminus, proline-rich domain, microtubule biding repeats (MTBRs) and C-terminus. The core of tau fibrils from the human post-mortem AD brain (AD fold) spans residues 273/304-380, while the CTE fold spans residues 274/305-379. Pick's fold contains residues 254-378. CBD fold spans from 274-380. PHF6* (275VQIINK280, red segment) and PHF6 (306VQIVYK311, purple segment) are considered to be crucial for fibril formation[98], and PHF6 is included at least partially in the all of the disease folds.

Tau fibrils from the human postmortem AD brain has a C-shaped core spanning R3, R4, and the early C-terminus region (residues G273/G304-E380, Figure 1.2)[5, 6], while tau fibrils extracted from post mortem CTE brains assume a more open C-shaped

core spanning a similar region (residues K274/S305-R379, Figure 1.2)[10]. In contrast, tau fibrils from PiD adopt a J-shaped core (residues K254-F378, lacking R2, Figure 1.2).[7] As for tau fibrils from 4R tauopaties, including CBD, PSP, GGT, and AGD that were reported thus far, comprise of R2-R4, and 10-18 amino acids of the C-terminal region (such as the CBD fold spanning residues K274-E380, Figure 1.2).[8, 12] They were further categorized into two classes based on the layers of the fold [12]: CBD fold and AGD fold adopt a four-layered conformation while PSP fold and GGT fold assume a three-layered core. Within these two classes, tau fibrils differs on a substructure level; AGD fold resembles CBD fold but is slightly longer, and has a smaller non-tau cavity between R2 and C-terminal segment; GGT fold is similar to PSP fold in the three-layered arrangement but has distinct chain turns and C-terminal packing direction. For several of these fibril structures, non-proteinous molecules have been suggested to be associated within the core of CTE[10], CBD[8], and PSP[11] fibril. Although the identity of these cofactor molecules is not known, their presence appears to be disease-specific.

The discovery that tau in different disease contexts can generate fibrils with distinctive shapes that imprint disease phenotypic diversity is reminiscent of the characteristics of prion proteins in the prion disease.[99] The pathological prion scrapie (also known as "prion seeds" or "prion strains") has distinct conformations and properties and is known to self-propagate by seeding the misfolding and aggregation of normal prion protein into a pathological misfolded state as part of amyloid fibrils.

1.4 Seeded aggregation of tau hints at a prion-like behavior

Similar to prion seeds, misfolded tau aggregates (referred to as "tau seeds") have been shown to transmit some features *in vivo* and in cells, such as the microscopic morphology of tau fibril or cell-type specificity. Studies with animal models have demonstrated the spread of tau pathology upon intracerebral injection of tau aggregates from patients, mouse models, or recombinant tau containing disease mutations, as verified by immunoanalysis with anti-tau antibodies.[16, 17, 18, 19, 20, 21, 22, 23, 24] The induced pathology was found in brain regions anatomically connected to the injection sites and propagate in a time- and dose-dependent manner, indicating that tau seeds from different sources are able to convert endogenous tau into pathological inclusions with some key properties preserved. Such properties include the type of cell that can be infected, the spatial patterns and distributions of the lesions in the brain regions.[24, 49, 50] Although antibodies (e.g. GT-38) have been used to show that AD patient-derived tau seeds generate tau inclusions in mouse brains that may be conformationally similar to that of the seed,[23, 51] high-resolution structural insight as to what protein folding motif is propagating in seeding is missing.

Tau seeding has also been demonstrated in cells, where the formation of cellular tau inclusions is monitored by the local increases of fluorescence-based signal in biosensor cells, such as Forster resonance energy transfer (FRET)-based biosensor seeding assay.[50, 49, 27, 100] The Diamond lab created monoclonal clonal HEK293T cell lines expressing truncated tau consisting of the microtubule-binding repeats (MTBR) (residues 244-372, also known as K18) and the aggregation-enhancing mutations P301L and V337M, fused with fluorescent sensors at the C terminus. This cell line serves as a platform to test the competency of tau seeds derived from patient brain tissue samples, mouse brain-derived

tau, and recombinant tau fibrils in inducing the misfolding and aggregation of naive K18 tau, and identifying emerging tau strains.[50] Based on the difference in the morphology of cellular inclusions, limited proteolysis, and the seeding activity in a split-luciferase assay, the Diamond lab proposed to have generated 18 distinct strains.[49] Strikingly, tau seeds from brain homogenates of disease patients with AD, CBD, CTE, PiD, AGD, and GGT were competent to generate inclusions with distinct macroscopic morphology in cells.[27, 101] These observations offer promising circumstantial evidence that core protein shape properties are propagated in seeding. A recent study cautioned that fluorescent protein tags on K18 could inhibit aggregation of tau due to steric hindrance, and the fluorescence signal increase in the cellular seeding assays may be due to factors other than seeded tau aggregation[102]. However, another study presented more supporting findings by employing live cell imaging using the K18-based biosensor cellular seeding assay, and observed three phases of amyloid aggregation according to the nucleation polymerization model: a nucleation phase, a subsequent exponential elongation phase, and a final plateau phase.[103] The height of the plateau phase is dependent on the amount of AD patient brain-derived seeds added initially to the cells, so the biosensor cellular seeding assays are still of interest for clinical applications. In summary, templated seeded aggregation of tau is a highly potent hypothesis that must be verified with direct structural biology studies. For this, it is key to collect molecular-level structural information on the evolving and aggregating tau populations, which in turn requires *in vitro* measurements at the current state of the art.

1.5 Tracking structural evolution of tau in seeded aggregation

Given the distinct structural differences observed in different tauopathies[5, 6, 7, 10, 8, 11, 12, 9], structural biology tools with sufficiently high resolution are needed to differentiate between the different disease phenotypic fibril shapes and to verify the seed-induced fibrils shapes. Ultrastructural and biochemical properties are often used as evidence for tau conformations, such as low-resolution morphology[47, 104], secondary structure[47], and proteolysis patterns[105, 106]. Similar features between the seed-induced fibrils and the seeds are used as indications of tau templated seeding.[47, 42, 25, 46, 38, 106, 107, 104, 105] For example, Xu et al. showed in a recent study that recombinant tau fibrils generated with AD-tau seeds are similar to AD-tau in terms of their ultrastructure, solubility, and conformation, as detected by conformation-dependent antibody DMR7 and MC1 that selectively bind to AD tau aggregates, indicating that AD-tau may have templated the aggregation of recombinant tau.[108] However, some studies found that the seeded tau fibrils are different from the seeds due to unsimilar proteinase digestion patterns and EM morphology.[105, 41] Therefore, tools that can directly track protein shape formation and evolution are needed to resolve these critical questions of direct relevance to therapeutics development.

Cryo-EM[5, 6, 7, 10, 8, 11, 12, 9], crystallography[109, 110], and nuclear magnetic resonance spectroscopy (NMR) [111, 112, 113] can be used to study the structure of mature fibrils with atomic resolution and molecular level details. However, they require a significant degree of homogeneity in the sample or crystallization and are demanding of sample type, quality and/or quantity. They are also challenging for discovery work on heterogeneous samples or to capture transient conformational ensembles along the course of aggregation. In contrast, EPR-based DEER spectroscopy provides an efficient

and direct approach to characterize partial features of heterogeneous samples, even of disordered proteins and partially aggregated biomolecules. It resolves the probability distribution of intramolecular distances in the 1.5 to several nm ranges across a pair of spin-labels attached to the molecule.

1.6 DEER for tracking structural evolution of tau aggregation

DEER can obtain structural information of molecules of different sizes and complexity by intramolecular distance measurements.[114, 115, 116] It yields the mean distance and distance distribution between a pair of paramagnetic spin-labels (commonly nitroxide-based). If the molecule adopts multiple conformations, the labeled positions are separated by multiple distances. When one of the conformations becomes dominant, a specific distance between the labeled positions dominates and the distribution of this distance is well defined. In this dissertation, I used DEER as the key technique to obtaining structural information of tau. This section is dedicated to giving a brief overview of DEER and its capabilities for elucidating tau structures.

For best performance, DEER is conducted with a pulsed Q-band EPR spectrometer with high microwave power (such as 100-300 Watt from a traveling wave tube amplifier). In DEER, pump and observer microwave pulses are used to selectively excite and observe two distinct spin populations. When spins between these populations are spatially proximal, they experience dipolar coupling that scales with $\frac{1}{r^3}$, where r is the distance between pairs of spins of the spin population selected by the pump and observer pulses. A time-domain dipolar signal, S(t), is acquired by measuring the decay of the dipolar coupling between an ensemble of spin-label pairs. The intramolecular distance,

r, and probability distribution of distances, P(r), between the two labeled residues can be reconstructed from S(t) [117, 118, 119, 120, 121].

1.6.1 Measuring mean distances and distance distributions of disordered and ordered structures

Rigid oligo(para-phenylene ethynylene) molecules serve as ruler models to showcase DEER-derived distance measurements (Figure 1.3a). As shown in Figure 1.3c, the end-to-end distance distribution of three of these ruler molecules of different lengths shows a single narrow peak, reflecting the well-defined end-to-end distance of the ruler molecules (monomer is 2.8nm, trimer is 4.1nm, and 5-mer is 5.4 nm). The capability of DEER to capture multiple well-defined distances is well-documented [107, 122, 123, 124]. More interestingly, DEER can quantify a broad distribution of distances originating for instance from a conformational ensemble of IDPs or polymers. For example, poly(ethylene oxide) (PEG, as shown in Figure 1.3b) is highly disordered, but still yields distinct end-to-end distance distributions for the 13-mer, 25-mer, and 36-mer PEG [125]. As the chain length increases, the mean distance moves to longer distances and the distance distribution broadens (Figure 1.3c). The scaling of the DEER-derived mean end-to-end distance with PEG molecular weight verified that PEG follows excluded volume behavior–a property that has been known in the literature but never directly measured until recently.[125] This example showcases the ability of DEER to capture the conformational state of disordered molecules via the peak position and shape of the distance distribution, P(r). DEER can furthermore characterize partially ordered macromolecules, such as tau that in part has adopted fibrillar structures and in part remains disordered.

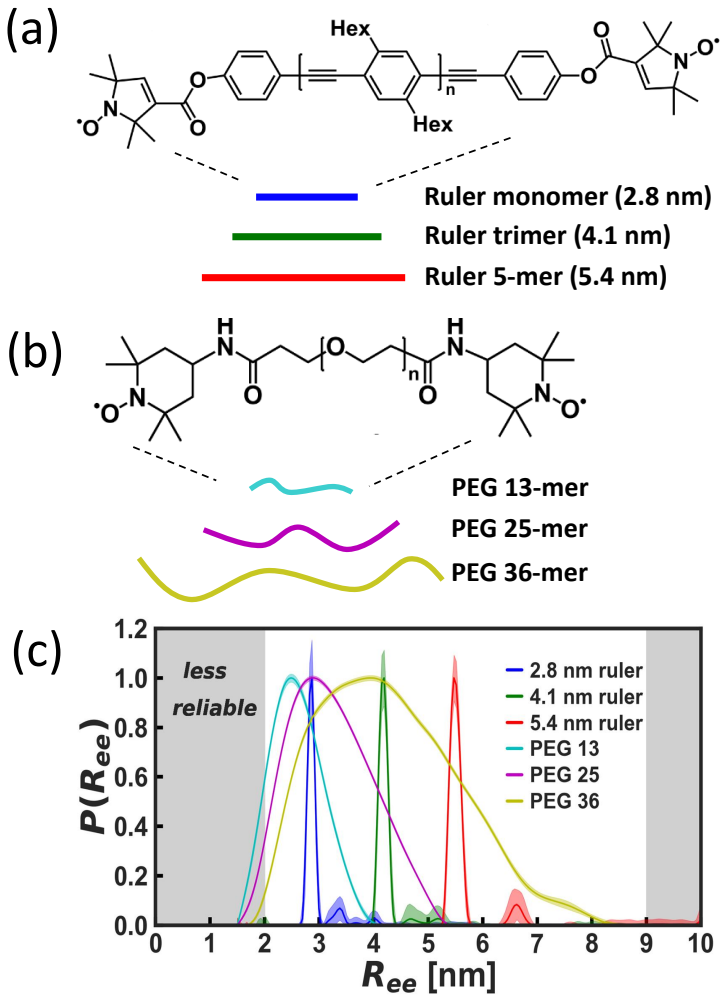

Figure 1.3: Chemical structure and schematic of (a). DEER ruler molecules of different sizes, and (b). PEG of different sizes (31-, 35-, 36-mer). Since the ruler molecules are more rigid, they are illustrated as a straight line. As for PEG molecules, curved lines are used to demonstrate their flexibility. (c). End-to-end distance distribution measured by DEER of the rulers and PEG molecules. The P(r)s of rulers are sharp and narrow, while the P(r)s of disordered PEG molecules are broad.

1.6.2 Capturing structural heterogeneity to assess conformational convergence in seeding

DEER spectroscopy coupled with site-directed spin-labeling (SDSL) provides a direct solution to characterize partial features of the tau ensemble. A pair of cysteines are introduced at residues of interest by site-directed mutagenesis, while the endogenous cysteines are mutated into other residues, such as serines. The double-cysteine construct is then labeled with nitroxide spin-labels, such as S-(1-oxyl-2,2,5,5-tetramethyl-2,5-dihydro-1H-pyrrol-3-yl)methyl methanesulfonothioate (MTSL, represented with red dots in Figure 3). The sites for SDSL are carefully chosen to be terminal sites or residues that lie at the exterior of the tau fibril core, once formed, to minimize adverse effects of the mutation and spin-labels on the protein folding and aggregation process. To avoid intermolecular spin interaction, at least 10-fold molar excess of mutation-free and label-free WT tau is mixed with spin-labeled tau, so that doubly spin-labeled tau monomers will be stacked between non-labeled tau along the fibril axis during fibrillization. By ensuring that spin-labeled tau modified by SDSL constitutes a fraction (e.g. 5 or 10%) of the tau population, intramolecular distances of tau incorporated into fibrils can be measured.[126, 127, 128]

DEER-based distance measurements can therefore be used to capture emerging conformations and fibril structures of tau starting from IDP. The exact shape and maximum peak position of P(r) sensitively depend on which segment of tau is flanked by the pair of spin-labels. For instance, when tau is labeled by SDSL at residues 316 and 337, as shown in Figure 1.4a, the pair of spin-labels spans most of R3, and its end-to-end distance distribution should be different for the different tauopathy fibrils derived from human post-mortem tissues. The IDP state of tau before aggregation has occurred yields a characteristically broad P(r)(Figure 1.4b). When tau stacks to fibrils with β-sheet structures and form a C-shaped core found in AD or a J-shaped core found in PiD (Figure

1.4a), the emergence of distinct shapes and the narrowing of the distance distribution is expected. This is illustrated in Figure 1.4b with model data, in which the blue and green P(r) data are generated based on the relative position of residue 316 and residue 337 observed from the PDB of AD fold [5, 6] and PiD fold [7], respectively. To verify or refine the folding pattern of tau, one can choose pairs of labels spanning different segments that will fold differently into distinct shapes. Figure 1.4c illustrates tau that is doubly labeled at residues 342 and 360. When tau is folded into a C-shaped fibril, the labeled segment collapses, generating a short mean distance with a narrower distribution (Figure 1.4d). When a J-shaped core is formed, the labeled segment extends, yielding a longer mean distance.

DEER-derived P(r) has been used in the literature to characterize the structural property of heparin-induced and seeded tau fibrils.[129, 45, 25] Heparin is a polyanionic cofactor commonly used to induce tau aggregation *in vitro*. The Margittai group observed that the heparin-induced fibril of K18 tau gives rise to multiple broad features in its intramolecular distance distribution, while heparin-induced fibril of K19 tau (truncated tau with R1, R3, and R4) generates a single narrow distance distribution.[129] The authors concluded that heparin-induced K19 fibrils are more homogeneous than K18 fibrils. Interestingly, seeding naive K18 monomer using K19 heparin-induced fibrils generated homogeneous fibrils, resembling the property of the K19 seed, indicating that certain conformers are selectively propagated and can converge towards a more homogeneous fibril population in the seeding process. DEER has been used to demonstrate conformational selection in the literature upon multiple generations of seeding with heparin-induced fibrils[45] or with transgenic mouse brain-derived fibrils.[25] In the study of Fichou et al., N-terminus truncated 4R tau (referred to as tau187, spanning amino acid 255-441) monomer was seeded with transgenic mouse-derived fibrils, resulting in multiple narrow peaks in the distance distribution.[25] This implied that seeding generated structurally

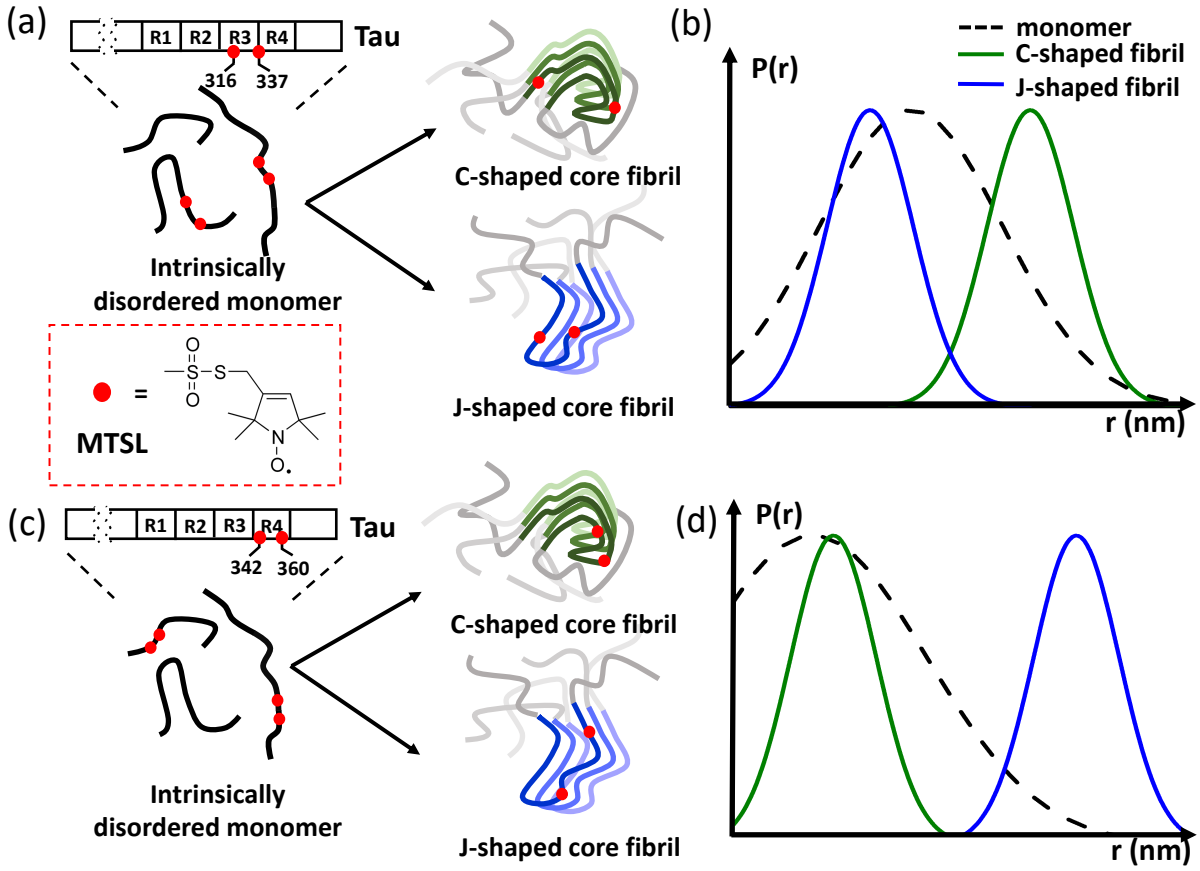

Figure 1.4: Schematic of applying pulsed DEER spectroscopy for tracking the structural evolution of doubly spin-labeled tau from a modeled ensemble of intrinsically disordered state (black) to a fibril state adopting distinct structures. Red dots represent nitroxide spin-labels MTSL that are introduced pairwise to tau. (a). Tau is spin-labeled at residues 316 and 337 with MTSL in monomer, and the monomer aggregates into either J-shaped core or C-shaped core fibrils. (b). Modeled P(r) spanning 316-337 of disordered monomers (black dash line) and structured fibrils of tau (blue: J-shaped core fibrils, and green: C-shaped core fibrils). The distribution will be narrower as tau changes from the intrinsically disordered state to an ordered fibril state. (c). Tau is labeled at residues 342 and 360. (d). Modeled P(r) spanning 342-360 of disordered monomers and fibrils in different structures.

better-defined fibrils compared to heparin-induced fibrils.

The above mentioned studies used truncated recombinant tau, but they demonstrate the potential of DEER method to assess structures of tau fibrils and derive information on seeding or aggregation mechanisms. Recently, modulation depth-based DEER anal-

ysis was used to obtain conformational information during the binding process of the molecular chaperone Hsp90 to full-length tau.[130] The authors observed that Hsp90-tau interaction results in the exposure of the MTBR regions of tau, followed by tau oligomerization, shedding light on the mechanism of the Tau/Hsp90 interaction on a molecular level. This study also shows that DEER methodology is versatile and transferable to full-length tau.

The absolute distance represented in P(r) can be furthermore compared with known atomic structures. Such evaluation was used to show that heparin fibrils[26] are distinct from the AD fibril fold as established by cryo-EM[5]. Tau187 was labeled at selected positions, and the measured distance distributions between multiple pairs of spin-labels were compared against the expected distance distributions from the AD fold by simulating the spin-labels onto the PDB structure at the same sites using the RotamerConvolveMD method.[131] The distance distribution of the heparin fibrils indicated that the conformational ensemble is not only different from but also more heterogeneous than, that of AD fibrils. Subsequent cryo-EM studies of heparin-induced 2N4R tau fibrils confirmed the presence of heterogeneous structures with a dominant conformation.[52] Interestingly, studies using solid-state NMR found that heparin-induced 0N4R[132] and 0N3R[133] fibrils are homogeneous, but distinct from the disease folds.

The DEER approach can determine whether the tau fibrils, once fully formed, adopt disease phenotypic structures, and/or whether homogeneous fibrils are formed. Figure 1.5a-h illustrates a set of pairs of sites strategically selected for spin-labeling to distinguish different folds, including disease folds and heparin folds established by cryo-EM [5, 6, 7, 10, 8, 11, 12, 9]. The addition of spinn-labels might affect the fibril formation and it is important to properly select the labeling sites and verify their effect on aggregation. This matter is discussed in the later section “Challenges of DEER-based Distance Distribution Measurements and Analysis”.

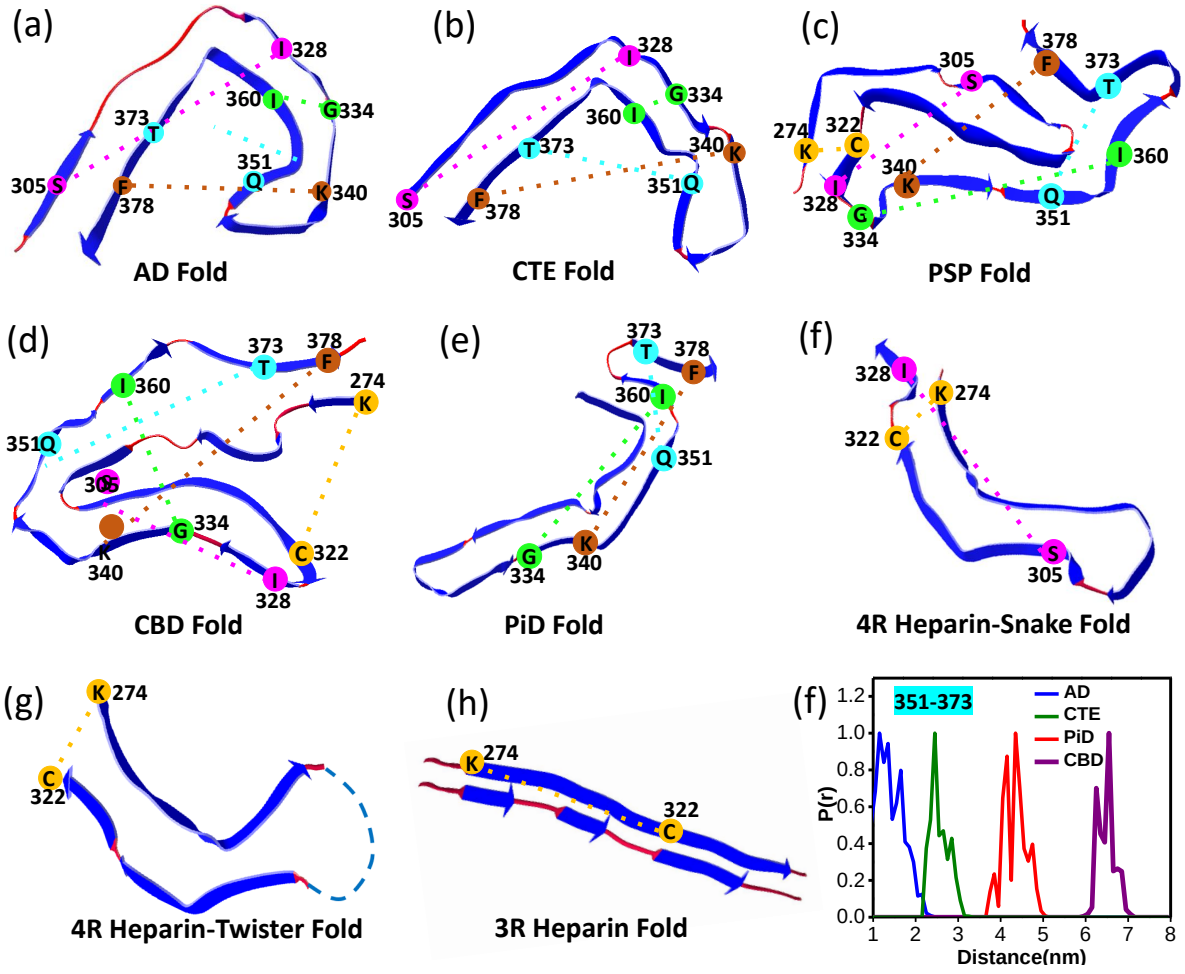

Figure 1.5: (a-e). Hypothetical spin-label pairs for P(r) measurements highlighted on the published atomic structures of different tau folds found by cryo-EM[5, 6, 7, 10, 8, 11, 12, 9]. Pairwise labeling sites are color-coded in the same color. Pairs of distances including 351-373, 340-378, 274-332, 334-360, and 305-328 can be used to distinguish different folds and can be used as "fingerprints" to identify whether a certain fold is formed, only partially or not. (i). Simulated P(r) of pair 351-373 from different folds using the RotamerConvolveMD program[131].

The distances between the alpha carbon of the residues in these pairs derived from the published PDBs can be used to estimate the mean distances measurable by DEER. For example, as measured in the PDB files, the distances between sites 274 and 322 in the snake fold of heparin-induced 2N4R tau fibrils[52] is 1.4 nm, while this distance in the CBD fold[8] is 3.9 nm. Hence, the P(r) of the pair 274-322 can differentiate

between the CBD fold and heparin folds. Moreover, the P(r) of pairs spanning 351-373 and 334-360 can distinguish different disease folds, including AD, PiD, CBD, and CTE. To be more accurate on the expected distance, we can simulate the expected distance distribution by modeling the spin-labels onto the corresponding PDB structures by the RotamerConvolveMD method,[26, 131] as shown in Figure 1.5i for spin-label pairs 351-373. This simulation demonstrates that DEER-derived P(r) of even a single strategic spin-label pair can be used as fingerprints to distinguish between the AD, CTE, PiD, or CBD folds. As for seeding, the comparison of the measured P(r) of seeded fibrils with the computed P(r) fingerprints can reveal whether the expected shapes emerge and become dominant. Once homogeneous and converged fibrils are formed, their final structure needs to be determined by techniques such as cryo-EM, crystallography, and/or solid-state NMR spectroscopy. However, even after converged fibril structures are solved, it is important to gain an understanding of the mechanism by which disease-phenotypic tau fibrils are formed and/or factors to enhance structural convergence to fibrils found in tauopathies. Such goals have not been achieved to date.

1.6.3 Tracking evolving structures along the course of aggregation

DEER-based distance measurements can be used to capture evolving conformations along the course of aggregation along different pathways by flash freezing at different time points. Following this procedure, Eschmann et al. discovered that the R2 and R3 regions of tau, specifically the hydrophobic hexapeptide segments of tau known as PHF6* (275VQIINK280) and PHF6 (306VQIVYK311), extend within the lag phase upon the addition of aggregation inducer heparin.[134] Both hexapeptides are known to promote the β-strand formation, while the PHF6 segment is included in the core of every known type

of tau fibril structure published to date[5, 6, 7, 10, 8, 11, 12, 9]. By directly measuring the distance across sites encompassing the PHF6 and PHF6* regions using DEER, the authors observed that these two segments are relatively protected in the soluble monomeric state. The addition of heparin extends the conformations of these segments well before they stack into β-sheets, indicating the formation of partially structured intermediates with an extended conformation. Therefore, when homogeneous and converged fibrils are formed through different aggregation pathways (such as the hypothetical model shown in Figure 1.6), one could use DEER-based distance measurements to track evolving structure of tau along these pathways and study how different folds are formed. Further therapeutic development efforts can be focused on the fold formation regions to disrupt the process.

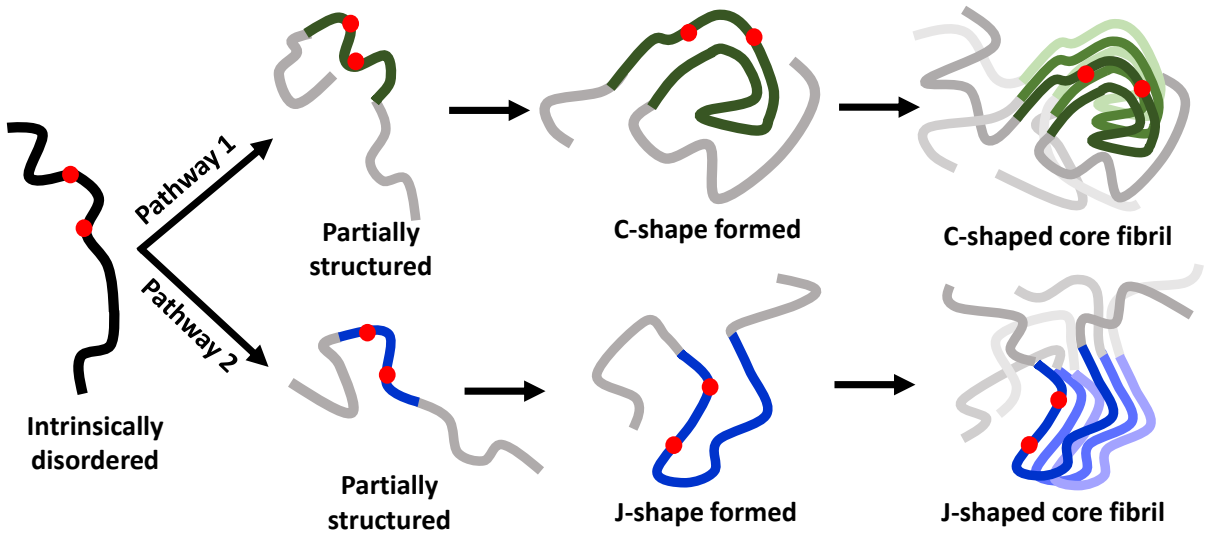

Figure 1.6: Schematic of the hypothetical model for the formation of AD C-shaped fibril (pathway 1) and PiD J-shaped fibril (pathway 2). The red dots represent the nitroxide spin-labels MTSL that are used to track evolving structures.

1.7 Challenges of DEER-based Distance Distribution Measurements and Analysis

DEER-based distance distribution measurements rely on spin-labels that are tethered to the protein. This prevents characterizing tissue-extracted protein and requires a labeling procedure most often practiced on recombinant proteins. Since the addition of spin labels may affect fibril formation, one should try to label the region that forms the outer layer of disease folds based on which disease fold is under investigation, and multiple pairs should be used to confirm the result. In addition, one needs to be concerned about the effect of the labels on the observed aggregation pathways and structures, albeit the spin-labels used for DEER are relatively small (264 Da for MTSL) compared to other tags such as fluorophores. The aggregation kinetics and low-resolution morphology of the mature aggregates are compared with and without labels to test the impact of the spin-labels. If some labeling sites appear disruptive, a series of nearby sites can be used for labeling to validate the distance results. Once converged structures are found by DEER with multiple spin-label pairs, other techniques such as cryo-EM should be used to confirm the formation of disease fold.

Another obstacle of DEER-based distance distribution measurements is imposed by the background signal arising from intermolecular spin interactions and the effect of spin-labels of neighboring proteins.[135] To weaken the effects of the intermolecular spin interaction, 5-10% of the doubly spin-labeled protein is used to produce the protein assembly. In principle, the contribution from intermolecular interactions can be accounted for by background correction, but current methods of doing so are not always robust.[119] In particular, protein aggregates exhibit, by definition, a high local concentration of proteins that are not randomly distributed (i.e. partially ordered aggregates). In the case of amyloid fibrils, proteins stack along one direction, which tends to align spins along

one dimension, i.e. the fiber axis. These situations make accurate correction of intermolecular interactions challenging. Further study of background signals will be critical for accurate determination of intramolecular distances within aggregates.

As for DEER data analysis, the distance distribution reconstruction can be challenging because ambiguity can arise in determining the shape, width, and the number of peaks of P(r), especially when the conformer population is heterogeneous and/or the types of structures present are unknown. The P(r) reconstruction from time-domain DEER data is an ill-posed problem and typically requires the use of a smoothing parameter when using model-free least-square minimization approaches relying on Tikhonov regularization.[136] In some cases, especially when the signal-to-noise ratio is poor, this leads to ambiguity in the extracted distance distribution. Alternative approaches, such as Srivastava-Freed Single Value Decomposition (SF-SVD)[118, 137], in combination with WavePDS based denoising algorithms[120], have been developed to provide a reliable and automated reconstruction of P(r) for capturing multiple and partially ordered structures. When the exact knowledge of the number of conformers present in the sample is inaccessible, one can use a model-based fitting strategy with standard functions such as Gaussians.[138, 139] Model-based fitting is robust and can provide an average of the distance as well as how far these average distances deviate from the expected distances. This approach was sufficient to show that heparin-induced fibrils are heterogeneous and distinct from AD's fibrils,[26] but it could not identify how many and what types of conformers were present.

1.8 Final Remark

Based on the high-resolution structures of tau fibrils from post mortem tauopathies patients solved by cryo-EM, [5, 6, 7, 10, 8, 11, 12, 9] we know that the defining differ-

ences between tauopathy phenotypes may lie at the atomic structural detail of the fibril structure. It is impossible to recreate the exact biological conditions needed to generate the disease-relevant end structures of tau fibrils, not only because of the complexity of the biological milieu but also because the timescale of tau fibril formation occuring over decades during aging. Yet, very recently, astudy using high-throughput cryo-EM showed that the AD and CTE folds can be reproduced *in vitro* using a particular fragment of tau and very specific aggregation conditions [140]. However, the propagation of disease folds still relies on the structural propagation in seeding, which has not yet been verified at high-resolution. Although *in vivo* and *in vitro* data provide strong circumstantial evidence that seeding can propagate given tau fibril structures [141, 36, 27, 16, 17, 19, 20, 21, 22, 24, 49, 50, 23, 51, 142, 143, 144, 145, 146, 147, 103, 148, 149, 150, 151, 152, 153, 154, 100, 155, 108, 148, 44, 42, 156, 157, 158, 103, 159, 160, 161, 162, 163, 164, 17, 165], molecular-level structural characterization is needed to show what motifs are propagating in seeding and what environmental factions are required for faithful structural replications. Compared to NMR or cryoEM, performing DEER to obtain a full distance distribution P(r) is a fast approach to obtain valuable structural information in evolving and heterogeneous samples. Such DEER-derived P(r) data can serve as a critical intermediary tool to characterize partial features of the tau conformational ensembles, irrespective of structural heterogeneity in the sample, and to investigate the structural propagation of tau during seeded aggregation and to inform future study with cryo-EM or NMR. DEER offers an approach to explore key factors that lead to structural convergence to disease-phenotypic fibril structures in seeding, including the physico-chemical conditions (e.g. effects of liquid condensate, crowding, lipid membranes), the chemical property of the tau protein (PTMs, mutations, fragmentation, etc.), the nature and origin of tau seeds, and external cofactors. Once disease-phenotypic fibril structures are converged to *in vitro* by DEER-derived P(r) data, cryo-EM and NMR will be needed to confirm the

findings.

1.9 Permissions and Attributions

1. A part of the material presented in chapter 1 is submitted to The Journal of Physical Chemistry B, and is currently under review.

Chapter 2

Disulfide Bonds Hinders Tau Aggregation

2.1 Introduction

Tau is an intrinsically disordered protein (IDP) found in neurons of the central nervous system, and its physiological function is mainly to bind with and stabilize microtubules[166]. Tau is also found to form insoluble aggregates in the brain, known as neurofibrillary tangles (NFTs)[167, 168]. The formation and accumulation of NFTs is the pathological hallmark of various neurodegenerative diseases called tauopathies, including Alzheimer's disease (AD)[169]. NFTs are high molecular weight amyloid fibrils with β-sheet structure[113]. It has been shown that NFTs formation is related to the disintegration of microtubules and the interruption of organelle transport along the neuron, resulting in neuronal loss[170, 171, 172]. Therefore, it is of great interest to study tau aggregation, especially the underlying mechanism and structure change on the molecular level, in the hope of finding methods to inhibit or prevent this process.

To study tau aggregation *in vitro*, polyanionic inducers like heparin, RNA, or proteoglycans are used to trigger tau aggregation[173, 174, 175, 176]. The fibrils formed have similar macroscopic morphology to those from AD patients' brain[177, 178, 174]. A recent study revealed that upon the addition of heparin, tau forms partially structured aggregation intermediates first, and rearrange them into β-sheet structured aggregates[179]. However, the driving forces for this process are still elusive. It's been suggested that noncovalent intermolecular interactions, such as hydrogen bonds between pairs of adjacent β-sheet fibril strands, can drive tau aggregation[180]. Electrostatic interactions between the negatively charged heparin and the positively charged lysine residues of tau[181], and hydrophobic interactions between tau molecules as well as between tau and heparin[182] were also suggested to lead to tau aggregation. Furthermore, covalent bonds like disulfide bonds formed between two thiol groups from cysteine residues were also proposed to play a role in tau aggregation[28, 29, 30]. It has been reported that intramolecular disulfide

bonds would impede tau aggregation[31, 28], but the view of intermolecular disulfide bonding's role in tau aggregation has not yet reached consensus. Some studies showed that intermolecular disulfide bonds facilitate tau aggregation[31, 32, 33], while another suggest otherwise[34]. Interestingly, recent evidence suggests that disulfide cross-linked tau dimers induce tau aggregation and transmission in HEK293 biosensor cells and primary neuron culture[35], indicating the importance of tau disulfide bond formation in tau pathogenesis. The precise mechanisms underlying these observations remain unclear[183]. Besides, reducing agents are often used in various *in vitro* studies to avoid disulfide bond formation; NFTs are found to seed in vitro aggregation of recombinant tau in the presence of DTT[17, 36]. In this study, we focused on investigating the precise role of disulfide bonding in tau aggregation. Is it a driving or hindering force of tau aggregation?

To systematically study the role of intermolecular and intramolecular disulfide bonds in tau aggregation, we measured the aggregation of two-, one- or zero-cysteine-containing tau by thioflavin T (ThT) fluorescence, which probe for the presence of cross-β structures. Size exclusion chromatography (SEC) was used to isolate tau monomers and disulfide-linked dimers. Blue native polyacrylamide gel electrophoresis (BN-PAGE) was performed to confirm species formed by disulfide bonds. In the present study, we found that incubation in reducing conditions or mutating the cysteines into another uncharged residue leads to enhanced aggregation. Both intermolecular and intramolecular disulfide bonds hinder tau aggregation, and disulfide bonding is not a driving force for tau aggregation.

2.2 Results

2.2.1 Disulfide bonding has a strong influence on tau aggregation kinetics

Disulfide bond formation is spontaneous under non-reducing conditions. The longest tau isoform has two naturally occurring cysteine residues at positions 291 and 322 (C291 and C322. Hence, it can form both intermolecular and intramolecular disulfide bonds. Here, a truncated variant of the longest isoform, Tau187, is used. It spans from residue 255 to 441 (Fig. 2.1a), including both C291 and C322. This construct contains all four microtubule-binding repeat domains and the C-terminal region, including the region that forms the tau fibril core. Previous studies showed two hydrophobic hexapeptide stretches, 275VQIINK280 (PHF6*) in the R2 domain and 306VQIVYK311 (PHF6) in R3 domain, form the core of the tau fibrils with β-sheet structure[4, 184, 185]. Several studies carried out on heparin-induced fibers have shown that mostly the four repeat domains are packed into a cross-β structure, forming the fiber core, and the rest remains disordered, forming the so-called fuzzy coat[186]. A recent study discovered with cryo-EM that heparin-induced full-length tau fibrils are heterogeneous, with a dominant structure spanning residues 272 to 330[52]. With the fibril core-forming regions included and the fuzzy coat N-terminal truncated, tau187 aggregation rate is enhanced and the fibril morphology is similar to full-length tau[179].

The overall effect of disulfide bonds on tau aggregation was studied by ThT fluorescence assay, which probes the formation of amyloid β-sheets, under non-reducing and reducing conditions (Fig. 2.1b). ThT fluorescence assay allows us to compare the rate of tau aggregation by comparing the slope of the increment, and the relative aggregation extends by comparing the plateau of the curve. Three mutants of Tau187 were studied:

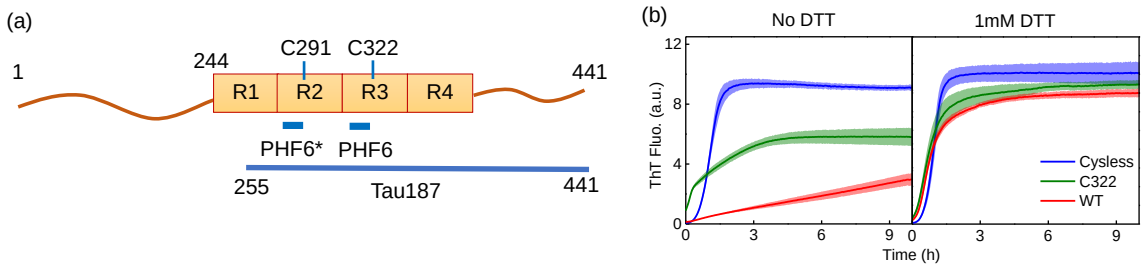

Figure 2.1: (a) Schematic of full-length tau sequence including Tau187. Tau187 consists of four microtubule-binding domains (R1-R4) and C-terminal, including the PHF6* and PHF6 regions. The two cysteines at the position of 291 and 322 are in the R2 and R3 regions respectively. (b) ThT fluorescence of heparin-induced aggregation of Tau187 (50 μM) under non-reducing conditions (with no DTT) and reducing conditions (with 1 mM DTT). Heparin was added at t=0h to initiate aggregation.

wild-type tau (referred to as WT), containing two native cysteines at locations 291 and 322; C291S mutant containing one cysteine at position 322 (C291 was mutated into serine, and the sample is referred to as C322 below); and C291S/C322S mutant, containing no cysteine (referred to as Cysless). Heparin was added to all the samples to initiate aggregation.

As shown in Fig. 2.1b left panel, upon addition of heparin, all three tau mutants aggregated under non-reducing conditions. Cysless had the highest aggregation rate, reaching the plateau the fastest within about 3 hours. It also had the greatest relative aggregation extend. C322 showed a lower aggregation rate compared with Cysless, reaching the plateau in about 5 hours, with a lower aggregation extend. As for WT, it had the lowest aggregation rate and likely the smallest aggregation extent.

Under reducing conditions where an excessive amount of dithiothreitol (1mM DTT) was used, the aggregation propensity of C322 and WT changed dramatically while Cysless remained similar (Fig. 2.1b right panel). When DTT was used to break disulfide bonds and keep the cysteines reduced, the aggregation extended and the rate of both C322 and WT increased, reaching the plateau within 3 hours like Cysless. The kinetics

of their aggregation became comparable to Cysless. The aggregation behavior of these samples under reducing conditions was slightly different due to the influence of mutations on aggregation, which was independent of disulfide bonding and markedly minor. Despite these differences, we still could assign a drastic change of tau aggregation behavior to the prevention of disulfide bond formation. Both WT and C322 have an increased rate of aggregation under reducing conditions, suggesting that disulfide bonds impede aggregation.

2.2.2 Intermolecular disulfide bonds hinder tau aggregation

To clarify the role of intermolecular disulfide bonds in tau aggregation, C322 Tau187 was used to perform heparin-induced assembly in the presence or absence of DTT (Fig. 2.1b). C322 mutant possesses a single cysteine residue and therefore can only form intermolecular disulfide bonds but no intramolecular disulfide bonds. As in Fig. 2.1b, upon the addition of heparin, C322 under reducing conditions reached a plateau faster, indicating a higher aggregation rate than that under non-reducing conditions. Moreover, the relative positions of plateaus showed a higher aggregation extend under reducing conditions. Therefore, breaking intermolecular disulfide bonds would increase the aggregation rate and extent. Furthermore, the addition of DTT did not change the fibril morphology (SI Figures, Fig. S2.1).

To confirm the formation of intermolecular disulfide bonds in C322, we conducted SEC and BN-PAGE to verify the presence of dimers formed via intermolecular disulfide bonds. C322 were run on the HiLoad XK 16/600 prepacked with Superdex 200 equilibrated with degassed running buffer (20 mM ammonium acetate, 100 mM sodium chloride, 0mM DTT). As shown in Fig. 2.2a, two distinct elution peaks were present. Based on the characteristics of the column used (see Materials and Methods) and the molecular

weight of Tau187 (22 kDa), we assigned the first elusion peak to the intermolecular disulfide-linked dimer and the second elution peak to the monomer. To further confirm these species, each peak was collected separately (two samples are referred to as C322-Dimer and C322-Monomer) and concentrated immediately after elution and run on BN-PAGE. Note that tau is intrinsically disordered and migrates slower on native-PAGE than structured proteins and standard protein markers with the same molecular weight. Tau187 dimers show up around 146kDa standard protein marker, while monomer is around the 66kDa marker. As in Fig. 2.2a, the sample of C322 before SEC showed both bands of monomer and dimer. However, in C322-Dimer obtain from SEC, dimer was the main species. In C322-Monomer, a strong band for monomer was observed. Besides, a light dimer band was also observed because no reducing agent was used in BN-PAGE, and disulfide-linked dimer could form spontaneously even though we ran the BN-PAGE immediately after the SEC to minimize the formation of the dimer. The overall intensity of the dimer band was higher, which was consistent with the result from SEC where the dimer peak has a bigger area than the monomer peak. These results suggested that C322 was a mixture of monomers and dimers, and the number of dimers was greater than monomers. Taken together, these data confirm the formation of intermolecular disulfide bonds.

To further verify that the intermolecular disulfide bonds hinder tau aggregation, we ran the ThT fluorescence assay on the C322 monomer and disulfide-linked dimer separately (Fig. 2.2c). C322 dimer showed a lower aggregation rate by reaching the plateau later, indicating that intermolecular disulfide bonding decreases aggregation kinetics. Moreover, the relative positions of the plateaus were consistent with the fact that the intermolecular-disulfide-linked dimer had the lower aggregation extend with the least amount of fibril formed, while the C322 monomer had a higher aggregation extend. Therefore, intermolecular disulfide bonds impede tau aggregation.

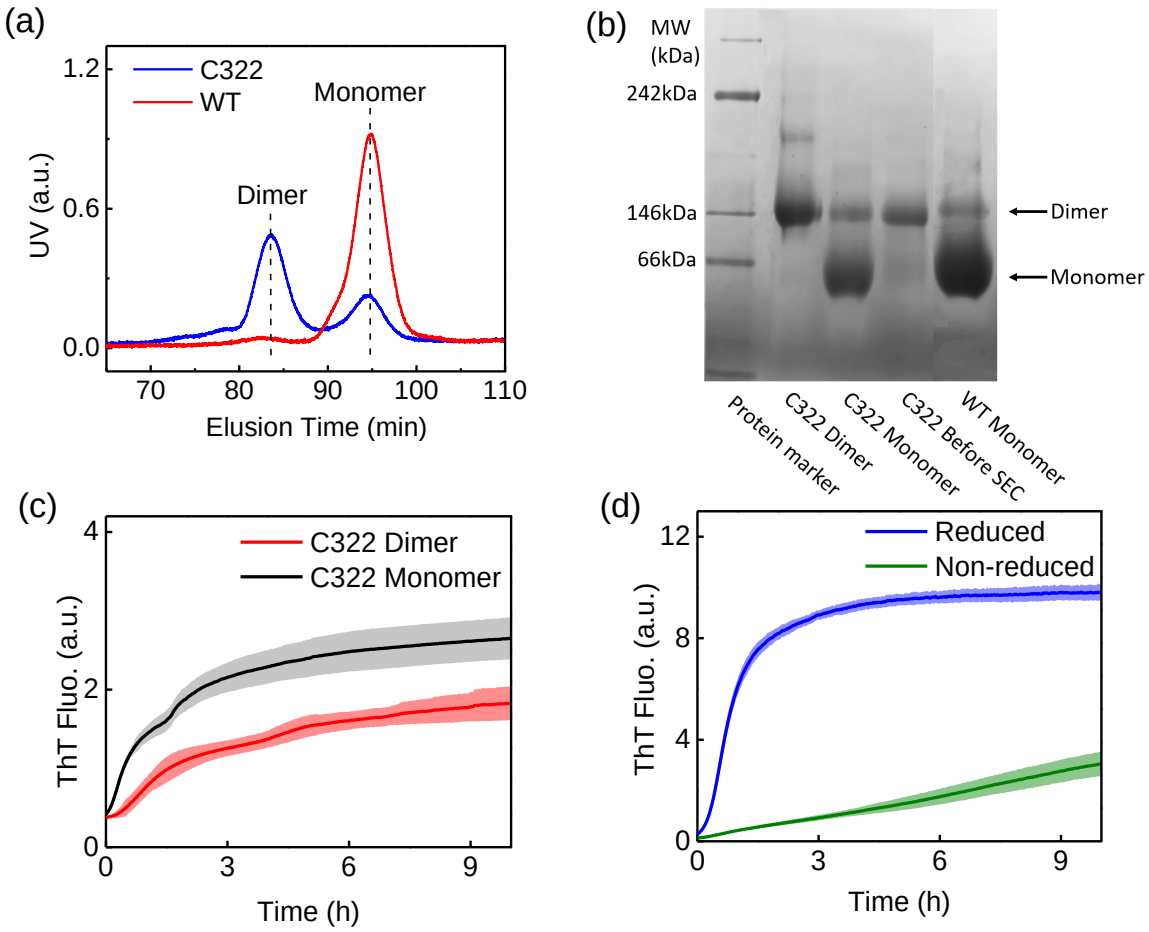

Figure 2.2: (a) Elusion peaks of C322 and WT from size exclusion chromatography using HiLoad XK 16/600 prepacked with Superdex 200. C322 has both disulfide-linked dimers and free monomers, while WT mainly consists of monomers. (b) Blue Native–PAGE of C322-Dimer and C322-Monomer from SEC, the C322 sample before SEC, and WT monomer sample separated from SEC. All samples were run under non-reducing conditions. It is important to note that, since tau is intrinsically disordered, the electrophoretic mobility of tau on native-PAGE will be different from structured proteins and standard protein markers with the same molecular weight. Our results show that tau187 monomer will show up at a molecular weight of 66 kDa of protein marker, and dimer will show up at 146 kDa of protein marker. (c) Heparin-induced aggregation of C322-Monomer and C322-Dimer from SEC, monitored by ThT fluorescence. (d) Heparin-induced aggregation of reduced WT monomer separated from SEC (with 1mM DTT) and non-reduced WT monomer, monitored by ThT fluorescence.

2.2.3 Intramolecular disulfide bonds impede tau aggregation

To probe the role of intramolecular disulfide bonds, we examined WT Tau187 which possesses two cysteine residues and could therefore form both intramolecular and intermolecular disulfide bonds. SEC and BN-PAGE (Fig. 2.2a and b) showed that monomer was the dominant species in WT Tau187 and a neglectable amount of intermolecular-disulfide-linked dimer was observed. Assume that the monomer fractions separated with SEC had mostly intramolecular disulfide bonds, they were collected and concentrated. This sample is referred to as WT-Monomer. The aggregation propensity of WT-Monomer under non-reducing and reducing conditions was investigated with ThT fluorescence. As shown in Fig. 2.2d, reduced WT-Monomer showed an accelerated aggregation rate and greater aggregation extend compared with the non-reduced WT-Monomer, indicating that breaking intramolecular disulfide bonds promotes tau aggregation. In other words, intramolecular disulfide bonds impede tau aggregation.

2.3 Discussion

Our results showed that both intermolecular and intramolecular disulfide bonds would impede tau aggregation. Breaking disulfide bonds using a reducing agent could promote tau aggregation. Therefore, the disulfide bond cannot be a driving force of tau aggregation. Using WT Tau187 with two cysteines, we showed that intramolecular disulfide bonds hinder tau aggregation. This is likely due to the formation of monomers with a compact conformation by intramolecular disulfide bonds[28]. When the compact conformation is formed, fibril formation core regions are buried in the monomer, making it harder for tau to interact and form fibrils. Besides, recent studies using cryo-electron microscopy on the structure of tau fibril from tauopathies patients showed that the two naturally occurring cysteine residues at positions 291 and 322 are not next to each

other[5, 6, 7, 10, 8, 11, 12, 9], indicating the lack of intramolecular disulfide bond in human tau fibrils.

As for the role of intermolecular disulfide bonds, we separated C322 monomers from disulfide-linked dimers using SEC. The heparin-induced aggregation of disulfide-linked dimers showed a lower aggregation rate and extend compared with monomers, indicating that the intermolecular disulfide bonds impede tau aggregation. It is possibly because the disulfide-linked dimers are less aggregation-prone than free monomers. According to a previous study, heparin extends the PHF6* (275VQIINK280) and PHF6 (306VQIVYK311) regions of tau well before β-sheet is formed and the extended conformation is aggregation-prone. We hypothesize that in the dimer linked by the cysteines at residue 322, PH6* and PHF6 regions may be more enclosed so it's harder for heparin to extend its PHF6* and PHF6 regions, leading to a lower aggregation active.

Our finding is consistent with a recent study on the truncated tau fragment dGAE composed of residues 297–391 from full-length tau[34]. The aggregation of dGAE was enhanced under reducing conditions and its zero-cysteine variant aggregated rapidly, forming long fibrils. The authors concluded that disulfide bonds inhibit tau aggregation due to the formation of assembly-incompetent dimers via disulfide bonding. Moreover, in the structure of AD tau fibril, cysteines are buried in two neighboring sheets and no sign of an inter-sheet disulfide bond is shown. This finding also suggests that the intermolecular disulfide bond does not assist tau aggregation.

However, our result is in contrast with other previous studies, where intermolecular disulfide bonding was found to promote tau aggregation[35, 33, 187, 31]. The exact reason behind these different findings is still unclear and further test is needed. In summary, our in vitro study demonstrated that disulfide bonding is not a driving force of tau aggregation. Both intermolecular and intramolecular disulfide bonds hinder tau aggregation due to the formation of less aggregation-prone species. Conditions that are

unfavorable to disulfide bond formation would promote aggregation.

2.4 SI Figures

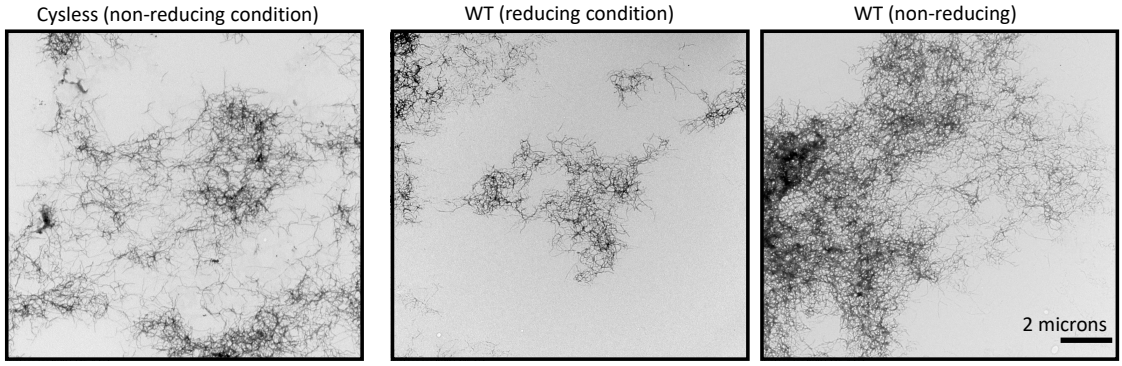

Figure S2.1. Transmission electron microscopy (TEM) images of cysless, WT under different conditions. WT fibril morphology is not changed when reducing agent DTT is added.

Chapter 3

Cofactors Are Essential Constituents of Stable and Seeding-active Tau Fibrils

3.1 Introduction

Amyloid aggregates are structured aggregates that are characterized by a high cross-β-sheet content. They rely on an extended intermolecular hydrogen-bond network that provides high stability, and allow even hydrophilic and charged domains to be dehydrated and tightly packed in a protein assembly [188]. Amyloid aggregates have been conjectured to be the most stable form of protein assembly [189]. The molecular forces from which this extreme stability originates were revealed mostly based on model peptides forming perfect cross-β-structures [190]. However, many amyloid aggregates are only partially composed of amyloid cross-β-sheets, and likely do not possess the high stability of model peptides.

The tau protein is an intrinsically disordered protein that is mostly present in neurons and can form amyloid fibrils in several neurodegenerative diseases including Alzheimer's disease (AD), frontotemporal dementia, and Pick's disease [191]. Tau is highly charged and hydrophilic, making it highly soluble and stable in aqueous environments across a wide range of pH and temperature. However, under pathological conditions, it can assemble into amyloid fibrils in which parts of its microtubule-binding domain, predominantly positively charged, densely pack into a cross-β-sheet arrangement [5]. However, the triggering factors and driving forces of fibrillation of the highly soluble tau protein remain unknown, and consequently neither the mechanism that achieves convergence to a unique fibril structure nor the main fibril feature that contributes to its stability is understood.

Aggregation mechanisms are most often studied with recombinant tau proteins or fragments. In vitro fibrillation of tau is typically triggered with the help of cofactors, most commonly heparin [192], but also other cofactors such as RNA [193] or arachidonic acid [194]. In the last few years, seeding tau aggregation has been shown to be possi-

ble by adding premade fibrils (seeds) to fresh monomers, but the seeding process is still improved by the presence of cofactors (RNA or heparin) in solution [195, 196]. It has been shown that heparin is a limiting factor in fibril formation [197, 198], but the exact nature of association of heparin with the mature fibrils remains unclear, with conflicting reports on whether heparin is part of [199] or not part of mature fibrils [169, 198]. As a result, the roles of heparin in tuning fibril formation, structure, and stability are unknown. For instance, heparin-induced fibrils were shown to be more stable than AD fibrils using chemical denaturation [156, 200], this stability was not addressed. In this study, we assess whether cofactors are crucial constituents of mature fibrils and contribute to their stability, or whether they only catalyze aggregation toward a self-sustained protein assembly.

Tau aggregates have been shown to propagate from neuron to neuron, and to be able to seed aggregation [200, 27], that is, convert naïve tau monomers into aggregates. This led to the hypothesis that, in vivo, monomeric tau can spontaneously polymerize into amyloid filaments when an appropriate seed template is provided. For that reason, pathological origins of tau aggregation have mostly been searched in the properties of tau itself, such as hyperphosphorylation, cleavage, high local concentrations, and alternative splicing, but marginally in abnormal interactions with other cofactors. Paradoxically, cofactors are always used for in vitro aggregation of tau, and even assumed to be biologically relevant. Therefore, gaining an understanding about the influence of cofactors on mature fibril properties will (i) provide key insight into the role of cofactors in fibril stability and conformation in vitro, and (ii) guide the search for cofactors that assist in seeding and spreading of tau aggregation in vivo. In this study, we used a set of biochemical tools together with electron paramagnetic resonance (EPR) to characterize the consequences of cofactor removal after fibril formation.

3.2 Results

3.2.1 Fibrils assemble when cofactors are present

We used a truncated version of the longest human tau isoform, 2N4R, that contains four repeat domains (R1 to R4), as well as the entire C-terminal region (residues 255 to 441, named here tau187), from which one of the two cysteines was mutated (C291S) to perform site-directed spin-labeling for EPR [179, 201]. The construct, with the addition of the aggregation-promoting disease mutation P301L [202], is referred to as tau throughout the manuscript (SI Figures, Fig. S3.1A). Polydisperse heparin (average molecular mass 15 kDa) and polyU (RNA, average molecular mass 900 kDa) were incubated with tau to induce fibrillation. The addition of heparin or RNA to tau resulted in amyloid fibril formation, as verified by significant increase of thioflavin T (ThT) fluorescence intensity (SI Figures, Fig. S3.2) and the presence of fibrillar structures captured by transmission electron microscopy (TEM; SI Figures, Fig. S3.1 B and C). We refer to the heparin-induced and RNA-induced tau amyloid fibrils as heparin fibrils and RNA fibrils, respectively.

3.2.2 Fibrils depolymerize when cofactors are digested

We tested whether these cofactors act as catalysts that assist fibril formation and subsequently dissociate from the product, or whether they are reactants that are part of the fibril scaffold and are necessary to ensure the stability of mature fibrils. To address this question, we investigated the amyloid fibril quantity by preparing heparin fibrils and RNA fibrils, and then degrading the cofactors via enzymatic digestion.

Heparin and RNA are cofactors that can be digested using heparinase and RNase, respectively (see Methods and Materials). In their digested form, both cofactors become

incapable of triggering fibril formation (SI Figures, Fig. S4). ThT fluorescence, which provides an in situ measure of cross-β sheet structures, was used to quantify the amyloid fibrils present in the sample. Heparinase and RNase were added to heparin fibrils and RNA fibrils after maximal ThT fluorescence was reached, and were incubated for 7 hours, resulted in a 20-30% and 60-70% decrease of ThT fluorescence, respectively (Fig. Fig. 3.1A). This reduction of ThT fluorescence was 2-3 times more significant than the effect of protein dilution (by enzyme addition). The control samples where buffer without enzymes was added showed a signal decrease of about 10% and 30%, respectively (Fig. Fig. 3.1A). These results show a significant loss of cross-β sheet when cofactors were digested.

The digestion of tau amyloid fibrils was further characterized by TEM (SI Figures, Fig. S3.3). Both heparin and RNA fibril images showed no discernable population of oligomeric or protofibrillar aggregates neither before nor after digestion (SI Figures, Fig. S3.3 A–D). A statistical analysis of the width of heparin fibrils was carried out before and after heparinase treatment. The distribution of fibril width (SI Figures, Fig. S3.3, E and F) did not distinguish different fibril populations neither before nor after digestion, and the average measured width was found to be similar before (15.3 ± 3.9 nm) and after (14.9 ± 2.8 nm) digestion. Thus, within the resolution provided by TEM, no preferential fibril population subject to digestion could be identified.

The digestion of tau amyloid fibrils was independently investigated by continuous-wave EPR (cw-EPR). cw-EPR of paramagnetic spins tethered to tau has been previously used to assess the packing and mobility of tau fibrils (18). The cw-EPR spectra of spin-labeled amyloid fibrils can be decomposed into three components: a mobile component corresponding to soluble low molecular mass species, an immobile component corresponding to high molecular mass species (oligomers, aggregates, etc.), and a spin-exchange component resulting from spin-labels that are within 5-Å proximity due to

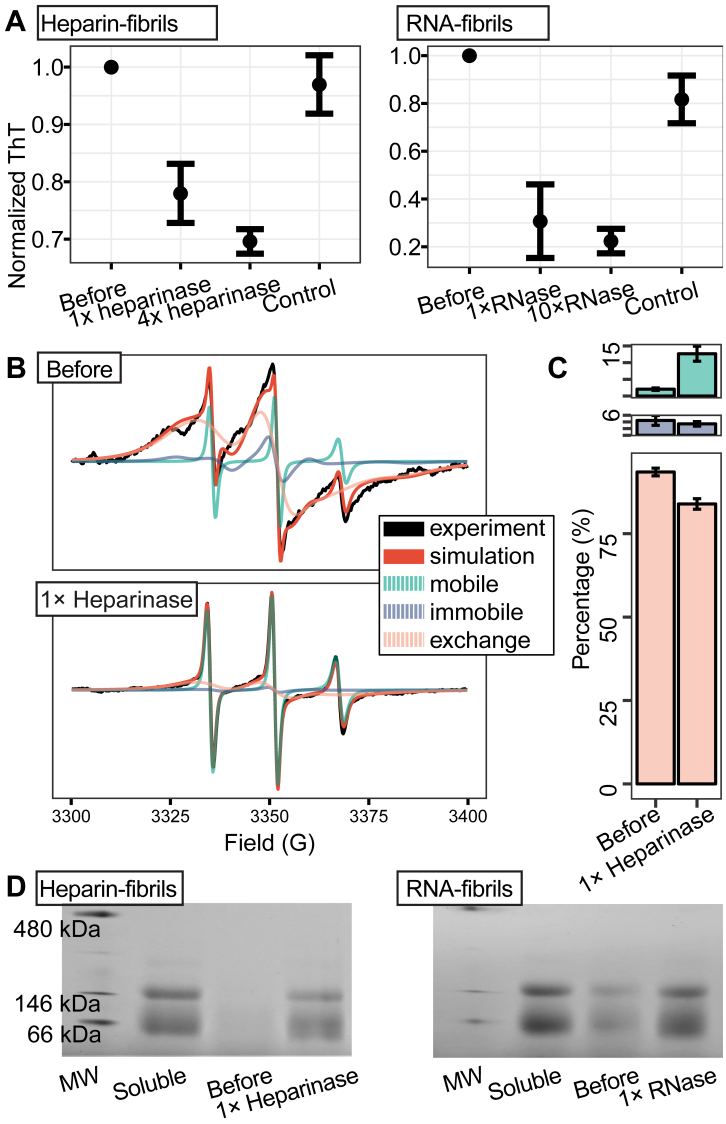

Figure 3.1: Fibrils depolymerize upon cofactor digestion. (A) ThT fluorescence of heparin-induced tau fibrils and RNA-induced tau fibrils before and after incubation with different concentrations of heparinase/RNase. ThT fluorescence value measured before enzyme addition was used as the normalization value. (B) cw-EPR spectra (black) of tau heparin fibrils spin-labeled at site 322, before and after incubation with heparinase. The simulation spectra (red) are composed of mobile (green), immobile (purple), and spin-exchange components (orange). (C) Population of each component extracted from cw-EPR spectrum analysis. (D) BNPAGE of heparin and RNA fibrils before and after incubation. Freshly prepared tau monomers were loaded as reference (soluble). In all panels, 1× heparinase: 1 U enzyme per 1 μg heparin; 1× RNase: 1.5 μg/mL. Error bars show SD (n $\geq$e 3).

parallel, in-register, amyloid cross-β-stacking of tau (18). Here we spin-labeled the native cysteine 322, prepared tau fibrils with heparin, and acquired cw-EPR spectra before and after heparinase treatment. The spectra were fitted using an established simulation protocol (18) into populations of mobile, immobile, and spin-exchange components (Fig. 3.1B). Fitting results implied that 93 ± 1% of the spin-labeled tau in heparin fibrils is in in-register amyloid cross-β-stacking, which decreases to 84 ± 2% after digestion. This loss was mostly compensated by increase of low molecular mass species (2 ± 0.3% before and 13 ± 2% after digestion), while the high molecular mass species remains similar (4 ± 1% before and 3 ± 1% after digestion) (Fig. 3.1C).

The increase of low molecular mass species interpreted from cw-EPR after digestion was further tested for both heparin and RNA fibrils using blue native polyacrylamide gel electrophoresis (BNPAGE; Fig. 3.1D). The results showed that tau fibrils after digestion release a significant amount of solubilized monomer and dimer, in contrast to tau fibrils before digestion, where no corresponding band could be discerned. Note that the ratio of monomer/dimer remained unchanged for the sample before aggregation ("soluble" lane) and after digestion. These results are direct evidence confirming that the decrease of ThT fluorescence observed in Fig. 3.1A results from a depolymerization of tau fibrils.

3.2.3 Bound cofactors are required to stabilize tau fibrils

We learned that digesting cofactors depolymerized tau fibrils. However, extending the digestion for longer times or increasing heparinase and RNase concentration by 4 and 10 times, respectively, did not significantly decrease the remaining ThT fluorescence (Fig. 3.1A), which suggests that the maximal digestion had been reached and the remaining ThT fluorescence came from species that are not sensitive to heparinase/RNase digestion. These species can originate from either (i) fibril populations that are stable without a

cofactor, or (ii) fibril populations stabilized by cofactors that are undigestible due to steric hindrance. To answer this question, we quantified the amount of undigested cofactor by separating the soluble cofactors from fibrils. Mature RNA fibrils were pelleted, washed, and incubated with or without RNase, referred to as digested and nondigested RNA fibrils, respectively. Digested and nondigested RNA fibrils were subjected to dialysis, and the percentage of equilibrated RNA that flowed through the dialysis membrane was measured by UV absorption and regarded as effectively digested RNA. Digested and nondigested RNA (without tau) were used as controls. Results presented in Fig. 3.2B revealed a degree of RNA digestion of 81 ± 2% and 36 ± 3% for digested and nondigested RNA fibrils, respectively. These results confirm that the majority of the RNA in RNA fibrils was digested upon RNase treatment, while the small but significant difference between digested fibrils (81 ± 2%) and digested RNA alone (90 ± 4%) reveals that a fraction of the RNA in the fibrils is protected against digestion. The above difference of 9 ± 6% is in qualitative agreement with the remaining ThT fluorescence (8 ± 2%) observed after digestion of pelleted fibrils. Note that the 36 ± 3% of RNA flowed through in the nondigested fibrils is close to the nondigested RNA control (28 ± 5%), suggesting it originates mostly from RNase contamination inside the dialysis tube that digests RNA over the dialysis time of 24 h.

Heparin fibrils were prepared using spin-labeled heparin (heparin-SL), detectable by cw-EPR. The double integral of a cw-EPR spectrum is directly proportional to the quantity of spin-label, and hence yields the heparin concentration. We first confirmed using a ThT assay that heparin-SL triggers tau fibrillation (data not shown). Dialysis as a way of separating digested heparin from fibrils could not be applied because the dialysis membrane seemed to react with the heparin-SL, yielding unreliable results. Instead, digested and nondigested heparin-SL fibrils were subjected to filtration (0.2 μm) that allowed the soluble heparin to flow through, while retaining the large fibrils and associated

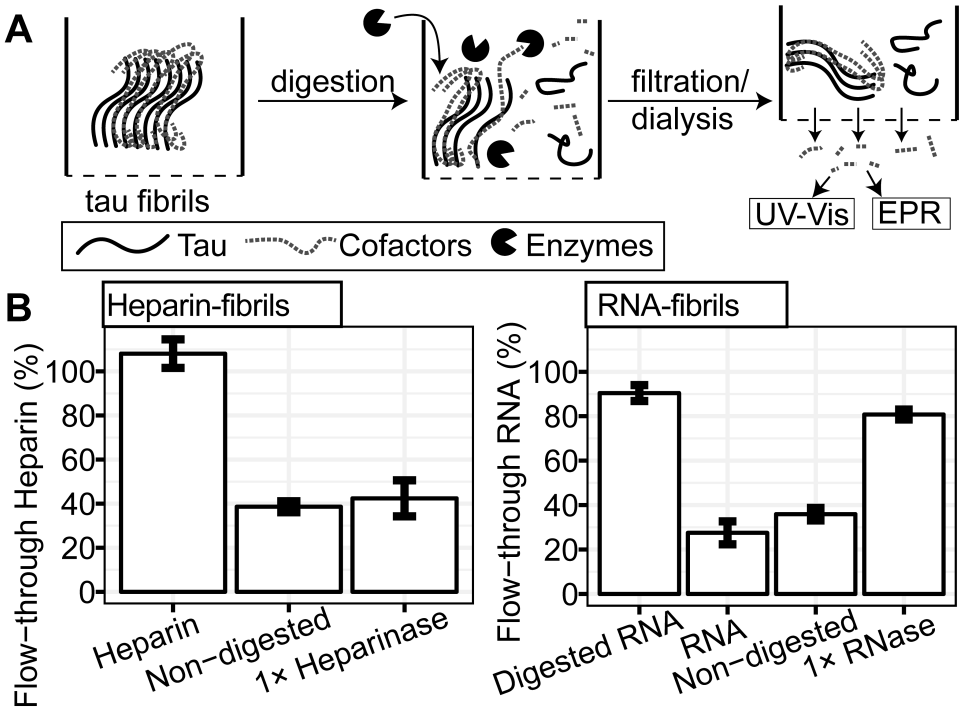

Figure 3.2: Cofactors are bound to fibrils and partially digested. (A) Schematic diagram of experimental procedures. Digested soluble cofactors were separated from tau fibrils via dialysis (RNA fibrils) or filtration (heparin fibrils) before measuring their concentration in the flow-through by cw-EPR (heparin) or UV absorbance (RNA). (B, Left) The concentration of spin-labeled heparin in the flow-through of a 0.2 μm filter for heparin and heparin fibrils before and after digestion. The concentration is given as the percentage of the concentration before filtration. (B, Right) RNA concentration outside a dialysis bag (12 kDa molecular mass cutoff) at equilibrium was measured and the percentage of RNA that flowed through is given on the y axis. Error bars show SD of three independent repeats.

heparin (Fig. 3.2A). The concentration of heparin in the filtrate was determined by cw-EPR and compared with the concentration before filtration to calculate the percentage of soluble heparin (Fig. 3.2B). Both digested and nondigested samples retained a significant amount of heparin (42 $\pm$ 8% and 39 $\pm$ 2% flowed through, respectively), while the control with only heparin-SL (no tau fibrils) flowed entirely through (108 $\pm$ 6%). The observation that even after digestion a large portion of heparin is bound to fibrils is in qualitative agreement with the ThT fluorescence that retains 80% of its intensity after digestion (Fig. 3.1A). We however could not detect a significant difference between

digested and undigested samples, in part due to the large variation in the measurement of spin concentration (±8% for the digested sample).

Furthermore, we detected a reproducible change in EPR lineshape of heparin-SL upon fibril formation (data not shown). A broadening of the central peak, implying slowed dynamics of the spin-labels, was observed upon aggregation. These results are consistent with the picture that (i) heparin is bound to fibril (line broadening between before and after aggregation), (ii) heparinase digestion detaches some heparin from the fibrils (line narrowing between before and after digestion), and (iii) the remaining heparinase-resistant fibrils still contain bound heparin (broadening after pelleting the digested fibers). Taken together, the quantification of cofactors as well as the cw-EPR lineshapes of heparin-SL strongly suggest that fibrils remaining after enzymatic digestion are stabilized by cofactors that are still associated with the fibrils and could not be digested (the second of the two posited scenarios).

3.2.4 Depolymerized Tau Monomers Have No "Memory" of the Fibril State

Tau undergoes drastic conformational rearrangements upon aggregation. We tested whether the released monomers after digestion recovered their original properties by measuring their conformational feature, their capacity to reform fibrils, as well as their capacity to seed aggregation.

We first tested whether or not released tau monomers were able to reaggregate. RNA fibrils were pelleted before digestion to ensure that only insoluble fibrils were subjected to digestion. The digested RNA fibrils were filtered and loaded onto a size-exclusion chromatography (SEC) column to purify the released monomers. The aggregation of these released monomers was then compared with freshly prepared monomers (i.e., that

did not go through the fibril state) at an identical concentration. ThT fluorescence presented in Fig. 3.3A showed that both fresh monomers and digested monomers displayed similar aggregation kinetics and maximal quantity. Note that heparin was used for this reaggregation experiment because of the difficulty of reliably removing RNase, even with SEC.

The reaggregation assay of heparin fibrils was slightly different because heparinase did not release enough monomers to rely on SEC purification. Instead, heparinase was inactivated by heating the sample at 65 °C for 15 min. We then added fresh heparin at a tau:heparin molar ratio of 10:1 to both digested and nondigested heparin fibrils (predigested fibrils and nondigested fibrils, respectively, in Fig. 3.3A). The change of ThT fluorescence was recorded and normalized to a scale from 0 to 1. Upon addition of heparin, the ThT fluorescence increased significantly more in the digested sample than in the nondigested sample, showing that the released monomers can reaggregate. The small increase in the nondigested sample might originate from the reaggregation of monomers that were released when heating the sample at 65 °C.

The conformational features associated with fibril digestion were further investigated. We have previously identified a signature of aggregation-prone tau conformations represented by a dramatic conformational extension around the amyloidogenic hexapeptides PHF6 (306VQIVYK311) and PHF6* (275VQIINK280) [203]. Following a similar procedure as shown in Eschmann et al. [203], we measured the distribution of intratau spin-label distance, r, spanning residues 272 and 285 by double electron–electron resonance (DEER). The distance distribution, P(r), was determined using the recently developed picard-selected segment-optimized (PICASSO) singular value decomposition (SVD) of the time-domain DEER decay [137, 120]. We first confirmed the expected distance extension around PHF6* when transitioning from monomer to heparin fibrils (Fig. 3.3B). The releasing of tau monomer upon heparinase treatment resulted in the partial rever-

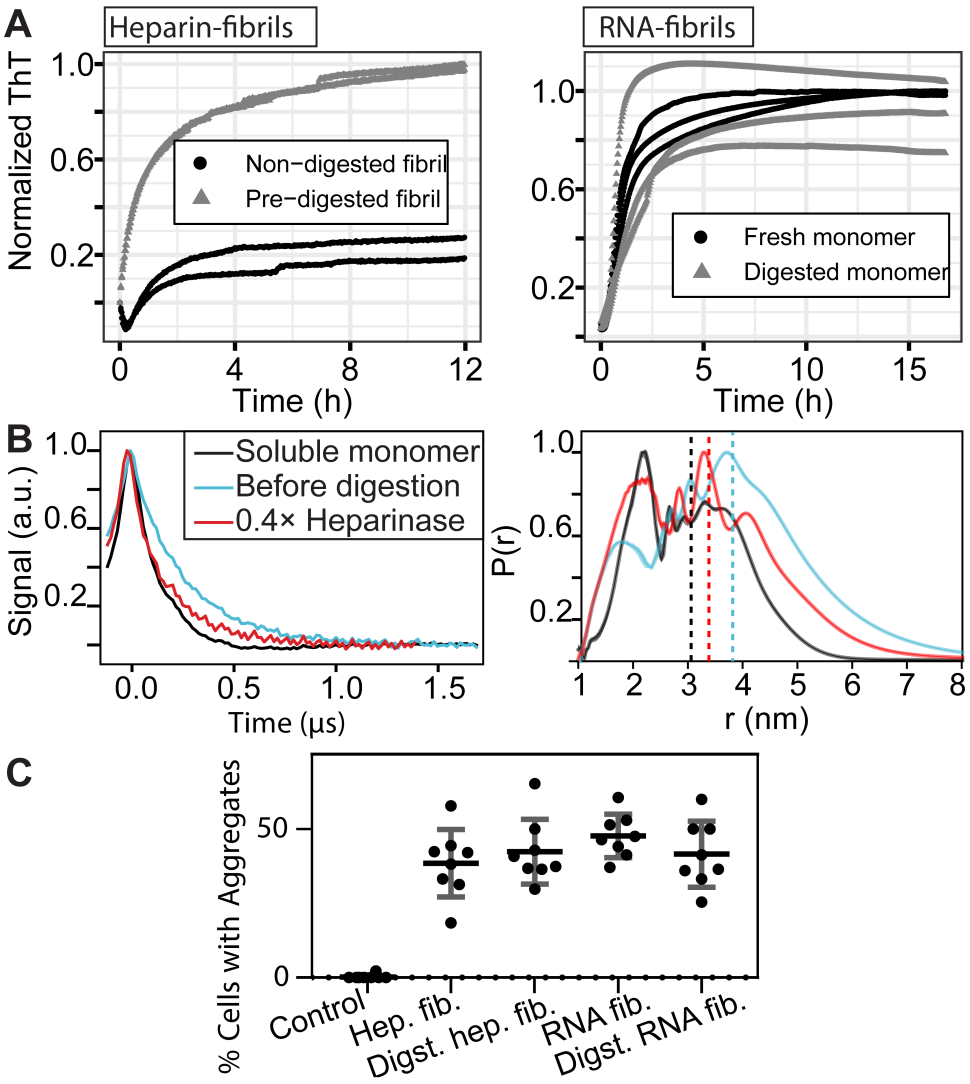

Figure 3.3: Refibrillization and conformation recovery of depolymerized tau monomers. (A, Left) ThT fluorescence of non/predigested heparin fibrils after heparin addition at time t = 0 h. (A, Right) Aggregation of monomers purified from digested RNA fibrils compared with fresh monomers. Curves of the same color show independent repeats. (B) DEER time-domain signal (Left) and corresponding distance distributions (Right), extracted with the SVD method, of tau labeled at residues 272 and 285 before and after digestion, compared with soluble monomer. (C) Quantification of in vivo seeding experiments. The ratios of cells that contain fluorescent puncta are reported. Digst, digested; fib, fibrils; Hep, heparin.

sal of the PHF6* distance extension (Fig. 3.3B), showing that the released tau lost its aggregation-prone conformational signature of solvent-exposed PHF6*. The P(r) of

the digested sample showed distinct features containing signatures of both the PHF6*-protected conformation (e.g., peak at 2.2 nm) and the PHF6*-exposed conformation (population at r ¿4 nm), indicating the coexistence of both fibril and released monomers.

It was recently proposed that after aggregation, tau, even in its monomeric form, maintains aggregate-templated conformations that provide high seeding capacities [39]. According to this hypothesis, the aggregation propensity of the tau monomers released from the digested fibrils should be much higher than that of fresh tau monomers, as the released monomers would populate fibrillation-prone conformations with increased numbers of nucleation sites in the sample. We tested this hypothesis by measuring the seeding propensity of heparin and RNA fibrils before and after cofactor digestion, both in vitro and in vivo. We used a cellular seeding assay similar to previously established assays [204, 100] in H4 neuroglioma. When the overexpressed proteins aggregate, they form fluorescent puncta [204] due to the fluorescent protein mCerulean tethered to tau (data not shown). Fig. 3.3C reports the percentage of cells that exhibited puncta. While all samples triggered seeding, there were no significant differences between digested and nondigested fibrils, suggesting that the monomers released from fibrils are not seeding-active. Furthermore, seeding was only possible when the fibrils were mildly sonicated. We interpreted this observation by suggesting that breaking the fibril is necessary for its efficient uptake, which again showed that monomers are not the active seeding species. The same results were obtained with H4 cells expressing tau187 instead of K18 (data not shown). Furthermore, we tested the seeding capacity of heparin fibrils in an in vitro assay where the premade fibrils were added to fresh monomers in the presence or absence of a cofactor (see next section for precise assay description). SI Figures, Fig. S3.4A shows that digested fibrils have lower seeding capacity compared with intact fibrils, as demonstrated with a smaller increase in ThT fluorescence (compare green with cinnamon curves). This result is in good agreement with the idea that depolymerized monomers

do not seed aggregation, and that the loss of seeding capacity is due to the loss of fibril content after cofactor digestion. The monomers derived from fibrils have no memory of the fibril state, neither in conformation nor in seeding capacity.

3.2.5 The Presence of Cofactor Sustains Fibril Seeding

To test the role of cofactors in seeding/spreading of fibrillation, we performed in vitro seeding assays of tau over two generations with and without cofactors, using either mouse-derived fibrils or heparin fibrils as seeds. The same tau construct as before was used, tau187C291S, but without the aggregation-promoting P301L mutation. We made this choice, as this tau variant is incapable of spontaneous fibril formation with RNA (SI Figures, Fig. S3.5B). Five percent (mass) of heparin fibrils were added as seeds to fresh tau in the presence or absence of RNA cofactor (polyU) while ThT fluorescence was monitored. Fig. 3.4A presents the ThT fluorescence of the seeding experiments after 10 h, while the full aggregation curves are shown in SI Figures, Fig. S3.5. The presence of the RNA cofactor significantly increased the seeding capacity of both digested and nondigested heparin-fibril seeds. For second-generation seeding, 10% of the end product of the first generation was added to the fresh monomers, with or without cofactor (Fig. 3.4A). As for first-generation seeding, the presence of cofactor significantly enhanced the seeding activity. The same experiments were carried out using mouse-derived fibril (rTg4510 mice expressing 2N4R-P301L) seeds (Fig. 3.4A). In contrast, the presence of a cofactor did not change the seeding capacity of mouse-derived fibrils in the first generation (Fig. 3.4A). For second-generation seeding, where 10% end product of the first-generation sample was used as the new seed, aggregation was observed only when a cofactor was supplied (Fig. 3.4A). The aggregation kinetics appeared to be slower compared with the other seeding experiment, as the ThT signal had not plateaued after

10 h. Altogether, the results presented in Fig. 3.4 show that cofactors are needed to promote templated seeding, and suggested that unknown cofactor species are present in mouse-derived material, which facilitated first-generation seeding without an extrinsic cofactor, while the second-generation fibrils were incapable of seeding, unless extrinsic cofactors were added.

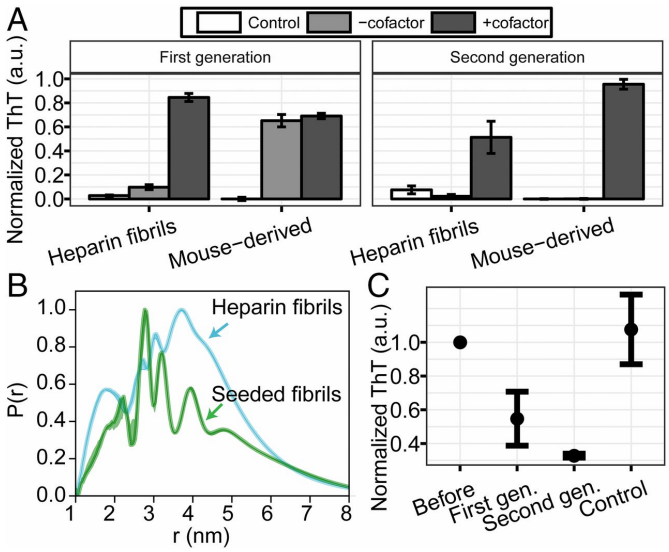

Figure 3.4: In vitro seeding of tau fibrils. (A) ThT fluorescence of recombinant tau187C291S seeded with heparin fibrils or mouse-derived fibrils (mouse-derived) in the presence or absence of cofactor (polyU RNA). In first-generation seeding (Left), 5% of preaggregated fibrils were added to fresh recombinant tau and incubated at 37 °C while shaking. In the second generation (Right), 10% of the end products of first-generation samples were added to fresh monomers. Control refers to the seeds with cofactor incubated without fresh tau. Error bars shows SD (n = 3). (B) DEER distance distribution between residues 272 and 285 of heparin fibrils and mouse-derived seed-induced fibrils (seed-induced fibrils) obtained from the SVD method. (C) ThT fluorescence before and after RNase addition to the first and second generations of mouse-derived seed-induced fibrils. Error bars shows SD (n $\geq$ 3). gen, generation.

To test whether seeding with mouse-derived material impacted the structure of the seeded tau fibrils, we performed DEER of doubly labeled tau187 at residues 272 and 285 (same sites as in Fig. 3.3B), whose aggregation was seeded with mouse-derived fibrils in the presence of polyU RNA cofactor (1% seed). The distance distribution was obtained using PICASSO [118] and compared with that of heparin fibrils (Fig. 3.4B). The P(r)s are

significantly different, implying that seeded and heparin-induced fibrils are structurally different, where specifically the seed-induced fibrils showed distinctly narrowed peaks reflecting multiple, highly ordered, fibril populations. In contrast, heparin-induced fibrils exhibited broader P(r) features that represent imperfectly packed (at least locally around PHF6*) fibrils populating a continuum of distances. This result agrees with the view that in vivo tau aggregates populate specific tau strains [49] that are structurally well-defined [140], while heparin fibrils are highly heterogeneous [26]. This result shows at high resolution a structural convergence of recombinant fibrils guided by mouse-derived fibrils, suggesting that in vivo aggregates can transmit their structural properties to naïve tau by templated seeding. When the just-discussed mouse-seed-induced fibrils, formed in the presence of polyU cofactor, were subjected to RNase treatment, again a partial decay of the ThT signal was observed (Fig. 3.4C), implying that the loss of β-sheet packing also occurs when the fibrils are structurally templated by mouse-extracted fibrils, underscoring the importance of the presence and nature of the cofactor.

3.3 Discussions

We have demonstrated that mature recombinant tau fibrils require cofactors to be sustainably stable. Upon cleavage of cofactors by enzymatic digestion, the fibrils depolymerize, releasing soluble monomeric tau. The incomplete digestion of the cofactor molecules (heparin or RNA) is likely due to allosteric hindrance that prevents the enzymes from accessing and cleaving their targets. The finding that in both RNA and heparin fibrils only a defined and reproducible amount of cofactor can be digested suggests that the fibrils are polymorphic, where in some types of aggregates the cofactors are protected from digestion while in others they are accessible to the enzyme. Note that single-point mutations change the extent to which ThT fluorescence is lost upon cofactor

digestion (data not shown), suggesting that the mutations affect the tau conformational ensemble within the fibril structure, and therefore the accessibility to the cofactors. The significant difference seen in Fig. 3.1A between the maximum digestible RNA (60 to 70%) and heparin (20%) could be explained by different molecular arrangements of the fibrils and/or by the nature of the enzymes, where RNase A (14 kDa) may be less sensitive to steric hindrance than heparinase I (43 kDa) to process its target.

Our work suggests that the high stability of heparin-induced fibrils previously observed [156, 205] is largely due to tau–cofactor interactions, and not due to superior tau fibril packing and stability. This highlights the need to further understand the role of cofactors in tuning the properties of tau fibrils of structure, stability, and seeding capacity.

The finding that a polyelectrolyte cofactor is essential for the stability of fibrils prepared in vitro has two major potential implications with respect to in vivo aggregates. (i) Polyanion-induced recombinant tau fibrils make limited models (of in vivo aggregates) that overestimate the role of the cofactor, and (ii) there is an unknown cofactor in the fibrils formed in neurons, whose roles have been underestimated to date. While we cannot rule out (i), the data presented here make a strong case for (ii). We have successfully performed in vitro seeding of recombinant protein with heparin-induced fibrils and mouse brain-derived fibrils. Without providing additional cofactors, no significant seeding was observed with heparin-induced tau seeds, but the seeding capacity of brain-extracted fibril seeds was high (Fig. 3.4A), in agreement with previous work [205, 17]. When fibrils extracted from this successful seeding experiment were used as pristine seeds for a second-generation seeding, no fibrils were formed (Fig. 3.4D), showing limited propagation of mouse-extracted fibrils through seeding. However, when a cofactor (polyU RNA) was provided in the reaction buffer, mouse-derive seeds, as heparin-induced seeds, were made competent over multiple generations (Fig. 3.4A). This result is in good agree-

ment with the hypothesis that an unknown cofactor is present in the mouse-extracted aggregates that permits first-generation seeding, but not subsequent generations, as the cofactor present in the original seed gets consumed. In contrast, when a cofactor is provided in the buffer, seeding can be sustainably carried out over successive generations, as previously reported [135].

Fibrils seeded with mouse-extracted fibrils in the presence of RNA populated better-defined fibril structures compared with heparin fibrils (Fig. 3.4B), but they too could be partially digested (Fig. 3.4C), showing that RNA gets incorporated into the seed-induced fibrils. Interestingly, 45% of the ThT intensity is lost in the digestion of the first generation aided by RNA, while 70% of the ThT signal is lost in the second generation, approaching the level of digestion of RNA fibrils (Fig. 3.1A). This is in good agreement with the view that in the first generation, aggregation is partially aided by the unknown cofactor from the mouse fibrils that is insensitive to RNase, while in the second generation mostly extrinsic RNA is supporting the structures of the fibrils that are subject to the same levels of degradation as the nonseeded RNA-induced fibrils. Consistent with this picture is the observation that the mouse-extracted seed without the added RNA cofactor is completely insensitive to RNase (data not shown) and is degraded by neither DNase nor heparinase I. Studies to determine the stoichiometry and nature of the unknown cofactor originating from the brain-extracted seed will be timely.

There is a large variety of bioelectrolytes that could interact with tau in vivo, including DNA, RNA, glycoaminoglycan (GAG), and ATP. Although tau is mostly present in axons [206], it is also found in neuronal nuclei [206] and is suspected to traffic in the extracellular matrix [207]. The complexity of the cellular environment and trafficking makes it very hard to unambiguously assess in situ the roles of a given cofactor in tau aggregation and the pathogenicity. GAG, in particular heparan sulfate (HS), has been the most studied interaction partner to tau [see, for instance, a recent review [208]], likely because (i) it

was found colocalized with tau neurofibrillary tangles (NFTs) in AD brain [192], (ii) heparin is a very efficient cofactor in promoting aggregation in vitro [192], and (iii) HS has been shown to play an important role in tau internalization [208]. Although it is unclear when and how HS interacts with tau, as the former is exclusively present on the extracellular surface while the latter is mainly found in the cytoplasm, the fact that the NFTs colocalize with HS [192] suggests that HS might be incorporated into in vivo tau fibrils. Similarly, RNA has also been found to specifically associate with tau in neurons [209], to be sequestered in tau pathological assemblies, not only in AD brains but also in Pick bodies [210], suggesting that RNA might also be part of the final tau fibrils. Recent advances in cryo-EM have allowed the identification of two very different fibril structures in AD brains [5] and Pick's disease [7], showing that different strains have very distinct atomistic fibril structures. If polyelectrolyte cofactors were present in the mature tau aggregates, they would not necessarily be visible on a cryo-EM electron density map (their high flexibility would likely compromise their resolution), while their interactions with tau could in fact modulate the differentiation toward a given strain.

3.4 SI Figures

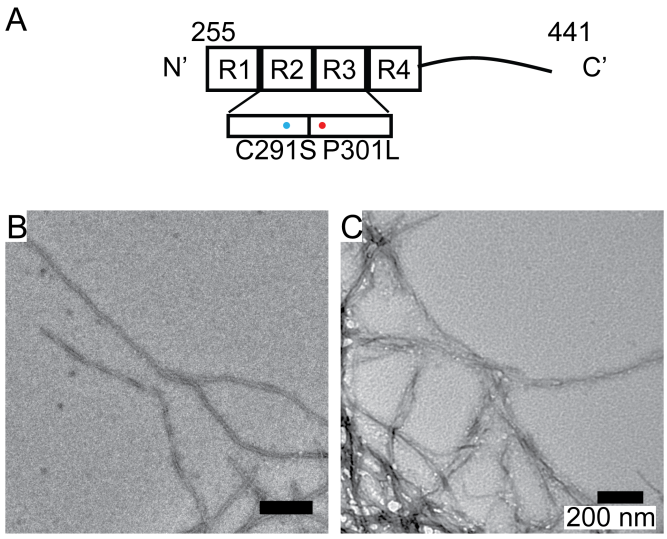

Figure S3.1. Assembly of tau fibrils with cofactors. A. Schematic representation of the tau construct used in this work (2N4R 255-441) that include the four repeat domains (R1-R4) as well as the C terminal region; B. Representative TEM image of heparin-induced tau fibrils and C. RNA-induced tau fibrils.

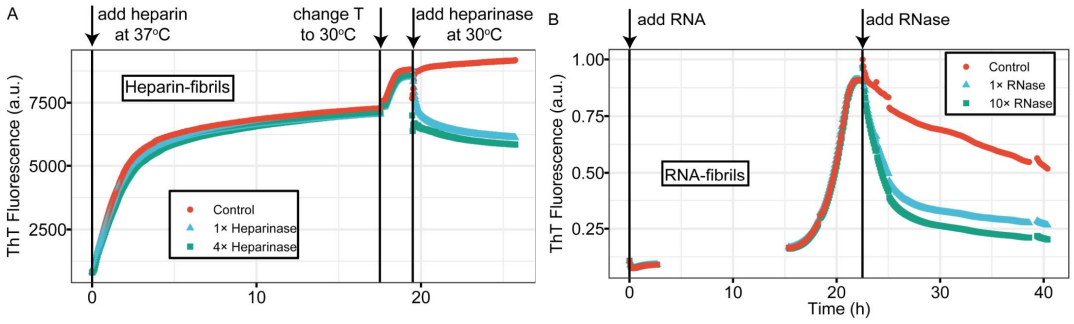

Figure S3.2. ThT fluorescence trace of heparin-/RNA-induced tau fibrillation followed by cofactor enzymatic digestion. A. Heparin-induced samples were incubated at 37°C until heparinase treatment where temperature was decreased to, and stabilized at, 30°C. B. RNA-induced fibrillation and RNase treatment were performed at room temperature. In the control samples buffer was added instead of enzymes.

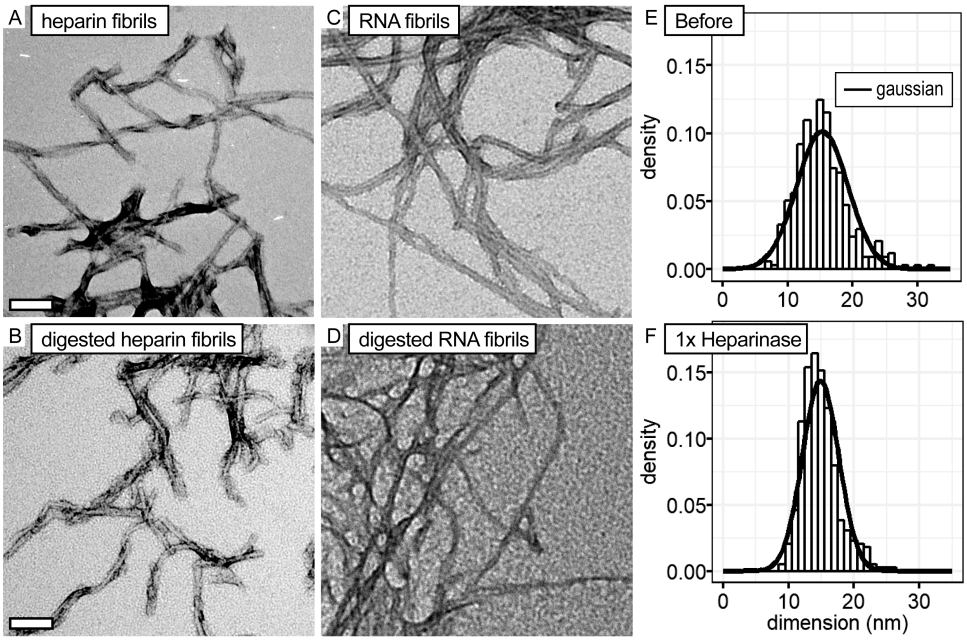

Figure S3.3. Dimension quantification of fibrils before and after digestion. TEM images show heparin fibrils A. before and B. after 1× heparinase treatment; RNA fibrils C. before and D. after 1× RNase treatment. Histograms with gaussian fits of the measured heparin fibril widths showed two similar populations of fibrils E. before and F. after 1× heparinase treatment.

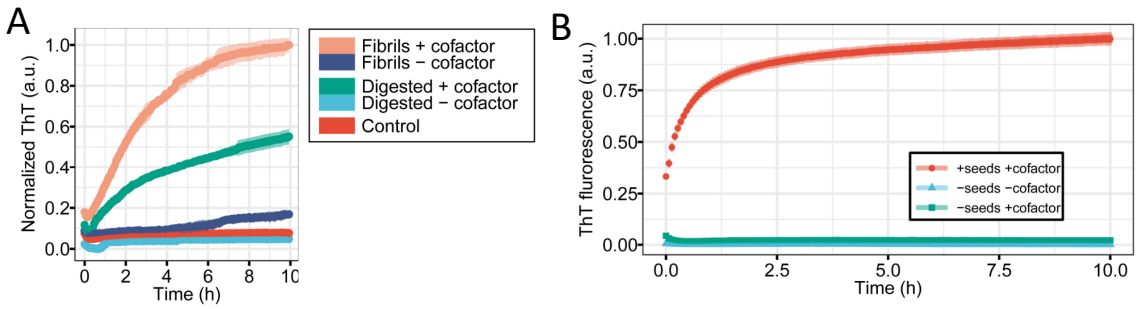

Figure S3.4. (A) ThT fluorescence of in vitro seeding experiments. Time resolved ThT curves of the seeded tau under the same conditions as in Fig. 4A. The control represents seed with cofactor and without monomeric tau. Digested fibrils have a lower

capacity to seed aggregation than undisturbed fibril seeds. (B) Controls of in vitro seeding assays. ThT fluorescence of 20 μM tau187C291S incubated with and without cofactor (polyU RNA at 120 μg/ml) showed that fibrils were not seeded in the absence of seeds. As a reference, mouse-fibrils seeds were added in the same condition (+seeds +cofactor).

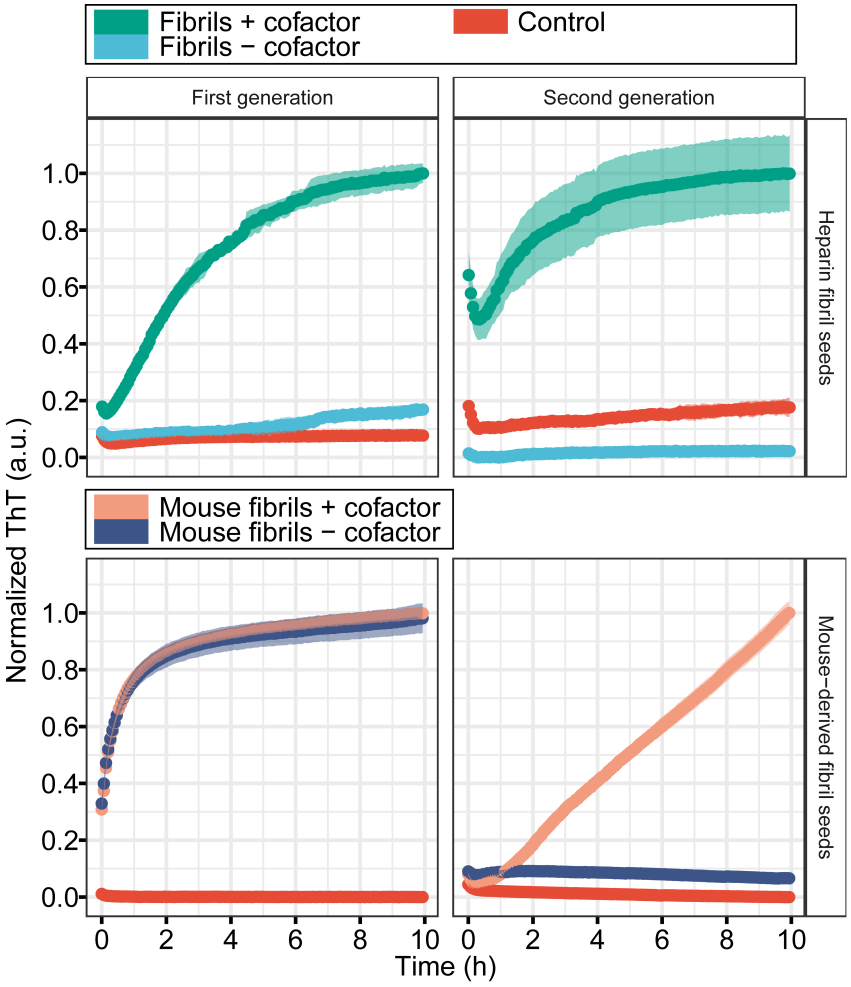

Figure S3.5. Full aggregation curves of seeding experiments presented in Fig. 3.4.

3.5 Permissions and Attributions

1. The content of is reproduced from Fichou, Yann, Yanxian Lin, Jennifer N.Rauch, Michael Vigers, Zhikai Zeng, Madhur Srivastava, Timothy J. Keller, Jack H. Freed, Kenneth S. Kosik, and Songi Han. "Cofactors Are Essential Constituents of Stable and SeedingActive Tau Fibrils." *Proceedings of the National Academy of Sciences* 115, no. 52 (December 26, 2018): 13234–39. The author of this dissertation, among coauthors of the reprinted article, retains copyright of the reproduced material, and needs not obtain permission to reproduce it in this dissertation. For details, please visit https://www.pnas.org/page/about/rights-permissions.

Chapter 4

Tau Fibril Fragments Constitute The Seeding Active Species in Sonicated Tau Fibrils

4.1 Introduction

Tau misfolding and aggregation into neurofibrillary tangles (NFTs) is one of the pathological hallmarks of tauopathies such as Alzheimer's disease (AD). Tau pathology in the brain is suggested to follow 'prion-like' behavior [18], with a cross-neuronal spread of tau aggregates (referred to as "seeds") from one brain region to another that triggers aggregation of monomeric tau. Recombinant tau fibrils and tau aggregates extracted from tauopathies brains or mouse model brains have been shown to act as seeds in various model systems to spread tau pathology [18, 211, 212, 20, 107, 27, 213]. Despite the evidence supporting the existence of seed in the initiation of aggregation, the biochemical and biophysical properties of the seed responsible for tau seeding are still controversial. Some studies argue that insoluble tau fibrils are the primary seeding competent species [214, 20, 215, 36, 196]. Others suggest that monomer [39, 216] or oligomer [38] are seeds and can trigger tau aggregation in cells and *in vitro* . However, in these studies, insoluble tau fibrils were subjected to sonication before the treatment of cells or recombinant tau monomer. Sonication may result in fibril breakage into a mixture of short fibrils and peptides. It was hypothesized that short fibrils provide more fibril ends for tau monomer to attach to and elongate [217] and thus seeding can be promoted. On the other hand, some studies found seeding-competent oligomers [38] and monomers [39, 37] based on sonication of fibrils. Therefore, the effect of sonication on tau fibril and the nature of the infectious seeding agent remains unclear.

Here, we show that sonication induces artificial fragmentation in tau fibrils and product fibril fragments are seeding-competent to trigger tau aggregation *in vitro* and *in vivo*. Mass spectrometry shows that upon sonication, tau fibrils are more protected than monomer. However, fragmentation induced by sonication is a stochastic process and due to the difficulty to identify which fragment of tau fibrils generated during sonication is

responsible for seeding, we argue that sonication should be used to process fibrils with caution.

4.2 Results

4.2.1 Recombinant heparin-induced tau fibrils upon sonication exhibits seeding activity *in vitro* and in cells

First, we tested the effect of sonication on the seeding ability of heparin-induced recombinant tau fibrils. Specifically, truncated tau (22kDa, referred to as tau187) spanning residues 251 to 441 of the longest isoform of tau that lacks any internal cysteines due to serine substitutions (C299S and C322S) and contains disease-associated P301L mutation was expressed and purified as described previously [134, 26]. Monomeric tau187 was incubated with heparin for 24 hours to make mature fibrils. To test the seeding activity of tau187 fibrils, fresh tau187 monomer was seeded with sonicated tau187 fibrils (xh-seed refers to the sample derived from heparin-induced tau fibrils upon sonication for x hours). Fibril formation was monitored by ThT fluorescence. As shown in Figure. 4.1a, pristine tau187 heparin-induced fibrils (0h-seed) exhibited minimal seeding activity, while fibrils upon 1 hour sonication (1h-seed) and 3 hours sonication (3h-seed) showed increased ThT fluorescence, indicating that sonication improved the seeding activity of heparin-induced tau fibrils. To ensure the formation of fibrils, fibrils grown from 3h-seed as well as the seeds were visualized by negative stain TEM (Figure. 4.1b).

To further test the seeding activity of the sonicated tau fibrils, we used previously described biosensor cells [100]. These cells stably express 4R tau repeat domain (RD) containing the disease-associated P301L-V337M mutation. All cells express 4R-RD-Cyan fluorescent protein and 4R-RD-yellow fluorescent protein (RD-CFP/YFP). Exogenously

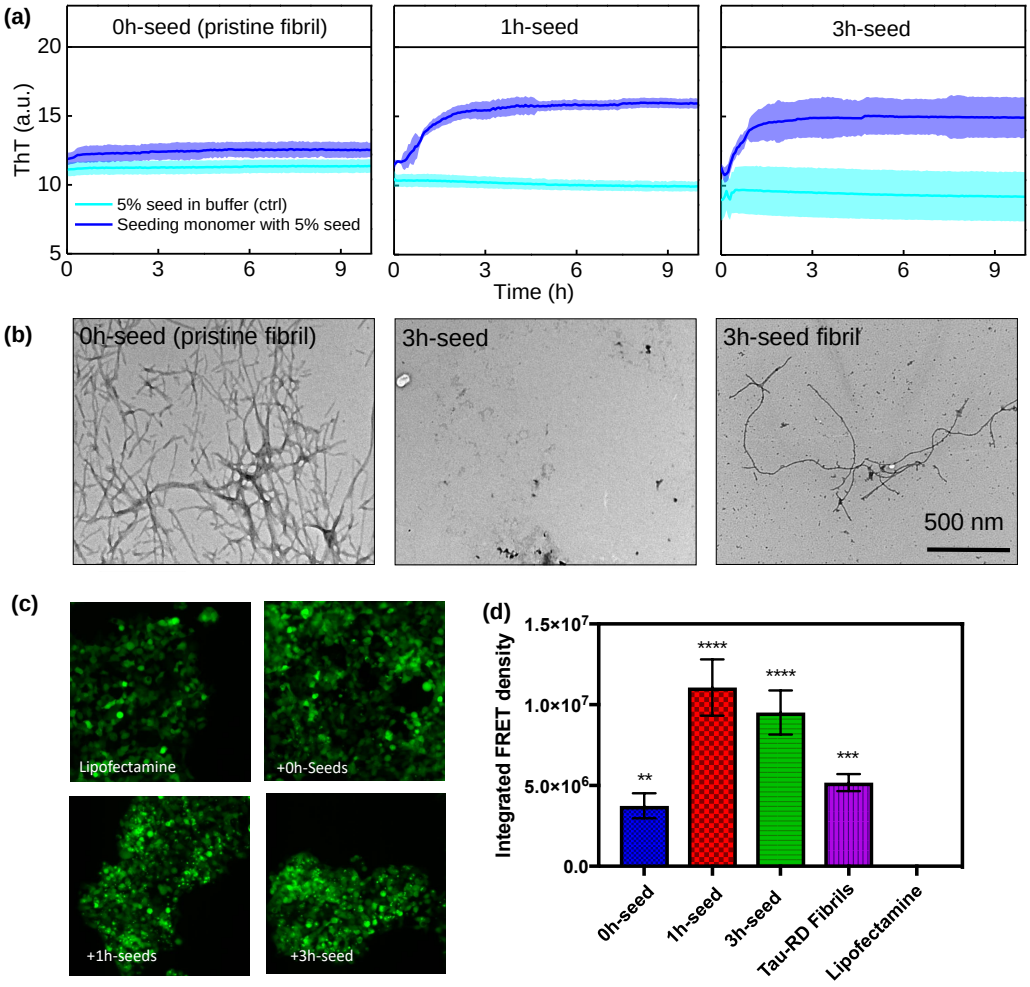

Figure 4.1: ThT fluorescence of in vitro seeded aggregation, TEM images, and cell assay of in vivo seeding. (a)ThT fluorescence of seeding tau monomer with 5% (molar ratio) of 0h-seed, 1h-seed, and 3h-seed. Here, Xh-seed refers to the sample derived from heparin-induced tau fibrils upon sonication for x hours. 0h-seed is non-sonicated pristine fibril. (b) TEM images of 0h-seed, 3h-seed, and seeded fibril generated with 3h-seed. (c) seeding cells with short time sonicated heparin-induced fibril

applied seeds induce intracellular aggregation with resultant fluorescence resonance energy transfer (FRET) between CFP and YFP that can be measured via flow cytometry [100]. Lipofectamine directly transduces tau aggregates across the plasma membrane and increases the assay's sensitivity by approximately 100-fold. Upon incubation with

Lipofectamine and the seeds, we observed seeding in cells by the 0h-seed, 1h-seed, and 3h-seed (Figure. 4.1c. The degree of seeding activity is scored using 'integrated FRET density', which is the product of the percent positive cells and the mean fluorescence intensity of FRET-positive cells, and from this, we determine the extent of tau seeding activity in cells [100]. As shown in Figure. 4.1d, 1h-seed, and 3h-seed have a higher seeding activity than 0h-seed and pristine tauRD fibrils. Interestingly, heparin-induced fibrils upon mild sonication (3min sonication) did not show any seeding activity *in vitro* but showed some seeding in cells. Therefore, we concluded that sonication improves the seeding ability of recombinant heparin-induced tau fibrils, especially in cells.

4.2.2 Sonication induces artificial fragmentation in recombinant tau monomer and fibril

To understand the effect of sonication on tau protein integrity, we sonicated tau187 monomer and fibrils for different amounts of time and ran the sonicated products on SDS-PAGE. As shown in Figure. 4.2a, the intensity of the tau187 monomer band at 22kDa decreased as sonication time increases, while the intensity of bands lower than 22kDa increased. The total band intensity of the monomer upon 3h sonication is lower than that of the monomer without sonication, indicating that the monomeric tau was broken into smaller peptides with a molecular weight below 10kDa by sonication and cannot be detected. As for heparin-induced fibrils (Figure. 4.2b), the band at 22kDa showed the existence of the mature tau187 fibrils in all sonicated products, implying that the tau is more protected in the fibril samples. However, the total band intensity of fibrils upon sonication was lower than the sample without sonication. We hypothesized that the flanking segments of the fibrils surrounding the fibril core were more ready to be fragmented by sonication than the core, and the sonication product is too small to be

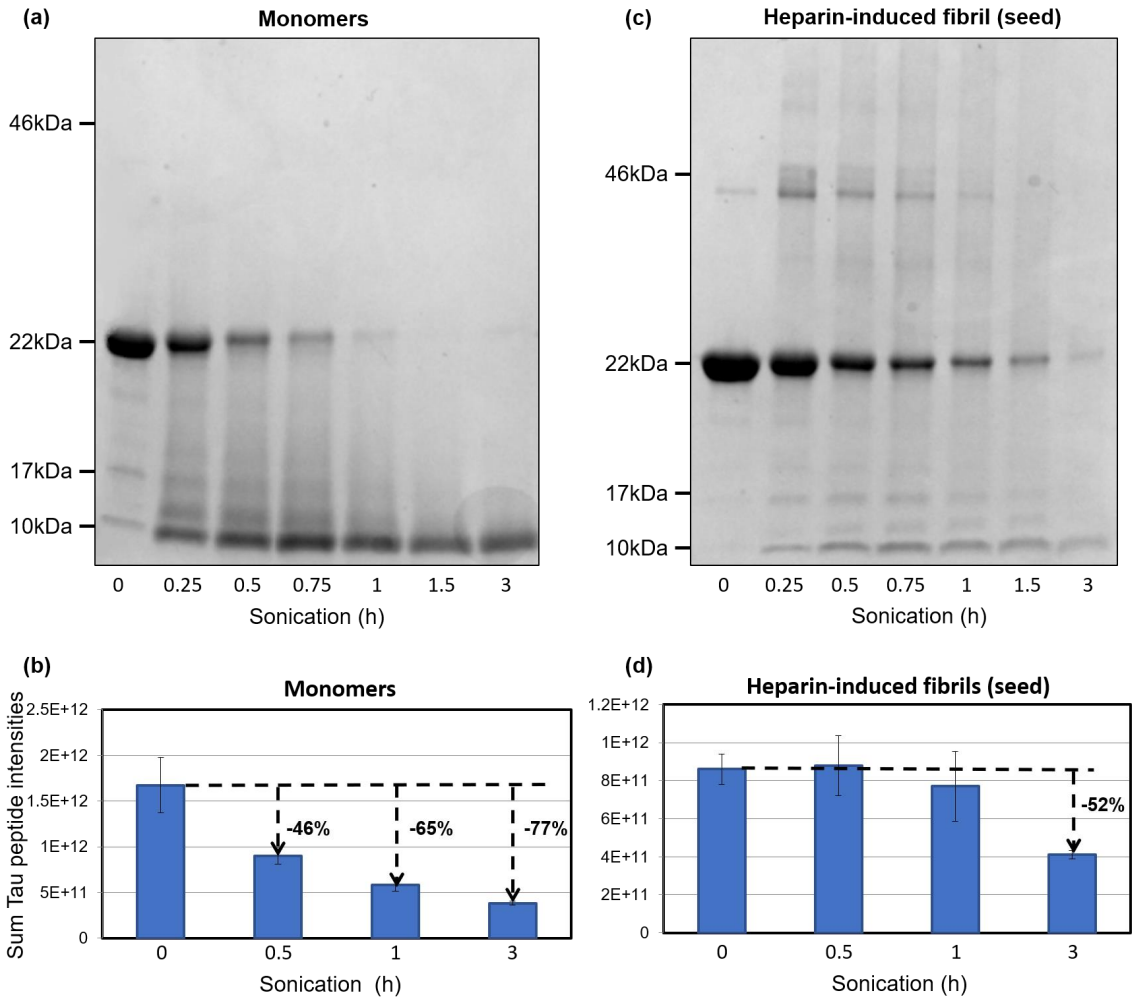

Figure 4.2: SDS-PAGE and the MS sum peptide intensity of tau upon sonication. (a) SDS-PAGE of tau187 monomer and fibril after sonication. Tau187 monomers or fibrils were sonicated for different amounts of time, and 2 μg of each sample was resolved by SDS-PAGE and coomassie stain. (b) Sum tau peptide intensities found by MS in monomer and (c) heparin-induced fibril upon sonication.

visualized on the gel.

Mass spectrometry was used to further understand the fragmentation effect of sonication on tau and to identify cleavage sites. Tau monomer and fibrils (with or without sonication) were run on liquid chromatography-tandem mass spectrometry (LC-MS/MS)

and the peptide population was analyzed by the sum tau peptide intensities. As shown in Figure. 4.2c, the decrease in the intensity of MS sum tau peptide intensities showed that 0.5-3h sonication fragmented tau monomer into peptides too small for MS to detect. This is consistent with the SDS-PAGE result. As for the heparin-induced fibril (Figure. 4.2d), the MS sum tau peptide intensities decreased drastically when 3h sonication was applied, indicating that tau fibrils were more protected from the artificial fragmentation by sonication than tau monomers. Further analysis of the MS data (SI Figures, Fig. S4.1 and S4.2) showed that the artificial fragmentation induced by sonication happens at random sites, and no tau187 monomer or oligomer was found in the sonicated products.

4.3 Discussion

In Alzheimer's disease and related neurodegenerative disorders, Tau protein is deposited in the form of large neurofibrillary tangles. These are bundles of long fibrils that are poor candidates for disease propagation, and sonication has been widely used to prepare seeding-competent materials. Our findings demonstrate that sonication induces artificial fragmentation in tau fibrils, and tau fibril fragments (small aggregates) have enhanced seeding activity compared to pristine, unsonicated fibrils. Fibril fragmentation is essential for tau seeding and the spread of tau pathology [218]. It may facilitate secondary pathways [219, 220] such as branching [221] or secondary nucleation from the fibril surface [222, 223] and thus contribute to enhanced aggregation. Seeding recombinant tau with sonicated tau fibrils for multiple cycles has shown to select tau fibril populations with different fragility and growth rates [45]. In contrast, another possibility is that long-time sonication can break off seed-competent monomers from heparin-induced fibrils; a study isolated monomeric species from heparin-induced full-length tau fibrils upon 3h sonication and the monomers are seeding active [106]. The authors discovered the struc-

tural difference between the seed-competent monomers and inert monomers, indicating that monomers are able to maintain stable seed-competent conformations. However, our data show that tau fibrils upon 3h sonication under a similar condition were fragmented, and no monomer was generated. Further experiments are needed to investigate whether this is due to the use of truncated tau here.

In addition, we found that artificial fragmentation induced by sonication is a stochastic process but whether this process mimics what happens in biological systems remains unclear. In fact, the mechanisms that fragment tau fibrils and produce small aggregates in cells are not well understood, but it may be in place because although small aggregates and short fibrils can be taken up by cells [224, 225], and tau oligomers can be taken up by cells more efficiently [150]. High molecular-weight fibrils derived from patients or made with recombinant tau can also be internalized by cells [226, 151, 227]. The internalized fibrils may undergo fragmentation in cells to provide a new surface to recruit monomers to the fibril ends. Therefore, efficient seeded aggregation may depend on the ability of these fibrils to break. Interestingly, a correlation between aggregate fragility and strain spread was observed in yeast prions, where the more fragile conformer (or strain) had a selective advantage [228]. In these organisms, the molecular chaperone HSP104, along with other factors, is thought to provide the mechanical force that disrupts fibrils and allows the separation of smaller aggregates into daughter cells [229]. However, no homolog of HSP104 exists in mammalian cells. Whether molecular chaperones mediate the fragmentation of tau fibrils is unknown. It could be another clearance-related mechanism causing the fragmentation, or multiple mechanics running in parallel. Regardless of the molecular details of these processes, fibril fragmentation appears to be a critical part of tau seeding. Although sonication treatment of seeds is an easy way to enhance *in vitro* seeding, due to the artificial fragmentation and the difficulty of identifying which fibril fragment is responsible for seeding, sonication should be used with caution.

4.4 SI Figures

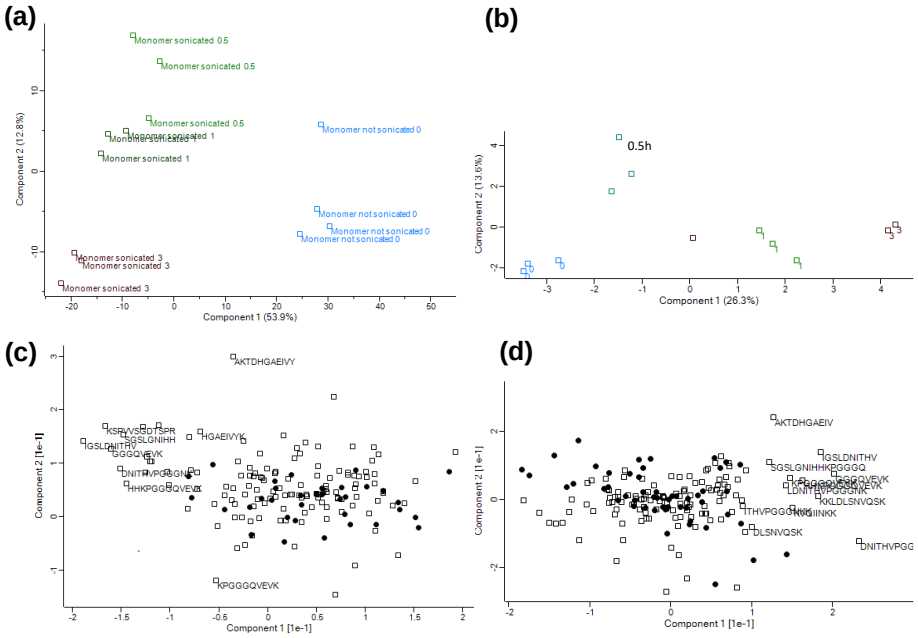

Figure S4.1.(a)(b) Principal Component Analysis (PCA) from MS. The plots show how sonication separates the groups along with component 2. Sonication clearly separates the groups. (c)(d) loading plot shows which peptides contribute most to the separation. There is no obvious cluster in one region so we concluded that the fragmentation induced by sonication is a stochastic process. It produces some fragments that are seeding active. Here, filled circles represent tryptic peptides, and squares represent semitryptic peptides (fragments). The semitryptic species do not increase compared to controls - their signal rather decreases over time as the peptides are getting further fragmented.

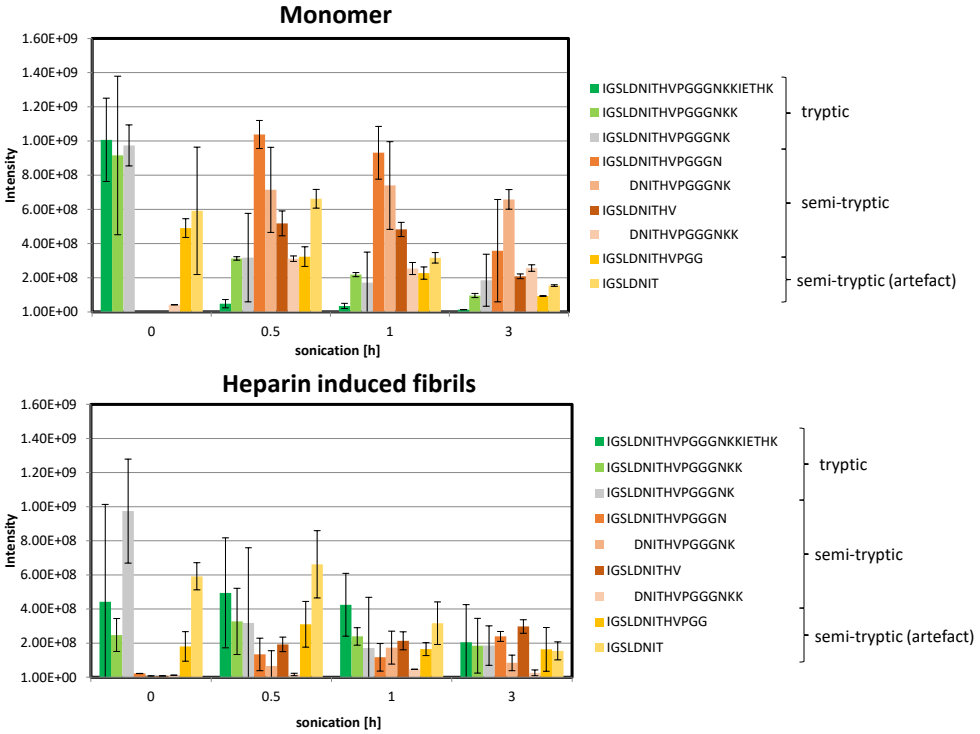

Figure S4.2. Tryptic and semi-tryptic peptide intensity from MS. For the first misscleaved tryptic peptide one can see that the decay is faster compared to the two other tryptic peptides as these peptides are being generated through the fragmentation of the first. The artifact was generated either by trypsin unspecificity or in-vitro synthesis. However, noting that these peptides intensity also decreased with sonication since peptides are getting fragmented by sonication

4.5 Permissions and Attributions

1. The content of chapter 5 is the result of a collaboration with Professor Judith Steen from the Boston Children's Hospital (Harvard University), and a manuscript is in preparation.

Chapter 5

CBD and PSP Cell-derived Tau Seeds Generates Heterogeneous Fibrils with A Subpopulation Resembling Disease Folds

5.1 Introduction

Tauopathies are a varied group of neurodegenerative diseases defined by the deposition of fibrillar aggregates of microtubule-binding protein tau in the brain, the prevalence of which is closely related to neurodegeneration.[230, 231] In the disease state, tau misfolds from a soluble monomer into a β-sheet-rich structure capable of self-propagating; thus, tau becomes a prion. Although tau pathology in these diseases varies in morphology and isoform composition [77], the defining difference between the clinical phenotypes is thought to arise from the shape, or conformation, that tau misfolds into. This phenomenon is explained by the strain hypothesis. Efforts to understand this disease mechanism began in 2009 when Clavaguera *et al.* showed that brain homogenate from a spontaneously ill tau mouse model induced intracellular tau aggregation and spread of pathology in wild type mouse brain [18]. Subsequently, the Diamond and Lee labs reported that recombinant tau fibrils alone induce aggregation of tau *in vitro* [232, 47, 36, 153] and *in vivo* [20]. These findings confirmed that the transmission of tau pathology reported by Clavaguera *et al.* was due to the prion-like behavior of the protein tau. Subsequently, the Goedert lab showed that brain homogenates prepared from deceased patients with a variety of tauopathies, including progressive supranuclear palsy (PSP), corticobasal degeneration (CBD), and argyrophilic grain disease (AGD) could induce tau pathology following inoculation in wild-type mice [162]. Moreover, the induced inclusions exhibited immunostaining patterns similar to those seen in the corresponding human pathology, implying the that each disease may be caused by a distinct tau strain. Testing this hypothesis, cell models expressing the repeat domain of tau fused to a fluorescent protein were used to demonstrate that each tauopathy is associated with a distinct tau strain that is isoform-dependent and capable of maintaining its biological properties after passaging in cells and mice [204, 49, 27]. Strains are distinct with respect to inclusion morphol-

ogy, sedimentation profile, seeding capacity, cell-type specificity, protease digestion and guanidine denaturation patterns, and spatial patterns and distribution of the induced lesions in the brain [204, 49, 27, 24, 105, 106, 158, 161].

Building from this initial work, cryo-electron microscopy (cryo-EM) studies have shown that tau strains arise due to differences in the conformation tau misfolds into. For example, while tau fibrils isolated from Alzheimer's disease (AD) patient samples adopt a C-shaped fold [5, 6], tau fibrils in Pick's disease (PiD) misfold into a J-shaped conformation [7]. These structures all differ from those found in CBD [8, 9], chronic traumatic encephalopathy (CTE) [10], PSP [11, 12], AGD [12], and globular glial tauopathies (GGT) [12] patient samples. However, it is most notable that the recombinant heparin-induced tau fibrils [52] adopt misfolded conformations that lack any homology with the patient-derived fibrils, indicating that research focused on tau misfolding in disease must use patient-derived fibrils as a starting material.

While cryo-EM has been a crucial tool to unravel the atomic basis of tau strains, it is limited by the ability to resolve the structure of tau fibrils at the disease endpoint. As a result, it remains unclear what factors govern the initial formation and propagation of strains in tauopathies. *In vitro* recombinant tau fibrils induced by polyanionic cofactors like heparin [175] are commonly used to study the formation mechanism of tau conformers, but the lack of homology between heparin-induced full-length tau fibrils and patient-derived fibrils [52] has shifted the field away from the use of recombinant fibrils generated using polyanionic cofactors. Interestingly, Lovestam *et al.* recently reported that recombinant tau seeded with brain homogenate from a post-mortem AD patient adopted the AD tau fold [140], establishing experimental conditions for studying the factors controlling structural specificity in tauopathies. With this tool in hand, it is now capable to use biophysical approaches to understand *how* tau templates its misfolded conformation in a strain-specific manner.

To investigate tau misfolding in PSP and CBD, we first amplified tau fibrils isolated from post-mortem patient samples in HEK293T cells engineered to express the repeat domain of tau (residues 244-378) with the P301L and V337M mutations fused to yellow fluorescent protein (YFP; Tau4RD*LM-YFP cells) to generated cell-passaged PSP and CBD seeds. Tau4RD*LM-YFP has been widely used in tau cellular seeding assays to understand tau strain biology [142, 50, 147, 152, 227, 233, 234, 100, 216, 149, 103, 145, 148]. We then used lysate from tau-infected cells to seed recombinant tau misfolding. Thioflavin T (ThT) and negative stain electron microscopy (EM) were used characterize the resulting fibrils and EPR-based double electron-electron resonance (DEER) spectroscopy was used to investigate protein structure during fibril formation. DEER provides an efficient and direct approach to characterize partial features of heterogeneous samples. It resolves the probability distribution of intramolecular distances from 1.5 to several nm ranges across a pair of spin-labels attached to the molecule of interest. Our results show that PSP and CBD seed-induced fibrils are conformationally distinct from heparin-induced recombinant tau fibrils, and a subpopulation recapitulates the CBD and PSP disease folds resolved using cryo-EM.

5.2 Results

5.2.1 Amplicfication of PSP and CBD patient materials in cultured cells requires expression of 4R tau

To investigate tau misfolding in CBD and PSP, we first established Tau4RD*LM-YFP cells that stably propagate tau aggregates isolated from deceased patient samples (schematic shown in Fig. 5.1a). Using a similar approach as previously described [27], tau prions were isolated from brain homogenates via sodium phosphotungstate (PTA), which

selectively precipitates aggregated proteins from soluble proteins [234, 235]. Protein pellets were then incubated with Tau4RD*LM-YFP cells for 4 days. The CBD and PSP patient samples induced YFP-positive tau puncta, whereas a control patient sample had no effect on the cells (Fig. 5.1b). Monoclonal cell lines stably propagating either CBD or PSP tau were generated following single-cell plating of infected cells. Expression of the 4RD-YFP construct was confirmed using lysate collected in RIPA buffer via Western blot (Fig. 5.1d).

Lysates from Tau4RD*LM-YFP cells infected with CBD and PSP patient samples were collected in 1X protease inhibitor, and were then used to seed recombinant truncated tau containing all four repeat domains with the familial P301L mutation, as well as the C-terminus (minus the first 10 residues of the first repeat; referred to here as Tau187). Importantly, the two naturally occurring cysteines in this construct were mutated to serines (C291S and C322S) to avoid the formation of disulfide bonds that may inhibit tau aggregation [31]. To determine if the cell-derived seeds could template tau misfolding, thioflavin T (ThT) fluorescence measurements were collected over the course of 24 hours. ThT is a fluorescent dye that has been established to bind specifically to β-sheet structures of amyloid proteins [236] and provides an *in situ* determination of β-sheet abundance. The CBD and PSP seeds induced an increase in ThT fluorescence, which was concentration-dependent (fluorescence intensity increased when 15% lysate was used compared to 5%; 5.2a. In comparison, polydisperse heparin (average molecular mass 15 kDa, Galen Lab Inc.) induce fibrillation and ThT fluorescence with a substantial increase in fluorescence emission, consistent with previous findings that heparin induces tau misfolding into conformations that are distinct from those present in CBD or PSP patient samples.

To confirm that the fluoresence increase in the ThT assay was due to the formation of tau fibrils instead of soluble molecules in the cell-derived lysates, we pelleted tau in

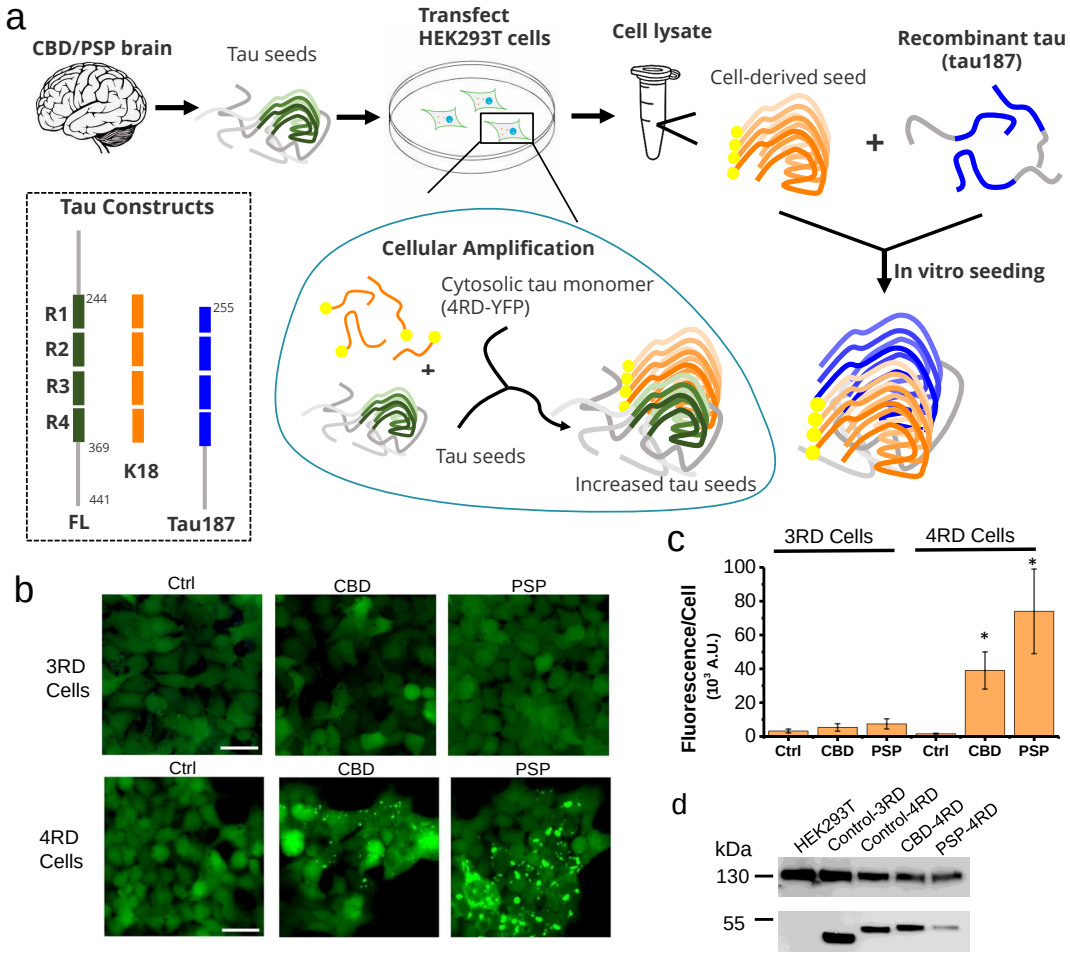

Figure 5.1: (a) Schematic of the cellular amplification of human materials and in vitro recombinant tau seeding with cell-derived seeds. The insert shows the tau constructs used in this study. (b-d) PSP and CBD human-derived materials propagated in Tau3RD(VM)-YFP cells (3RD cells) and Tau4RD(LM)–YFP cells (4RD cells). (b) Representative images of cells infected with CBD and PSP patient samples. YFP is shown in green. (Scale bar, 50 μm). (c) Quantification of cell infection of 3RD cells and 4RD cells using control (n = 6), CBD (n = 5), and PSP (n = 6) patient samples was determined by summing the total fluorescence in each image and normalizing to the cell count. Tau seeds isolated from CBD ($\{P < 0.001\}$), and PSP ($\{P < 0.001\}$) showed a significant increase in infectivity over the control samples in 4RD cells, whereas not in 3RD cells. Data are shown as the mean from five images per well in six wells. *$\{P < 0.05\}$.(d) Cell lysate from HEK293 cells, 3RD cells, 4RD cells, and CBD and PSP infected 4RD cells were analyzed for the presence of total tau-YFP by Westernblot with the YFP antibody.

the lysates by ultracentrifugation at 100,000 x g for 1 hour. Tau aggregates were then resuspended in 20 mM HEPES buffer (pH 7.4) and were used as seed. ThT fluorescence showed that the resuspended pellet induced aggregation of recombinant tau187 monomer while the supernatant did not (SI Figures, Fig. S5.1). The resuspended pellet generated a comparable plateau ThT value as non-centrifuged CBD seeds, indicating that the seeding capability of cell-derived seeds is from the tau aggregates. In summary, cell-derived seeds can induce recombinant tau to aggregate, and the amount of seeds used dictates the quantity of tau transforming into β-sheets. The capacity of the seeds to induce fibril formation is different from that of heparin since heparin-induced higher plateau ThT signal. To maximize the seeded fibril product, 15% seeds were used in subsequent experiments.

The morphology of the heparin- and seed-induced fibrils was characterized by negative stain EM. As shown in Fig. 5.2b, heparin-induced fibrils were long (straight and twisted, SI Figures, Fig. S5.1) whereas the CBD and PSP lysate-induced fibrils appeared twisted, with branching in some fibrils (SI Figures, Fig. S5.2). These findings are consistent with our ThT incorporation data indicating that heparin induced the formation of tau fibrils with a distinct conformation from the CBD- and PSP-induced fibrils.

To determine if the seed-induced fibrils exhibit prion-like activity, we infected the Tau4RD*LM-YFP cells with the heparin- and lysate-seeded fibrils. Visual comparison of the cells infected with heparin fibrils or seed-induced fibrils shows distinct aggregate morphologies (Fig. 5.2c).

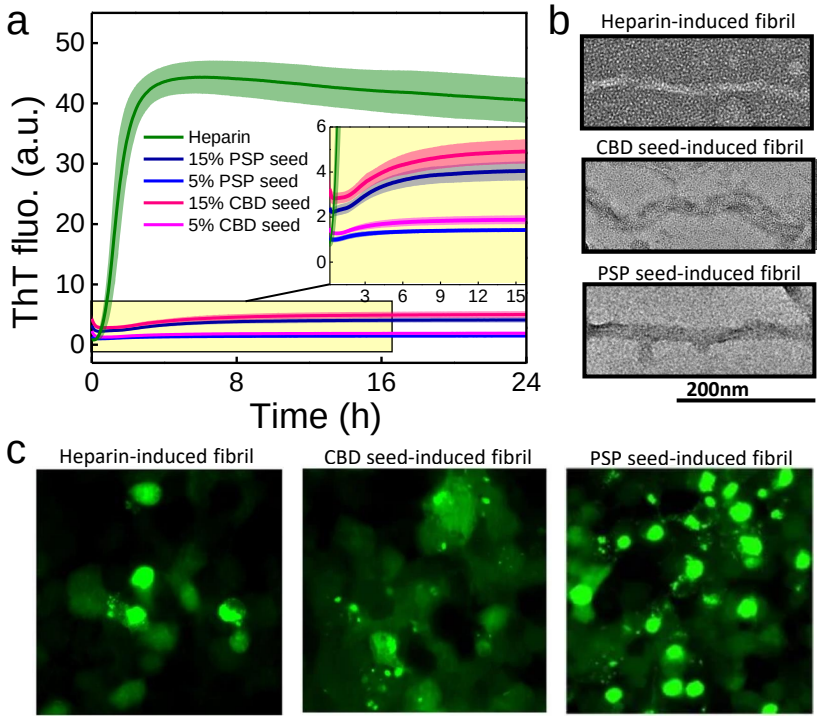

Figure 5.2: (a) ThT fluorescence of tau aggregation induced by heparin or seeds. The seeded aggregation has a relatively low maximum ThT and the curve was enlarged and shown in the insert. Tau187 at 25 μM concentration were mixed with stoichiometric amounts of heparin (8.25 μM), or 5% or 15% (w/w) of cell-derived seeds, and allowed to aggregate in the presence of ThT at 37 °C. (b) Representative negative stain TEM of heparin-induced fibrils and seed-induced fibrils. Full images are shown in Fig. S5.2. (c) Representative images of Tau(4RD*LM)–YFP(1) cells infected with heparin fibrils and seed-induced fibrils. YFP is shown in green. (Scale bar, 50 μm.)

5.2.2 PSP and CBD seeded tau fibrils have distinct conformations and a subpopulation recapitulates disease folds

To investigate the conformational features of the seed-induced fibrils, we employed DEER to probe local packing and intra-tau distances. DEER has the unique ability to measure distance distributions among samples in the 1.5–8 nm range between two electron spin-labels tethered to the protein. Because DEER is solely sensitive to paramagnetic probes, it is particularly well suited for tracking protein aggregation, where protein crowding and sample heterogeneity make the use of NMR, crystallography or cryo-EM

challenging. Previously, we have used DEER-based distance measurements to study the structure of heparin-induced fibrils and found that it is structurally heterogeneous and distinct from AD fibrils [26], and this result was later verified by cryo-EM [52]. Following a similar procedure as shown in Fichou et al. [26], the positions of the spin-label pairs were rationally chosen to locate on the outer layer of the fibril core in the CBD and PSP fibrils [10, 8] so that the spacial effect of spin-labels to tau protein aggregation and shape formation would be minimized. We also computed the expected distance distribution in CBD and PSP fibrils from patients using the RotamerConvolveMD method [131], and selected the spin-label pairs that are significantly different between the solution state and the aggregated states, as well as in CBD and PSP disease fold. Finally, three spin-label pairs were selected: 351-373, 334-360, and 340-378.

After the spin-label pairs were determined, we introduced two cysteines to tau187 at desired sites by site-directed mutagenesis. MTSL electron spin-labels were then tethered to the cysteine residues. In order to measure intramolecular distances, we diluted the spin-labeled protein (Tau-SL) with unlabeled tau187. Seeding performed with spin diluted tau187 (90% unlabeled tau + 10% Tau-SL) had ThT fluorescence result similar to unlabeled tau187 (SI Figures, Fig. S5.3). To prepare samples for DEER measurements, heparin or 15% seeds were added to spin diluted tau187 to induce aggregation, and after 24 hours of incubation, samples were subjected to dialysis (molecular weight cut off 25 kDa) against D_2O buffer to remove excess monomers. We then measured the distribution of intra-tau spin-label distance, r, by DEER. The distance distribution, P(r), was determined using Tikhonov regularization [136] in combination with WavePDS based denoising algorithms [120].

Fig. 5.3 demonstrates DEER-derived distances for heparin fibrils, CBD seed-induced fibrils, and PSP seed-induced fibrils compared with the simulated DEER distance distributions expected from cryo-EM CBD fold and PSP fold [10, 8] by the RotamerCon-

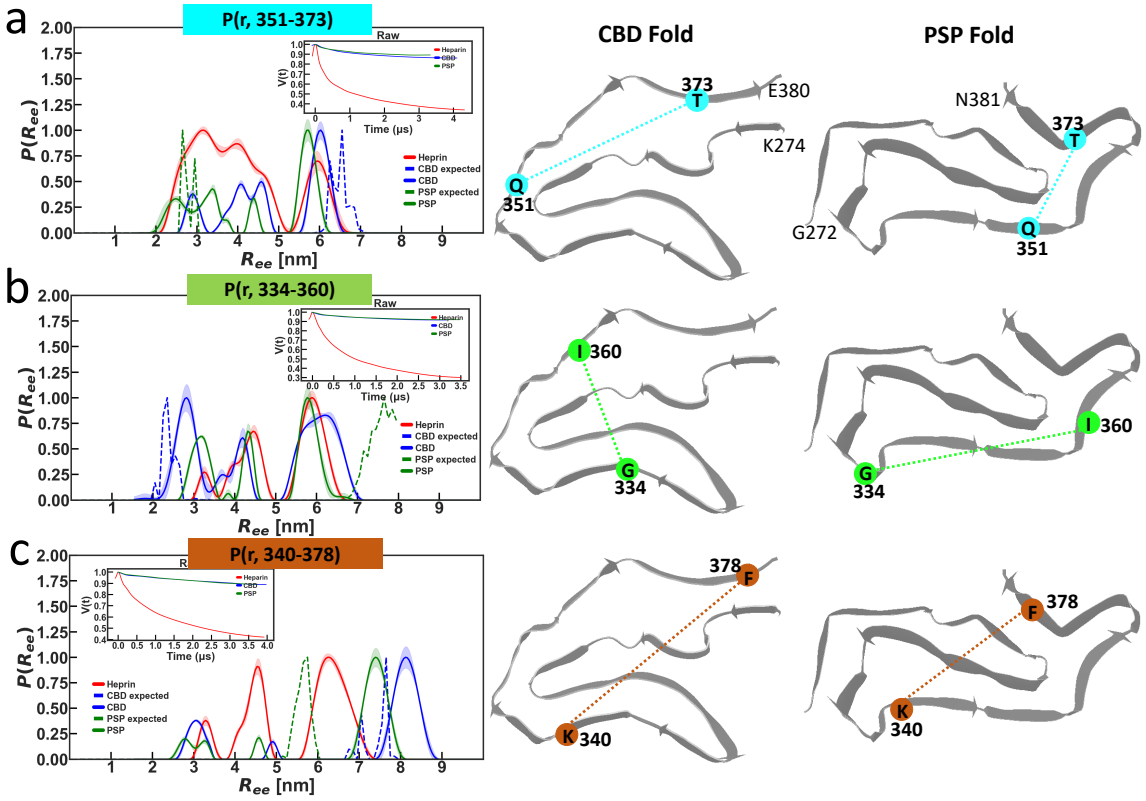

Figure 5.3: Intra-molecular DEER distance distribution, P(r), measured for heparin fibrils (red solid), CBD seed-induced fibrils (blue solid) and PSP seed-induced fibrils (green solid). Expected distances (doted curves) were similated from the published PDBs of cryo-EM CBD fold (6tjo) and PSP fold (7p65) [10, 8] by the Rotamer-ConvolveMD method [131] and were also illustrated on the schematic views of their cryo-EM folds. Three spin-label pairs were measured or simulated (a) residues 351-373 (b) 334-360 (c) 340-378. All replicates are shown in SI Figures, Fig. S5.4 and Fig. S5.5

volveMD method [131]. The schematic views of CBD and PSP folds are illustrated in grey, with the spin-label pairs highlighted for each P(r) for visualization. The spin-label pair at residue 351 and 373 was first used to compare the structures of different fibrils. As shown in Fig. 5.3a, heparin fibrils exhibited a broad distance distribution and were distinct from that of the CBD and PSP seed-induced fibrils, indicating that the heparin fibrils are structurally distinct from the seed-induced fibrils, and are more structurally heterogeneous (at least at this region). CBD and PSP seed-induced fibrils showed multi-

ple narrowed peaks, indicating multiple ordered conformers. The measured P(r) of PSP and CBD seed-induced fibrils had peaks close to the expected distances (marked in dotted lines), indicating that a subpopulation of the CBD and PSP seed-induced fibrils resembles the CBD and PSP fibrils found in patients, respectively. To investigate whether the same implication applies to full-length tau, we seeded recombinant 0N4R tau with CBD and PSP cell-derived seeds using the same protocol. 0N4R tau lack the acidic 29-residue inserts in the N-terminal and was found abundant in humans. The seed-induced 0N4R fibrils showed similar results as compared with tau187 (SI Figures, Fig. S5.6), so the conclusion is applicable to full-length tau.

We probe the existence of the C-shape found in the patient's CBD fibrils by measuring the distances between residues 334 and 360, and between residues 340 and 378. As shown in Fig. 5.3b, P(r, 334-360) of CBD seed-induced fibrils have multiple peaks, one of which was closed to the expected distance distribution. P(r, 334-360) of PSP seed-induced fibrils have a dominant, narrow peak centered around 7.5nm, close to the expected distance of 8nm. In contrast, the P(r, 334-360) of heparin fibrils is different from the measured P(r) of seed-induced fibrils. Similar results can be observed in Fig. 5.3c for the distance spanning residues 340 and 378, P(r, 340-378). Therefore, the results demonstrated that the seed-induced fibrils are structurally different from the heparin fibrils, and are more structurally defined. Besides, in R3 to early C-terminus region, a subpopulation of the seed-induced fibrils resembles the CBD and PSP fibrils derived from patients. These show, at high resolution, that cell-derived CBD and PSP seeds can guide partial structural convergence of recombinant tau, suggesting that cell-derived seeds may transmit their structural properties to naïve tau by templated seeding.

5.3 Discussion

We have demonstrated that patient-derived CBD and PSP seeds can be amplified in 4R-containing cells but not in 3R-containing cells, suggesting the isoform specificity of these 4R tauopathies as previously established [237, 27]. We have successfully performed *in vitro* seeding of recombinant tau with the cell-derived CBD and PSP seeds without any added cofactor or sonication treatment of the seeds. The cell-derived seeds recruited recombinant tau (either full-length or truncated tau) and formed seed-induced fibrils, albeit the extent of the seeded aggregation is relatively low compared with heparin-induced aggregation. Using DEER-based distance measurements, we have shown at high resolution that the CBD and PSP seed-induced fibrils had better-defined structures compared with heparin fibrils (Fig. 5.3). Importantly, partial features from the measured distance distributions of the seed-induced fibrils were similar to the expected distance distribution simulated from the CBD fold and PSP fold [10, 8], indicating a subpopulation of the seed-induced fibrils resembles the CBD and PSP fibrils derived from patients at the R3 to early C-terminus region.

Our results agree with the prevalent hypothesis that tau spreads in a "prion-like" behavior: pathological tau aggregates populate specific tau strains to native protein through seeding. The diverse tauopathies' fibril conformations revealed by cryo-EM [7, 8, 9, 10, 11, 12, 12] supports tau strain hypothesis and its unambiguous link to disease. However, what features the tauopathy fibril conformations are conserved in seeding, if at all, has not been shown at high resolution. Previously, morphological evidence and biochemical properties are often used as evidence for tau conformations, such as macroscopic morphology [47, 104], secondary structure [47], binding to conformation-dependent antibodies [108], and proteolysis patterns[105, 106]. Similar features between the seed-induced fibrils and the seeds are used as indications of tau templated seeding

[47, 42, 25, 46, 38, 106, 107, 104, 105, 108]. For example, Kaufman et al. [49] isolated and characterized 18 tau strains that originated from either recombinant protein, tauopathy mice, or patient brains. The isolated strains were distinguished by multiple methods including inclusion morphology, detergent solubility, seeding, proteolytic digestion, and toxicity. After inoculating transgenic mouse brains with the 18 strains, the unique neuropathology patterns of each strain were faithfully transmitted, indicating that the seed-induced fibrils in mice are similar to the seeds. In a more recent study, Xu et al. showed that recombinant tau fibrils generated with AD patient-derived seeds is similar to AD-tau in terms of their ultrastructure, solubility, and conformation, as detected by conformation-dependent antibody DMR7 and MC1 that selectively bind to AD tau aggregates, indicating that AD-tau may have templated the aggregation of recombinant tau. [108] However, some studies found that the seeded tau fibrils are different from the seeds due to different protease digestion patterns and macroscopic morphology [105, 41]. Therefore, high-resolution evidence is needed to verify the templated seeding in the tau strain hypothesis.

Here, we found that partial distance features of seed-induced fibrils were similar to the expected distance from cryo-EM CBD fold and PSP fold, indicating that we achieved partial convergence to these disease fibrils by seeding. A few factors may account for partial convergence instead of full convergence. Firstly, the cell-derived seeds were generated in cells expressing 4RD tau, which lacks N-terminus and C-terminus. Although the 4RD tau in cells may be templated by human materials, residues outside of the MTBR (especially the 369KKIETHKLTF378 segment in the C-terminal region which is lysine-dense) could contribute to tau folding and strain propagation, so the CBD and PSP folds may only be formed partially in cells. Moreover, a recent report suggests that the fusion of 4RD tau to fluorescent proteins may induce steric hindrance and inhibit tau aggregation [102]. Therefore, the cell-derived seeds may be imperfect and

further experiments with cells expressing full-length tau will be timely. Secondly, the *in vitro* seeding conditions used in this study may not favor the propagation of specific strains, so multiple conformers were populated. In fact, a recent study with cryo-EM [140] showed that the addition of salt such as sodium chloride changed the shape of tau fibrils and by changing the buffer condition of the tau construct used, the authors generated recombinant tau fibrils identical to the AD fold or CTE fold. Therefore, further optimization of the buffer conditions and tau monomer substrate is needed to investigate how to fully converge recombinant tau into disease fibrils.

Furthermore, our results showed that DEER-based distance measurements can serve as an important tool to study heterogeneous tau fibril samples and inform future cryo-EM studies. Although cryo-EM tau structures [7, 8, 9, 10, 11, 12, 12] have rightfully captured the field's attention, this method has limitations: a relatively small number of homogeneous brain samples can be studied, and only after extensive purification of fibrils from large quantities of brain material. Besides, there is no structural information for residues outside of the amyloid core that could contribute to strain formation, and only large detergent-insoluble fibrils have been successfully imaged, which may not represent the critical tau intermediates such as oligomers. In contrast, EPR-based DEER spectroscopy provides an efficient and direct approach to characterize partial features of heterogeneous samples, even of disordered proteins and partially aggregated biomolecules. It resolves the probability distribution of intramolecular distances in the 2 to several nm ranges across a pair of spin-labels attached to the molecule. Therefore, DEER can be used for discovery work on heterogeneous samples or to capture transient conformational ensembles along the course of strain formation or seeded aggregation. After the conditions for structural convergence is achieved, cryo-EM can and will be used to characterize the product.

In summary, we have demonstrated that the recombinant tau fibrils induced by CBD

and PSP cell-derived seeds are structurally distinct from heparin-induced fibrils, and a subpopulation of the seed-induced fibrils resembles the CBD and PSP fibrils from patients in the R3 to early C-terminus region. These findings established that disease folds are replicated at least partially through seeding, and the tau strains hypothesis is partially verified at high resolution. Awareness and knowledge of tau strains will guide both therapy and diagnosis. For example, unique conformations of tau will determine the efficacy of small molecules in positron emission tomography (PET). For example, tau strains found in tauopathies can guide us to design PET ligands that target a subset of tauopathies but not others by target binding with a specific local conformation [238], and seed-induced fibrils generated with recombinant tau can be used for molecule screening.

5.4 SI Figures

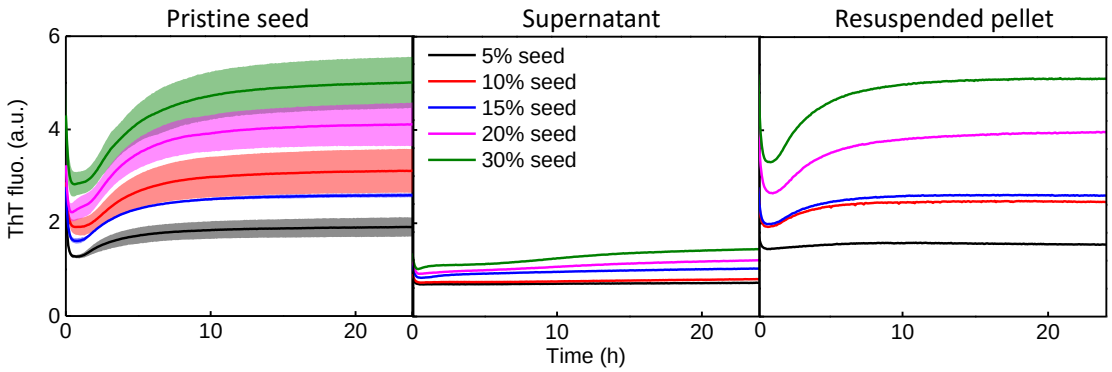

Figure S5.1. ThT fluorescence of aggregation of tau induced by prestine CBD seed, supernatant from ultracentrifuge, and resuspended pellet. Supernatant and pellet were obtained by ultracenrifuging cell-derived CBD seeds at 100,000 g for 1h at 4C. The pellet was resuspended in 20mM HEPES buffer (pH 7,4). Same volume of the buffer was used here as the non-centrifuge seed.

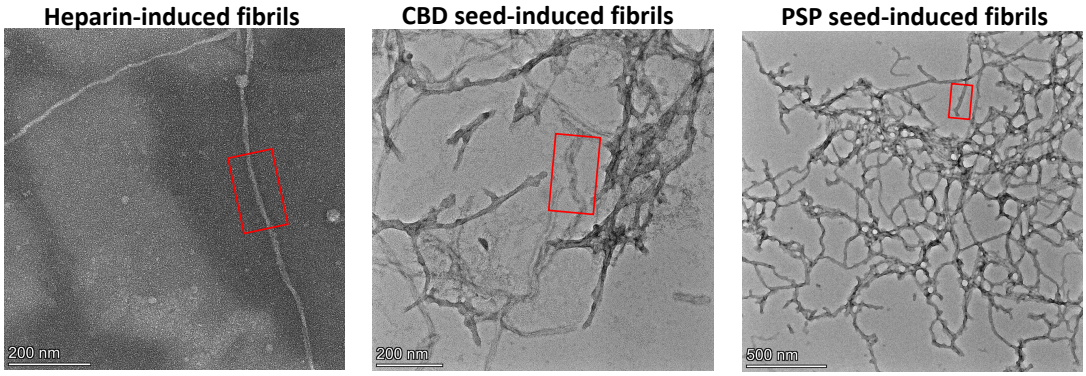

Figure S5.2. Full TEM images of tau hepafin fibrils and seed-induced fibrils. The red box in the images represent where the representative fibrils morphology was taken for Fig. 5.2,

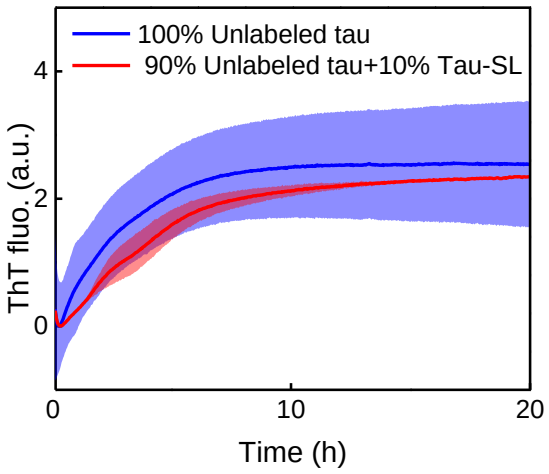

Figure S5.3.ThT fluorescence of CBD seed-induced aggregation of spin-dilute tau. 15% CBD seed was mixed with unlabeled tau or spin-dilute tau (90% unlabeled tau + 10% labeled tau). Absolute concentrations were 50 μM for tau, 20 μM for ThT respectively. 165 μg of seeds were added.

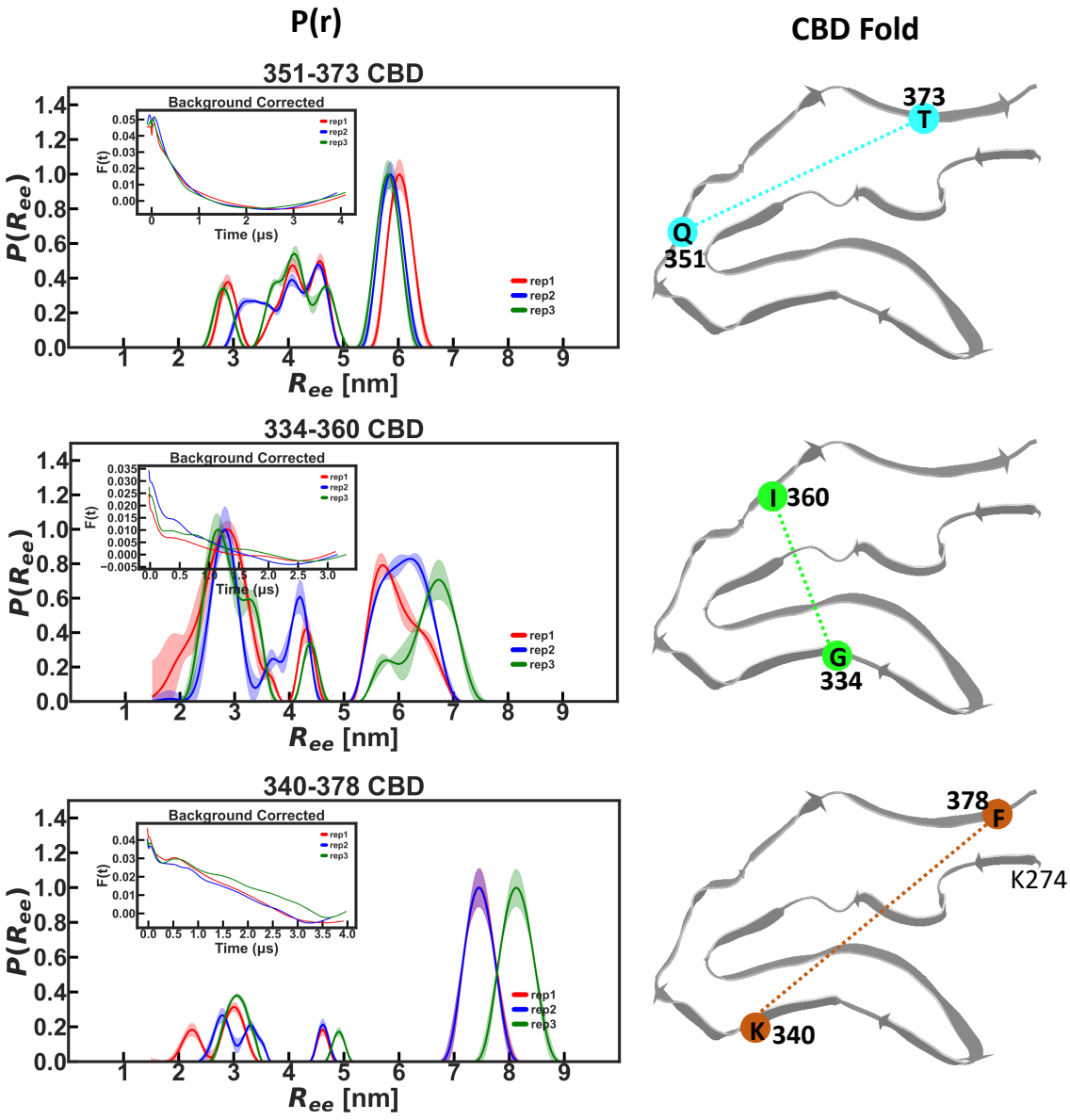

Figure S5.4. DEER distance measurements of CBD-induced fibril: replicates and background corrected data. Inserts in the P(r) are the background corrected time-domain data.

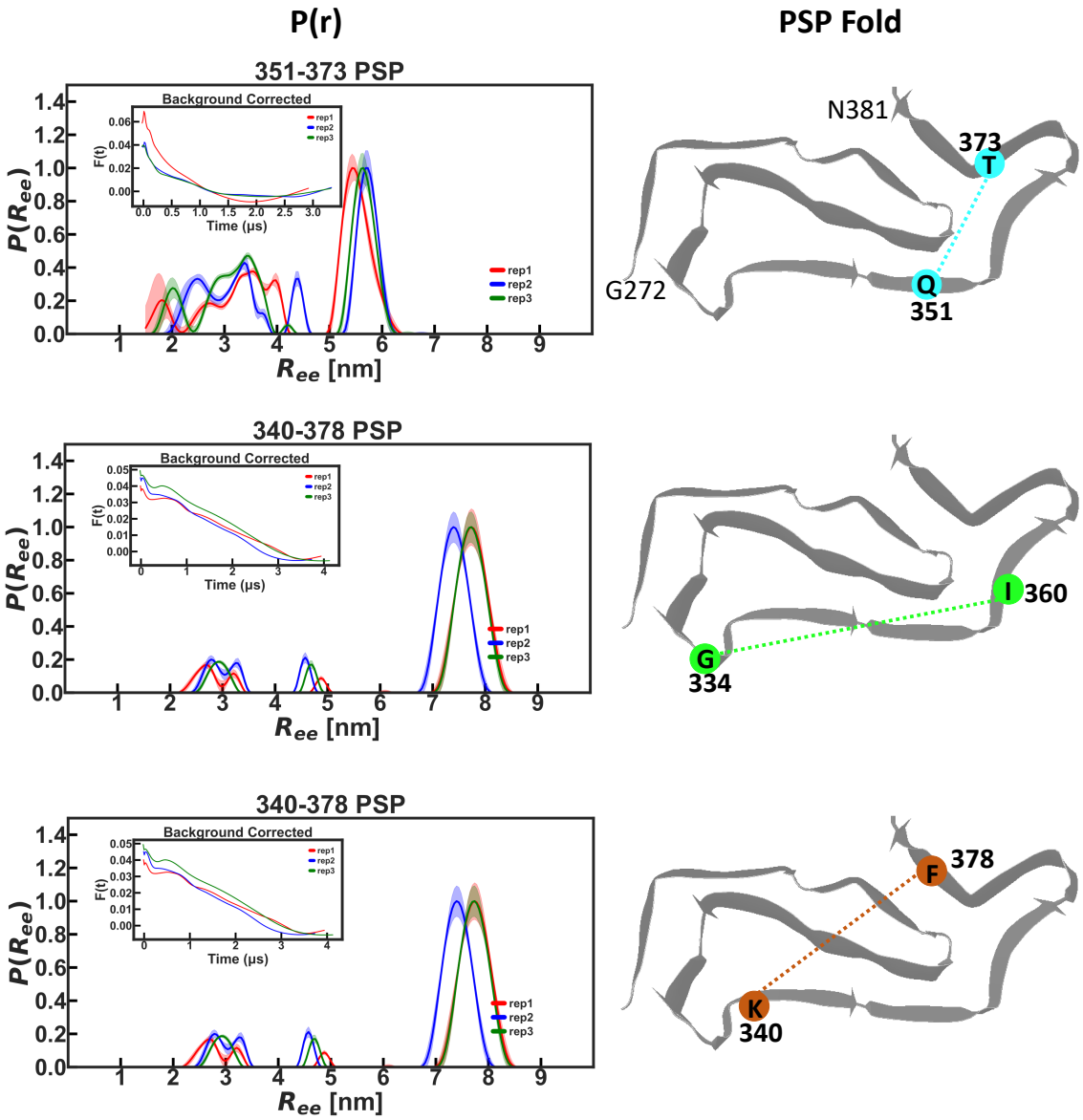

Figure S5.5. DEER distance measurements of PSP-induced fibril: replicates and background corrected data. Inserts in the P(r) are the background corrected time-domain data.

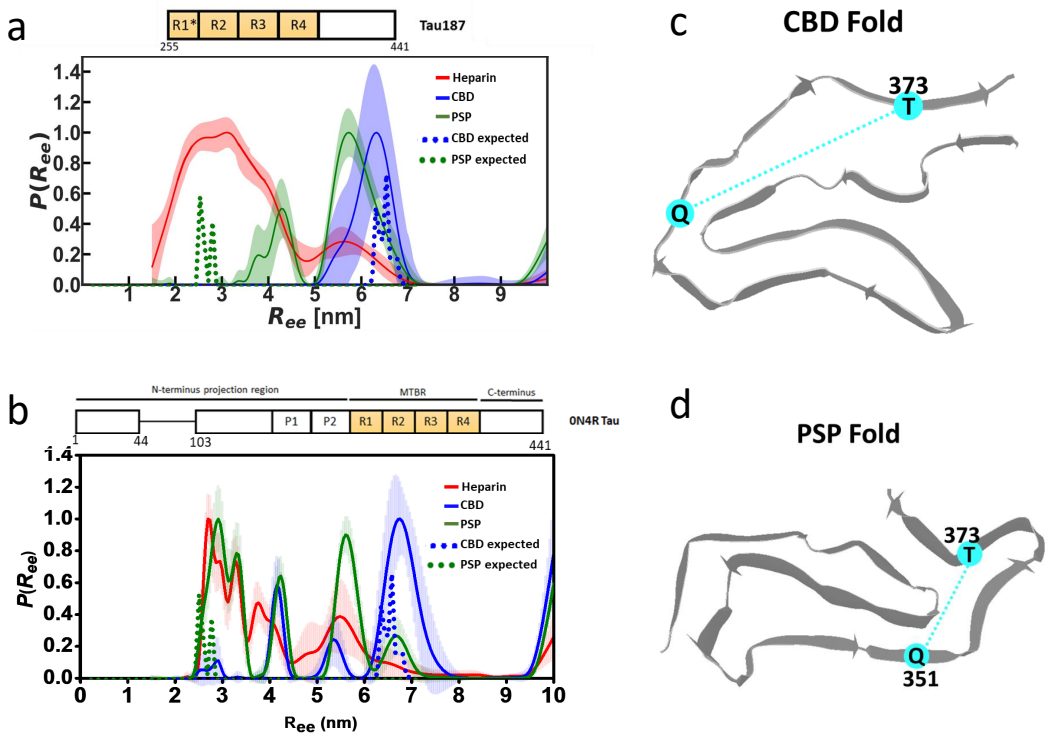

Figure S5.6. Comparison of tau187 and 0N4R tau including the schematic representation of tau, and the P(r) spanning 351-373 (a) Tau187 (b) P(r) 0N4R. (c) and (d) schematic views of CBD and PSP cryo-EM folds. Labeled sites at residue 351 and 373 are highlighted

5.5 Permissions and Attributions

1. The content of chapter 5 is the result of a collaboration with Professor Amanda Woerman from University of Massachusetts Amherst, and we are preparing the manuscript together. We plan to submit it to Nature Structural and Molecular Biology.

Chapter 6

Conclusion and Outlook

The concept that the spreading of tau pathology in tauopathy occurs by a "prion-like" mechanism is gaining popularity. The key elements of this hypothesis are that diverse conformational tau strains exist in different tauopathies and that they induce templated seeding of monomeric tau in cells. The distinct tauopathy fibril conformations revealed by cryo-EM [7, 8, 9, 10, 11, 12, 12] supports the theory of tau strains. However, despite the evidence hinting at the existence of prion-like tau seeds or strains in brain tissues in tauopathies that can induce templated seeding in mouse models or *in vitro* [16, 17, 18, 19, 20, 21, 22, 23, 24, 25, 26, 27], many present studies used similar patterns of neuropathological lesions in mouse, morphological appearance in cells at a microscopic level, or relative resistance to proteolytic enzymes as evidence for conformations. More work is needed to document at high resolution the structural characteristics of tau strains and the exact structural features that are transmitted and preserved in tau seeding. The work described in this dissertation employed the unique spectroscopic tools that the Han lab specializes in to investigate the role of commonly used experimental conditions in the determination of tau fibril shapes and to probe the structural properties of the fibril that are replicated and propagated in tau seeding at high resolution.

To achieve robust *in vitro* seeding with recombinant tau, I set out to explore experimental conditions that promote tau seeding, and to understand how these conditions affect tau aggregation and shape formation, which is presented in chapters 2 to 4. The first key condition I addressed was the use of reducing agents, such as DTT. I found that incubation under reducing conditions or mutation of cysteine to another uncharged residue leads to increased aggregation. Both intermolecular and intramolecular disulfide bonds hinder tau aggregation, and disulfide bonds are not the driving force for tau aggregation. Another key condition I addressed was the use of polyanionic cofactors (e.g. heparin). Tau fibrils in tauopathies have been observed to be associated with non-tau molecules so cofactors might play a role in disease pathogenesis [10, 8, 11]. Recombi-

nant tau assembly can be triggered in vitro by heparin and RNA. The strongly negative charges on each of these molecules are likely to act as critical motifs for interaction with tau. As *in vitro* seeding, some studies included cofactors in the seeding reaction buffer without explaining their roles [42, 43, 44, 45, 46]. Whether the cofactors serve as reactants that incorporate into the product fibrils or only act as catalysts that can be removed without breaking the fibrils has not been elucidated. In chapter 3, I have shown that cofactors, specifically heparin and RNA, bind to tau proteins, and are incorporated into tau fibrils at specific stoichiometry and that cofactors are essential for *in vitro* seeding. The results suggested that in neurons under pathological conditions, tau aggregation can be facilitated by interactions with polyanionic cofactors.

Besides the use of reducing agents and cofactors in seeding reaction, tau seeds are often subjected to sonication before the treatment of cells or recombinant monomer [37, 38, 39, 40, 41]. Inspired by a recent study showing that monomeric tau release from heparin-induced fibrils by sonication maintains aggregate-templated conformations that provide high seeding capacities [39], I set out to understand the effect of sonication on tau fibrils and the nature of tau seeds. In chapter 4, I have shown that sonication induces artificial segmentation in heparin-induced tau fibrils and fibril fragments are seeding competent to trigger further amyloid formation in cells and with recombinant tau. Mass spectrometry results have shown that upon sonication, tau fibril is more protected compared with monomer. Since tau fibrils are fragmented randomly during sonication and it is not clear which fragment is responsible for the seeding activity observed.

Finally, with the above-mentioned knowledge of the experimental conditions for seeding, I further optimized *in vitro* seeding protocol and achieved robust seeding using disease-relevant tau seeds derived from HEK293T cells expressing tau upon seeding with CBD or PSP patient materials, as described in chapter 5. In the final seeding protocol, no reducing agent or cofactor was needed, and the seeds were not subjected to sonication

treatment. Robust seeding was obtained by seeding recombinant tau with 15% (w/w) CBD or PSP cell-derived seeds. Electron paramagnetic resonance (EPR) based double electron-electron resonance (DEER) distance measurements coupled with site-directed spin-labeling (SDSL) were used to investigate the structure of tau fibrils produced from seeding at high resolution. I have shown that CBD and PSP seed-induced fibrils have distinct conformations compared with heparin-induced fibrils, and a subpopulation recapitulates part of CBD and PSP disease folds. These results indicated that by controlling the experimental conditions and by using shape-defined seeds, tau can be partially converged towards disease folds. Furthermore, I have shown that DEER-derived P(r) data can serve as a critical intermediary tool to characterize partial features of the tau conformational ensembles, irrespective of structural heterogeneity in the sample, and to investigate the structural propagation of tau during seeded aggregation. DEER offers an approach to exploring the key factors that lead to structural convergence to disease-phenotypic fibril structures and it will be useful to inform future cryo-EM or ssNMR studies.

As I have shown that recombinant tau can be partially converged towards PSP and CBD disease folds through *in vitro* seeding, it becomes crucial to understand how to achieve full convergence to the disease-phenotypic fibril structures. In fact, disease mutations may play a role. For example, the V337M mutation was identified in some patients with frontotemporal dementia with parkinsonism-17 (FTDP-17) and has been associated with prominent antisocial behavior and paranoia and severe frontotemporal and limbic degeneration [239, 240]. Consistent with the previous report, I found that V337M mutation promoted tau aggregation *in vitro* (as shown in Fig. 6.1a). Tau187 with both V337M and P301L mutation generated the highest plateau ThT value. Preliminary DEER distance measurements on heparin-induced fibrils of tau with and without V337M showed that V337M may shift the distance slightly to a larger distance (Fig. 6.1b).

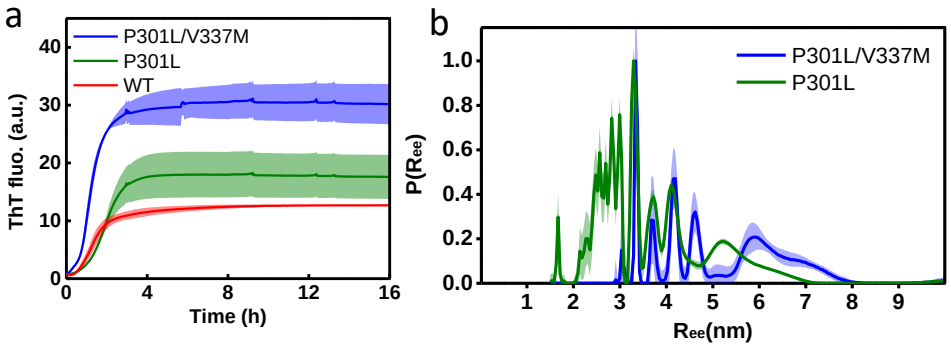

Figure 6.1: V337M mutation affect tau aggregation and fibril shape. (a) ThT fluorescence of heparin-induced aggregation of wilde-type tau without any disease mutation (WT), tau with aggregation promoting P301L mutation (P301L), and tau with both P301L and V337M mutations (P301L/V337M). (b) Intra-molecular DEER distance distribution spanning residues 351-373 measured for heparin fibrils of P301L tau and P301L/V337M tau.

Furthermore, our lab is currently working on generating structurally-defined fibrils with tau fragments, such as HP1-5 (Fig. 6.2). Specifically, HP2, spanning the residues 295 to 313 with P301L, is expected to form fibrils with a hairpin structure. We plan to use HP2 fibrils as seeds and investigate how they induce aggregation and folding beyond the core.

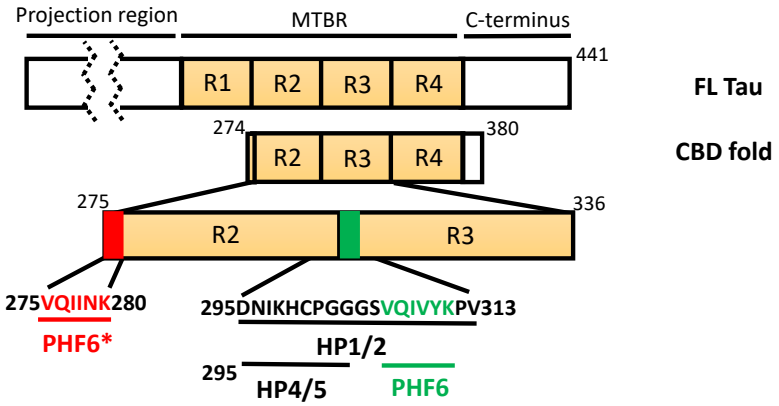

Figure 6.2: schematics of tau constructs

We are also employing post-translational modifications (PTMs) and different salts in buffers to screen conditions for generating structurally-defined fibrils with fibril mor-

phology similar to the paired helical filaments (PHFs). For example, HP2 forms more fibril bundles in buffer with ammonium sulfate or sodium chloride as compared with fibrils made in buffer without salt (ctrl) (Fig. 6.3). Besides, phosphorylation or pseudo-phosphorylation can be done with the serine at position 305. The phosphorylated HP2 peptide is then aggregated with heparin Preliminary results from TEM showed that the phosphorylated tau generates fibril morphologically different from HP2 without phosphrylation (Fig. 6.3). Whether these conditions affect structural convergence or how buffer conditions affect seeding is ongoing.

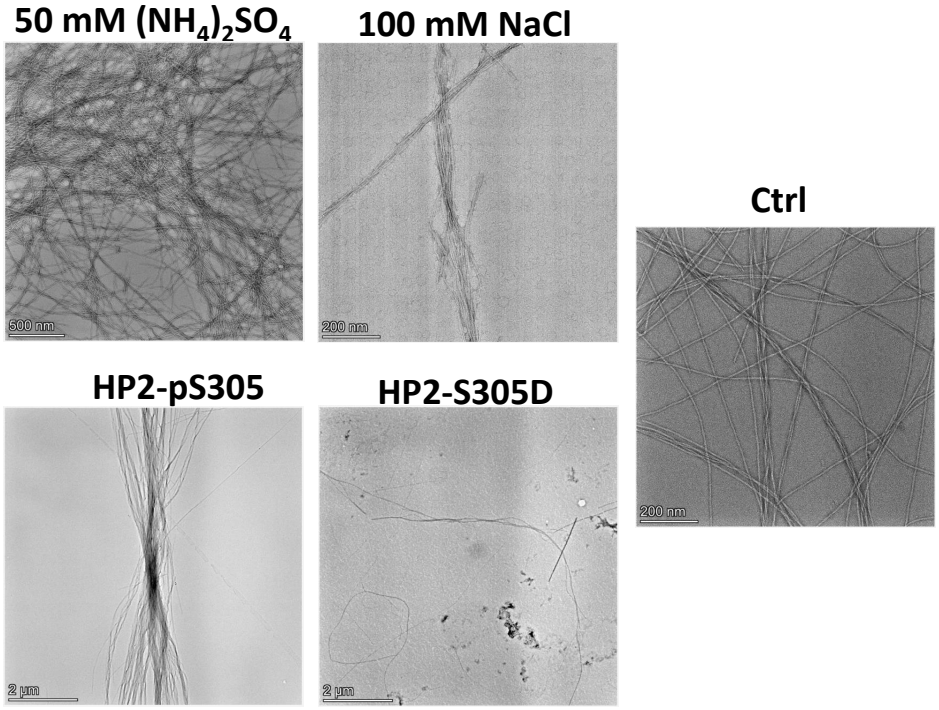

Figure 6.3: Representative TEM images of heparin-induced of HP2 made in 20mM HEPES buffer with different concentration of salts, with phosphorylation (HP2-pS305) or with pseudo-phosphorylation (HP2-S305D). Control is heparin-induced HP2 fibrils (ctrl) made in buffer without salt or phosphorylation.

Nonetheless, knowledge of tau strains and structural convergence through seeding will be useful for guiding therapy and diagnosis. Specifically, when a total structural

convergence to tauopathy folds with recombinant tau is achieved, these fibrils will be very useful for screening small molecules in positron emission tomography (PET) that binds specifically to these strains, allowing the diagnosis of tauopathies. Moreover, anti-seeding approaches may be developed to disrupt seed propagation to suppress neurodegeneration and lead to clinical benefits. The *in vitro* studies will further guide *in vivo* studies, and may soon translate to patients.

Appendix A

Materials and Methods

A.1 Protein expression and purification

In Chapter 2 to 4, 20 mM ammonium acetate buffer at pH 7.0 was used for tau or other stocks and as assays running buffer. In chapter 5, 20mM HEPES at pH 7.4 was used for tau or other stock and as assays running buffer.

N-terminal truncated, microtubule binding domain containing tau187 (residues 255-441 with a His-tag at the N-terminus) were used for *in vitro* studies. Mutated variants of tau187 were prepared using site-direct mutagenesi: C322 tau187 with C291S mutation, and cystein-less tau187 (cysless) with C291S and C322S muatation used in chapter 2; tau187 P301L contains P301L mutation, tau187 C291S/P301L contains C291S and P301L mutations, tau187 C291S/C322S contains C291S and C322S mutations, tau187 G272C/S285C contains C291S, C322S, G272C and S285C mutations, and cysless tau187 P301L/G272C/S285C contains C291S, C322S, G272C and S285C mutations used in chapter 3; cysless tau187 P301L/Q351C/T373C contains C291S, C322S, Q351C and T373C, cysless tau187 P301L/G334C/I360C contains C291S, C322S, G334C and I360C, cysless tau187 P301L/K340/F378C contains C291S, C322S, K340 and F378C. Besides, mutated

variants of full-length 0N4R tau used in chapter 5 was produced in a similar way.

The cloning, expression, and purification of tau have been previously described [179]. Shortly, the gene encoding desired tau187 tau or 0N4R tau was cloned into a pET-28a vector and was tranfected into E. coli. BL21 (DE3) competent cells (Novagen). E. coli BL21 (DE3) cells were cultured from frozen glycerol stock or from plates overnight in 10 mL luria broth (LB) which was used to inoculate 1 L of fresh LB. Culturing and inoculation were performed at 37 °C with shaking of 200 rpm. At OD 600 of 0.6-0.8, tau187 variant expression was induced by incubation with 1 mM isopropylß-D-thiogalactoside (Sigma Aldrich) for 2-3 h. Cells were harvested by centrifugation for 10 min at 5000 × g (Beckman J-10; Beckman Instruments,Inc.), and the pellets were stored at -20 °C until further use. Cell pellets were resuspended in lysis buffer (Tris-HCl pH 7.4, 100 mM NaCl, 0.5 mM DTT, 0.1 mM EDTA, 1mM PMSF) with 1 Pierce protease inhibitor tablet (Thermo Fisher). Lysis was initiated by the addition of lysozyme (2 mg/ml), DNase (20 μg/ml), and $MgCl_2$ (10 mM) and incubated for 30 min on ice. Lysate was then heated to 65 °C for 13 min, cooled on ice for 20 min and then centrifuged to remove the precipitant. The supernatant was loaded onto a Ni-NTA agarose column pre-equilibrated with wash buffer A (20 mM sodium phosphate pH 7.0, 500 mM NaCl, 10 mM imidazole, 100 μM EDTA). The column was then washed with 20 ml of buffer A, 15 ml buffer B (20 mM sodium phosphate pH 7.0, 1 M NaCl, 20 mM imidazole, 0.5 mM DTT, 100 μM EDTA). Purified tau187 was eluted with buffer C (20 mM sodium phosphate pH 7.0, 0.5 mM DTT, 100 mM NaCl) supplemented with varying amounts of imidazole increasing from 100 mM to 300 mM. The protein was then concentrated via Amicon Ultra-15 centrifugal filters (MWCO 10 kDa; Millipore Sigma) and the buffer was exchanged into final buffer (20 mM ammonium acetate buffer at pH 7.0, or 20mM HEPES at pH 7.4) by PD-10 desalting column (GE Healthcare). To further purify the protein, size exclusion chromatography was conducted by injecting 2-5 mL sample onto HiLoad 16/600 Superdex

200 Column (GE Healthcare Life Sciences) connected to a BioRad NGC Quest 10 FPLC system, and 1.5 mL fractions were collected with a BioFrac fraction collector (BioRad). Prior to sample injection, the column was washed by 130 mL degassed Milli-Q water at a flow rate of 0.8 mL/min and equilibrated with 160 mL degassed working buffer (20 mM ammonium acetate buffer at pH 7.0, or 20mM HEPES at pH 7.4) at 0.8 mL/min. Samples were eluted from the column with 150 mL working buffer at 0.6 mL/min after sample injection. Fractions of each elution peaks were collected right after elution. Elution peak assignment was done by comparing with the elution profile of purified tau187 monomers. Fractions corresponding to monomer were concentrated using Amicon Ultra-4 centrifugal filters (MWCO 10 kDa; Millipore Sigma). The final protein concentration of tau187 was determined by UV-Vis absorption at 274 nm using an extinction coefficient of 2.8 $cm^{-1}mM^{-1}$ calculated from absorption of Tyrosine. The final protein concentration of tau187 was determined by UV-Vis absorption at 274 nm using an extinction coefficient of7.45 $cm^{-1}mM^{-1}$ calculated from absorption of Tyrosine.

A.2 Thioflavin T fluorescence spectroscopy measurement of tau aggregation

In vitro tau aggregation were carried out in working buffer (20 mM ammonium acetate buffer at pH 7.0 was used in chapter 2-4, or 20mM HEPES at pH 7.4 was used in chapter 5). 20 μM ThT dye was added into 50 μM tau187 with or without 1 mM DTT in Corning™ 384-Well Solid Black Polystyrene Microplates (Thermo Fisher Scientific). Then, heparin was mixed in the samples at the mole ratio of 4:1 (tau187: heparin) to induce aggregation. In chapter 2, ThT fluorescence was monitored by Tecan infinite 2000Pro Plate Reader with the excitation at 440 nm and emission at 480 nm over a period of 14 18h at 37

°C (gain was set to 100). One data point was taken every 2 minutes. Measurements were done in triplicate. The figures showed the average and standard deviations. RNA-induced tau fibrils (RNA fibrils) in chapter 3 were prepared by mixing 20 μM of tau with 300 μg/ml RNA (polyU, Sigma, P9528). 20 μM ThT was added to the mixture, and the samples were immediately pipetted to a 384-well plate (Corning, 3844) and incubate at 37 °C. In chapter 3-5, fluorescence intensity was monitored in a Bio-Tek Synergy 2 microplate reader (excitation 440/30, emission 485/20, number of flash 16). When ThT fluorescence reached maximum, samples were collected to be heparin-induced tau fibrils.

A.3 Size exclusion chromatography

In chatper 2, disulfide-linked dimer and monomer of tau were separated by injecting 2 mL sample without DTT onto size exclusion column HiLoad XK 16/600 prepacked with Superdex 200 (GE Healthcare Life Sciences) connected to a BioRad Duoflow FPLC, and 1 mL fractions were collected with a BioFrac fraction collector (BioRad). Prior to sample injection, the column was washed by 130mL degassed Mili-Q water at a flow rate of 0.5mL/min and equilibrated with 260mL degassed running buffer (20 mM ammonium acetate, 100 mM sodium chloride) at 1mL/min. Samples were eluted from the column with 150 mL running buffer at 1mL/min after sample injection. Fractions of each peak were collected and concentrated using Amicon Ultra-4 centrifugal filters (Fisher Scientific, UFC801024) right after elution and were analyzed for monomeric and dimeric state by BN-PAGE. For SEC elution peak assignment, the elution of standard samples ranging from 17 kDa to 440 kDa (eluted at 1mL/min) was used for reference according to HiLoad Superdex 200 prep grade manual (data file 18-1100-52 AE). Dimeric tau187 is 44 kDa, whose elution peak matched the position of 44 kDa standard sample. Accordingly, monomeric tau187 elution peak could be assigned.

A.4 Tau fibrils digestion

Digestions of heparin were carried out by incubating heparin fibrils with Bacteroides heparinase I (heparinase, New England Biolabs Inc. P0735S) and incubated at 30 °C for 8 hours. Digestions of RNA were carried out by incubating RNA fibrils or seed-induced fibrils with RNase A (RNase, Thermo Scientific, AB-0548) at room temperature for 8 hours. Different concentration of heparinase/RNase were used (in all figures, 1× heparinase: 1 Units of enzyme per 1 μg of heparin; 1× RNase: 2.5 μg/mL). The sample denoted as "Control" in Fig. 3.1, "Non-digested" in Fig. 3.2 and "Non-digested fibril" in Fig. 3.3A followed the identical incubation times and temperatures than the digested samples but received buffer instead of enzymes. Pelleted fibrils (used in Fig. 3.2B RNA fibrils, and Fig. 3.3A) were prepared from tau fibrils before digestion, by centrifugation at 53,000 rpm (TLA-100.3 rotor) for 1h and resolubilizing in working buffer. The seed-induced fibril swere digested with 1x RNase. Quantification and characterization of digested heparin and RNA, and re-aggregation from digested fibrils were described in the published paper [25].

A.5 In vitro seeding

In chatper 3, in the first generation, 20 μM tau187C291S in (100 mM NaCl, 20 mM ammonium acetate) was seeded with 5% mass of either mouse-extracted fibrils or heparin-induced fibrils. The heparin-induced fibrils were sonicated in a bath sonicator for 20 min before uses. 20 μM thioflavin T was present in the buffer. "+cofactor" denotes the presence of 120 μg/ml polyU RNA while "-cofactor" demotes no RNA added. After seed addition, samples were placed in a 384-well microplate (Corning 3844) and ThT fluorescence was measured in a plate reader (Biotek Synergy 2) at 37 °C with shaking.

After 24 h, the samples were used as seeds for the second generation. 10% mass of the end product of the first generation was added, after 20 min sonication in a bath sonicator, to fresh tau187C291S with or without cofactor. First generation with/without cofactor was used to seed second generation with/without cofactor, respectively.

In chapter 4, 50 μM cysless P301L tau187 was preincubated with 12.5 μM heparin in 20 mM ammonium acetate overnight to prepare tau-heparin fibrils. Preincubated tau-heparin fibrils were subjected to sonication with probe sonicator (Omni International) and used as the seed for the seeding experiment. 5% (molar ratio) of seed was mixed with the freshly prepared tau monomer and designated concentration of polyanions in the presence of 20 μM ThT. Fluorescence was monitored with Bio-Tek Synergy 2 microplate reader.

In chapter 5, 5% to 15% (protein mass percentage) of CBD and PSP cell-derived seeds were incubated with 50 μM cysless P301L tau187 in 20 mM HEPES buffer to make seed-induced fibrils. 20 μM ThT was added to the mixture and the fluorescence was monitored Bio-Tek Synergy 2 microplate reader.

A.6 Blue Native Polyacrylamide Gel Electrophoresis (BN-PAGE).

BN-PAGE was prepared on Thermo Fisher Scientific NtivePAGE™ Bis-Tris Gel System. Cathode Buffer and Anode Running Buffer were prepared and cooled prior to use. 4μg of protein samples were premixed with NativePAGE Sample Buffer (4X) and NativePAGE 5% G-250 Sample Additive. Then, NativePAGE 3-12% Bis-Tris Protein Gels (1.0 mm, 10-well, Thermo Fisher Scientific) was prepared and oriented in Mini-Cell. All sample wells were filled with Cathode Buffer (1X) for better visualization. Samples and

protein standard were loaded. The upper buffer chamber was filled with Cathode Buffer (1X) and lower chamber was filled with Anode Running Buffer (1X). Then, electrophoresis ran for 110min at 150V constant. Once it was complete, the gel was fixed with fixing solution (40% methanol, 10% acetic acid), and distained with distain solution (8% acetic acid).

A.7 Negative stain TEM

10 μL of recombinant tau fibril samples were applied to copper grid (Electron Microscopy Science, FCF-300-Cu) cleaned with plasma for 20 s. Samples were stained with 10 μL 1.5 w/v % uranyl acetate and were analyzed using a FEI Tecnai G2 TEM microscope (FEI) at room temperature. For mouse-derived fibrils, tau fibrils extracted from rTg4510 mice cortex (0.5 μg) were adsorbed on 200-mesh formvar-coated copper grids, washed, and stained with a 2% uranyl acetate solution. Grids were then imaged with a JEOL JEM-1230 (JEOL USA, Inc) at the indicated magnifications.

A.8 spin-labeling

Protein was spin-labelled using MTSL ((1-Acetoxy-2,2,5,5-tetramethyl-δ-3-pyrroline-3-methyl) Methanethiosulfonate) purchased from Toronto Research Chemicals. Prior to labelling, samples were treated with 5 mM DTT, which was removed using a PD-10 desalting column. Then, 10× to 15× molar excess MTSL to free cysteine was incubated with the protein at 4 °C overnight. Excess MTSL was removed using a PD-10 desalting column. Labelling efficiency, defined as the molar ratio of tethered spin-labels over the cysteines, was measured to be 50-60% for double-cysteine mutants and about 90% for single-cysteine mutant used in chapter 4 or 5.

A.9 CwEPR and spectra analysis

Cw-EPR experiments were carried out on Bruker EMX X-band spectrometer with dielectric cavity (ER4123D). 4 μL of sample was loaded into a capillary tube (0.6 mm i.d., 0.8 mm o.d.) and sealed at one end with critoseal. Samples were irradiated with 2 mW incident microwave power at 9.8 GHz using a 1 G modulation amplitude and a sweep width of 150 G or 200 G. Spin counting was obtained by calculating the doubled integral of the acquired derivative spectra, which is proportional to the number of spin in the cavity. A 2nd polynomial fitted baseline was subtracted to the first integral before applying the second integration.

A.10 Double Electron Electron Resonance (DEER)

Double-cysteine tau187 was expressed and spin-labeled as doubly-labeled tau (tau-SL2) that contains two spin-labels in order to probe distances between two target residue (in chapter 4, residues 272 and 285 and in chapter 5, residues 351 and 373, residues 334 and 360, and residues 340 and 378). Cysless tau187 was expressed and purified to avoid disulfide bonding. In chapter 4, the protein stocks were concentrated, and buffer exchanged against D_2O-based buffer (100 mM NaCl, 20 mM ammonium acetate, 1.5 mM CaCl2) using Amicon centrifugal concentrators (10 kDa cutoff). A 1:10 molar ratio tau-SL2:cysless sample of 57 μM tau-SL2 and 570 μM cysless was incubated with 157 μM heparin at room temperature for 24 h to prepare heparin fibrils (denoted as "before digestion" in Fig. 3.3B). Heparin fibrils were then incubated with 120 U of heparinase at 30 °C overnight to prepare digested heparin fibrils (denoted as "0.4× Heparinase" in Fig. 3.4B). 35 μL samples were mixed with 15 μL D8-glycerol (30% volume) before transferring to a quartz tube (2 mm i.d.) and frozen using liquid nitrogen. Seeded-fibrils

sample (Fig. 3.4B) was prepared as follow: A 1:10 molar ratio tau-SL2:ysless sample of 15 μM tau-SL2 and 150 μM cysless was incubated at RT with 825 μg/ml polyU and 1% (protein mass) mouse braine-xtracted tau fibrils. After 12h, the sample was pelleted and the fibrils solubilized in 35 μL buffer and 15 L D8-glycerol before transferring to a quartz tube (2 mm i.d.) and freezing using liquid nitrogen.

In chapter 5, tau-SL2 and cysless were stored in 20 mM HEPES in H_2O. A 1:10 molar ratio tau-SL2:cysless sample of 57 μM tau-SL2 and 570 μM cysless was incubated with 157 μM heparin at 37 °C 24 h to prepare heparin fibrils. As for CBD and PSP seed-induced fibrils, a 1:10 molar ratio tau-SL2:cysless sample of 200 μM tau-SL2 and 200 μM cysless was incubated with 15% (mass) CBD or PSP seeds at 37 °C for 24 h to prepare seed-induced fibrils. 50 μL of fibrils were then dialyzed to 20mM HEPES in D_2O at room temperature for 6 h using Pur-A-Lyzer™ Mini Dialysis Kit (Mini 25000, MWCO 25 kDa). 35 μL samples were then mixed with 15 μL D8-glycerol (30% volume) before transferring to a quartz tube (2 mm i.d.) and frozen using liquid nitrogen.

Four-pulse DEER experiments were carried out at 85 K using the Q-band Bruker E580 Elexsys pulse EPR spectrometer operating at 4 GHz and equipped with a 300 W TWT amplifier. The following DEER pulse sequence was used: $\pi_{obs}/2$ – τ_1 – π_{obs} – (t-π_{pump}) – (τ_2-t) – π_{obs} – τ_2 – echo. Rectangular observe pulses were used with lengths set to πobs/2 = 10–12 ns and πobs = 20–24 ns. A chirp πpump pulse was applied with a length of 20–24 ns and a frequency width of 60 MHz. The observed frequency was 90 MHz higher than the center of the pump frequency range. τ1 was 180 ns, and τ2 was set to 2.4ms.

Bibliography

[1] J. Q. Trojanowski, T. Schuck, M. L. Schmidt, and V. M. Lee, *Distribution of tau proteins in the normal human central and peripheral nervous system*, *J. Histochem. Cytochem.* **37** (Feb., 1989) 209–215.

[2] M. Goedert, *Tau protein and the neurofibrillary pathology of alzheimer's disease*, *Neurobiology of Alzheimer's Disease* **777** (1996) 121–131.

[3] P. V. Arriagada, J. H. Growdon, E. T. Hedley-Whyte, and B. T. Hyman, *Neurofibrillary tangles but not senile plaques parallel duration and severity of alzheimer's disease*, *Neurology* **42** (Mar., 1992) 631–639.

[4] M. von Bergen, P. Friedhoff, J. Biernat, J. Heberle, E. M. Mandelkow, and E. Mandelkow, *Assembly of tau protein into alzheimer paired helical filaments depends on a local sequence motif ((306)VQIVYK(311)) forming beta structure*, *Proc. Natl. Acad. Sci. U. S. A.* **97** (May, 2000) 5129–5134.

[5] A. W. P. Fitzpatrick, B. Falcon, S. He, A. G. Murzin, G. Murshudov, H. J. Garringer, R. A. Crowther, B. Ghetti, M. Goedert, and S. H. W. Scheres, *Cryo-EM structures of tau filaments from alzheimer's disease*, *Nature* **547** (July, 2017) 185–190.

[6] B. Falcon, W. Zhang, M. Schweighauser, A. G. Murzin, R. Vidal, H. J. Garringer, B. Ghetti, S. H. W. Scheres, and M. Goedert, *Tau filaments from multiple cases of sporadic and inherited alzheimer's disease adopt a common fold*, *Acta Neuropathol.* **136** (Nov., 2018) 699–708.

[7] B. Falcon, W. Zhang, A. G. Murzin, G. Murshudov, H. J. Garringer, R. Vidal, R. A. Crowther, B. Ghetti, S. H. W. Scheres, and M. Goedert, *Structures of filaments from pick's disease reveal a novel tau protein fold*, *Nature* **561** (Sept., 2018) 137–140.

[8] W. Zhang, A. Tarutani, K. L. Newell, A. G. Murzin, T. Matsubara, B. Falcon, R. Vidal, H. J. Garringer, Y. Shi, T. Ikeuchi, S. Murayama, B. Ghetti, M. Hasegawa, M. Goedert, and S. H. W. Scheres, *Novel tau filament fold in corticobasal degeneration*, *Nature* (Feb., 2020).

[9] T. Arakhamia, C. E. Lee, Y. Carlomagno, D. M. Duong, S. R. Kundinger, K. Wang, D. Williams, M. DeTure, D. W. Dickson, C. N. Cook, N. T. Seyfried, L. Petrucelli, and A. W. P. Fitzpatrick, *Posttranslational modifications mediate the structural diversity of tauopathy strains*, *Cell* **180** (Feb., 2020) 633–644.e12.

[10] B. Falcon, J. Zivanov, W. Zhang, A. G. Murzin, H. J. Garringer, R. Vidal, R. A. Crowther, K. L. Newell, B. Ghetti, M. Goedert, and S. H. W. Scheres, *Novel tau filament fold in chronic traumatic encephalopathy encloses hydrophobic molecules*, *Nature* **568** (Apr., 2019) 420–423.

[11] X. Xiang, T. Arakhamia, Y. Carlomagno, S. Dhingra, M. Thierry, M. DeTure, C. N. Cook, D. W. Dickson, L. Petrucelli, and A. W. P. Fitzpatrick, "Role of molecular polymorphism in defining tau filament structures in neurodegenerative diseases." May, 2021.

[12] Y. Shi, W. Zhang, Y. Yang, A. G. Murzin, B. Falcon, A. Kotecha, M. van Beers, A. Tarutani, F. Kametani, H. J. Garringer, R. Vidal, G. I. Hallinan, T. Lashley, Y. Saito, S. Murayama, M. Yoshida, H. Tanaka, A. Kakita, T. Ikeuchi, A. C. Robinson, D. M. A. Mann, G. G. Kovacs, T. Revesz, B. Ghetti, M. Hasegawa, M. Goedert, and S. H. W. Scheres, *Structure-based classification of tauopathies*, *Nature* **598** (Oct., 2021) 359–363.

[13] G. S. Gibbons, R. A. Banks, B. Kim, L. Changolkar, D. M. Riddle, S. N. Leight, D. J. Irwin, J. Q. Trojanowski, and V. M. Y. Lee, *Detection of alzheimer disease (AD)-Specific tau pathology in AD and NonAD tauopathies by immunohistochemistry with novel Conformation-Selective tau antibodies*, *J. Neuropathol. Exp. Neurol.* **77** (Mar., 2018) 216–228.

[14] J. Verelst, N. Geukens, S. Eddarkaoui, D. Vliegen, E. De Smidt, J. Rosseels, V. Franssens, S. Molenberghs, C. Francois, E. Stoops, M. Bjerke, S. Engelborghs, M. Laghmouchi, S. Carmans, L. Buée, E. Vanmechelen, J. Winderickx, and D. Thomas, *A novel tau antibody detecting the first Amino-Terminal insert reveals conformational differences among tau isoforms*, *Front Mol Biosci* **7** (Mar., 2020) 48.

[15] M. Albert, G. Mairet-Coello, C. Danis, S. Lieger, R. Caillierez, S. Carrier, E. Skrobala, I. Landrieu, A. Michel, M. Schmitt, M. Citron, P. Downey, J.-P. Courade, L. Buée, and M. Colin, *Prevention of tau seeding and propagation by immunotherapy with a central tau epitope antibody*, *Brain* **142** (June, 2019) 1736–1750.

[16] G. S. Gibbons, V. M. Y. Lee, and J. Q. Trojanowski, *Mechanisms of Cell-to-Cell transmission of pathological tau: A review*, *JAMA Neurol.* **76** (Jan., 2019) 101–108.

[17] J. L. Guo, S. Narasimhan, L. Changolkar, Z. He, A. Stieber, B. Zhang, R. J. Gathagan, M. Iba, J. D. McBride, J. Q. Trojanowski, and V. M. Y. Lee, *Unique pathological tau conformers from alzheimer's brains transmit tau pathology in nontransgenic mice*, *J. Exp. Med.* **213** (Nov., 2016) 2635–2654.

[18] F. Clavaguera, T. Bolmont, R. A. Crowther, D. Abramowski, S. Frank, A. Probst, G. Fraser, A. K. Stalder, M. Beibel, M. Staufenbiel, M. Jucker, M. Goedert, and M. Tolnay, *Transmission and spreading of tauopathy in transgenic mouse brain*, *Nat. Cell Biol.* **11** (July, 2009) 909–U325.

[19] W. Hu, X. Zhang, Y. C. Tung, S. Xie, F. Liu, and K. Iqbal, *Hyperphosphorylation determines both the spread and the morphology of tau pathology*, *Alzheimers. Dement.* **12** (Oct., 2016) 1066–1077.

[20] M. Iba, J. L. Guo, J. D. McBride, B. Zhang, J. Q. Trojanowski, and V. M.-Y. Lee, *Synthetic tau fibrils mediate transmission of neurofibrillary tangles in a transgenic mouse model of Alzheimer's-Like tauopathy*, *Journal of Neuroscience* **33** (Jan., 2013) 1024–1037.

[21] E. Peeraer, A. Bottelbergs, K. Van Kolen, I.-C. Stancu, B. Vasconcelos, M. Mahieu, H. Duytschaever, L. Ver Donck, A. Torremans, E. Sluydts, N. Van Acker, J. A. Kemp, M. Mercken, K. R. Brunden, J. Q. Trojanowski, I. Dewachter, V. M. Y. Lee, and D. Moechars, *Intracerebral injection of preformed synthetic tau fibrils initiates widespread tauopathy and neuronal loss in the brains of tau transgenic mice*, 2015.

[22] I.-C. Stancu, B. Vasconcelos, L. Ris, P. Wang, A. Villers, E. Peeraer, A. Buist, D. Terwel, P. Baatsen, T. Oyelami, N. Pierrot, C. Casteels, G. Bormans, P. Kienlen-Campard, J.-N. Octave, D. Moechars, and I. Dewachter, *Templated misfolding of tau by prion-like seeding along neuronal connections impairs neuronal network function and associated behavioral outcomes in tau transgenic mice*, 2015.

[23] Z. He, J. D. McBride, H. Xu, L. Changolkar, S.-J. Kim, B. Zhang, S. Narasimhan, G. S. Gibbons, J. L. Guo, M. Kozak, G. D. Schellenberg, J. Q. Trojanowski, and V. M.-Y. Lee, *Transmission of tauopathy strains is independent of their isoform composition*, *Nat. Commun.* **11** (Jan., 2020) 7.

[24] S. Narasimhan, J. L. Guo, L. Changolkar, A. Stieber, J. D. McBride, L. V. Silva, Z. He, B. Zhang, R. J. Gathagan, J. Q. Trojanowski, and V. M. Y. Lee, *Pathological tau strains from human brains recapitulate the diversity of tauopathies in nontransgenic mouse brain*, *J. Neurosci.* **37** (Nov., 2017) 11406–11423.

[25] Y. Fichou, Y. Lin, J. N. Rauch, M. Vigers, Z. Zeng, M. Srivastava, T. J. Keller, J. H. Freed, K. S. Kosik, and S. Han, *Cofactors are essential constituents of stable*

and seeding-active tau fibrils, *Proc. Natl. Acad. Sci. U. S. A.* **115** (Dec., 2018) 13234–13239.

[26] Y. Fichou, M. Vigers, A. K. Goring, N. A. Eschmann, and S. I. Han, *Heparin-induced tau filaments are structurally heterogeneous and differ from alzheimer's disease filaments*, *Chem. Commun.* **54** (2018), no. 36 4573–4576.

[27] A. L. Woerman, A. Aoyagi, S. Patel, S. A. Kazmi, I. Lobach, L. T. Grinberg, A. C. Mckee, W. W. Seeley, S. H. Olson, and S. B. Prusiner, *Tau prions from alzheimer's disease and chronic traumatic encephalopathy patients propagate in cultured cells*, *Proc. Natl. Acad. Sci. U. S. A.* **113** (2016), no. 50 E8187–E8196.

[28] S. Walker, O. Ullman, and C. M. Stultz, *Using intramolecular disulfide bonds in tau protein to deduce structural features of aggregation-resistant conformations*, *J. Biol. Chem.* **287** (Mar., 2012) 9591–9600.

[29] K. Bhattacharya, K. B. Rank, D. B. Evans, and S. K. Sharma, *Role of cysteine-291 and cysteine-322 in the polymerization of human tau into alzheimer-like filaments*, *Biochem. Biophys. Res. Commun.* **285** (July, 2001) 20–26.

[30] O. Schweers, E. M. Mandelkow, J. Biernat, and E. Mandelkow, *Oxidation of cysteine-322 in the repeat domain of microtubule-associated protein tau controls the in vitro assembly of paired helical filaments*, *Proc. Natl. Acad. Sci. U. S. A.* **92** (Aug., 1995) 8463–8467.

[31] S. Barghorn and E. Mandelkow, *Toward a unified scheme for the aggregation of tau into alzheimer paired helical filaments*, *Biochemistry* **41** (2002), no. 50 14885–14896.

[32] M. M. Haque, D. Kim, Y. H. Yu, S. Lim, D. J. Kim, Y. T. Chang, H. H. Ha, and Y. K. Kim, *Inhibition of tau aggregation by a rosamine derivative that blocks tau intermolecular disulfide cross-linking*, *Amyloid-Journal of Protein Folding Disorders* **21** (Sept., 2014) 185–190.

[33] Y. Furukawa, K. Kaneko, and N. Nukina, *Tau protein assembles into isoform- and disulfide-dependent polymorphic fibrils with distinct structural properties*, *J. Biol. Chem.* **286** (2011), no. 31 27236–27246.

[34] Y. K. Al-Hilaly, S. J. Pollack, D. M. Vadukul, F. Citossi, J. E. Rickard, M. Simpson, J. M. D. Storey, C. R. Harrington, C. M. Wischik, and L. C. Serpell, *Alzheimer's disease-like paired helical filament assembly from truncated tau protein is independent of disulfide crosslinking*, *J. Mol. Biol.* **429** (2017), no. 23 3650–3665.

[35] D. Kim, S. Lim, M. M. Haque, N. Ryoo, H. S. Hong, H. Rhim, D.-E. Lee, Y.-T. Chang, J.-S. Lee, E. Cheong, D. J. Kim, and Y. K. Kim, *Identification of disulfide cross-linked tau dimer responsible for tau propagation*, *Sci. Rep.* **5** (Oct., 2015) 15231.

[36] J. L. Guo and V. M. Y. Lee, *Seeding of normal tau by pathological tau conformers drives pathogenesis of alzheimer-like tangles*, *J. Biol. Chem.* **286** (2011), no. 17 15317–15331.

[37] A. M. Sharma, T. L. Thomas, D. R. Woodard, O. M. Kashmer, and M. I. Diamond, *Tau monomer encodes strains*, *Elife* **7** (Dec., 2018).

[38] G. Ghag, N. Bhatt, D. V. Cantu, M. J. Guerrero-Munoz, A. Ellsworth, U. Sengupta, and R. Kayed, *Soluble tau aggregates, not large fibrils, are the toxic species that display seeding and cross-seeding behavior: Generation of tau aggregates via sonication*, *Protein Sci.* **27** (Nov., 2018) 1901–1909.

[39] H. Mirbaha, D. Chen, O. A. Morazova, K. M. Ruff, A. M. Sharma, X. Liu, M. Goodarzi, R. V. Pappu, D. W. Colby, H. Mirzaei, L. A. Joachimiak, and M. I. Diamond, *Inert and seed-competent tau monomers suggest structural origins of aggregation*, *Elife* **7** (July, 2018) e36584.

[40] B. Nizynski, H. Nieznanska, R. Dec, S. Boyko, W. Dzwolak, and K. Nieznanski, *Amyloidogenic cross-seeding of tau protein: Transient emergence of structural variants of fibrils*, *PLoS One* **13** (July, 2018) e0201182.

[41] W.-H. Nam and Y. P. Choi, *In vitro generation of tau aggregates conformationally distinct from parent tau seeds of alzheimer's brain*, *Prion* **13** (Jan., 2019) 1–12.

[42] A. Kraus, E. Saijo, M. A. Metrick, 2nd, K. Newell, C. J. Sigurdson, G. Zanusso, B. Ghetti, and B. Caughey, *Seeding selectivity and ultrasensitive detection of tau aggregate conformers of alzheimer disease*, *Acta Neuropathol.* **137** (Apr., 2019) 585–598.

[43] E. Saijo, M. A. Metrick, 2nd, S. Koga, P. Parchi, I. Litvan, S. Spina, A. Boxer, J. C. Rojas, D. Galasko, A. Kraus, M. Rossi, K. Newell, G. Zanusso, L. T. Grinberg, W. W. Seeley, B. Ghetti, D. W. Dickson, and B. Caughey, *4-repeat tau seeds and templating subtypes as brain and CSF biomarkers of frontotemporal lobar degeneration*, *Acta Neuropathol.* **139** (Jan., 2020) 63–77.

[44] E. Saijo, B. Ghetti, G. Zanusso, A. Oblak, J. L. Furman, M. I. Diamond, A. Kraus, and B. Caughey, *Ultrasensitive and selective detection of 3-repeat tau seeding activity in pick disease brain and cerebrospinal fluid*, *Acta Neuropathol.* **133** (May, 2017) 751–765.

[45] V. Meyer, M. R. Holden, H. A. Weismiller, G. R. Eaton, S. S. Eaton, and M. Margittai, *Fracture and growth are competing forces determining the fate of conformers in tau fibril populations*, *J. Biol. Chem.* **291** (June, 2016) 12271–12281.

[46] H. A. Weismiller, R. Murphy, G. Wei, B. Ma, R. Nussinov, and M. Margittai, *Structural disorder in four-repeat tau fibrils reveals a new mechanism for barriers to cross-seeding of tau isoforms*, *J. Biol. Chem.* **293** (Nov., 2018) 17336–17348.

[47] B. Frost, J. Ollesch, H. Wille, and M. I. Diamond, *Conformational diversity of wild-type tau fibrils specified by templated conformation change*, *J. Biol. Chem.* **284** (Feb., 2009) 3546–3551.

[48] P. D. Dinkel, A. Siddiqua, H. Huynh, M. Shah, and M. Margittai, *Variations in filament conformation dictate seeding barrier between three- and four-repeat tau*, *Biochemistry* **50** (May, 2011) 4330–4336.

[49] S. K. Kaufman, D. W. Sanders, T. L. Thomas, A. J. Ruchinskas, J. Vaquer-Alicea, A. M. Sharma, T. M. Miller, and M. I. Diamond, *Tau prion strains dictate patterns of cell pathology, progression rate, and regional vulnerability in vivo*, *Neuron* **92** (Nov., 2016) 796–812.

[50] D. W. Sanders, S. K. Kaufman, S. L. DeVos, A. M. Sharma, H. Mirbaha, A. Li, S. J. Barker, A. C. Foley, J. R. Thorpe, L. C. Serpell, T. M. Miller, L. T. Grinberg, W. W. Seeley, and M. I. Diamond, *Distinct tau prion strains propagate in cells and mice and define different tauopathies*, *Neuron* **82** (June, 2014) 1271–1288.

[51] B. Falcon, A. Cavallini, R. Angers, S. Glover, T. K. Murray, L. Barnham, S. Jackson, M. J. O'Neill, A. M. Isaacs, M. L. Hutton, P. G. Szekeres, M. Goedert, and S. Bose, *Conformation determines the seeding potencies of native and recombinant tau aggregates*, *J. Biol. Chem.* **290** (Jan., 2015) 1049–1065.

[52] W. Zhang, B. Falcon, A. G. Murzin, J. Fan, R. A. Crowther, M. Goedert, and S. H. Scheres, *Heparin-induced tau filaments are polymorphic and differ from those in alzheimer's and pick's diseases*, *Elife* **8** (Feb., 2019) e43584.

[53] M. Goedert, M. G. Spillantini, R. Jakes, D. Rutherford, and R. A. Crowther, *Multiple isoforms of human microtubule-associated protein tau: sequences and localization in neurofibrillary tangles of alzheimer's disease*, *Neuron* **3** (Oct., 1989) 519–526.

[54] K. S. Kosik and E. A. Finch, *MAP2 and tau segregate into dendritic and axonal domains after the elaboration of morphologically distinct neurites: an immunocytochemical study of cultured rat cerebrum*, *J. Neurosci.* **7** (Oct., 1987) 3142–3153.

[55] L. M. Ittner, Y. D. Ke, F. Delerue, M. Bi, A. Gladbach, J. van Eersel, H. Wölfing, B. C. Chieng, M. J. Christie, I. A. Napier, A. Eckert, M. Staufenbiel, E. Hardeman, and J. Götz, *Dendritic function of tau mediates amyloid-beta toxicity in alzheimer's disease mouse models*, *Cell* **142** (Aug., 2010) 387–397.

[56] H. Zempel, E. Thies, E. Mandelkow, and E.-M. Mandelkow, *Abeta oligomers cause localized ca(2+) elevation, missorting of endogenous tau into dendrites, tau phosphorylation, and destruction of microtubules and spines*, *J. Neurosci.* **30** (Sept., 2010) 11938–11950.

[57] A. Sultan, F. Nesslany, M. Violet, S. Bégard, A. Loyens, S. Talahari, Z. Mansuroglu, D. Marzin, N. Sergeant, S. Humez, M. Colin, E. Bonnefoy, L. Buée, and M.-C. Galas, *Nuclear tau, a key player in neuronal DNA protection**, *J. Biol. Chem.* **286** (Feb., 2011) 4566–4575.

[58] C. G. Gunawardana, M. Mehrabian, X. Wang, I. Mueller, I. B. Lubambo, J. E. N. Jonkman, H. Wang, and G. Schmitt-Ulms, *The human tau interactome: Binding to the ribonucleoproteome, and impaired binding of the Proline-to-Leucine mutant at position 301 (P301L) to chaperones and the proteasome**, *Mol. Cell. Proteomics* **14** (Nov., 2015) 3000–3014.

[59] G. Multhaup, O. Huber, L. Buée, and M.-C. Galas, *Amyloid precursor protein (APP) metabolites APP intracellular fragment (AICD), Aβ42, and tau in nuclear roles**, *J. Biol. Chem.* **290** (Sept., 2015) 23515–23522.

[60] M. Goedert, C. P. Baur, J. Ahringer, R. Jakes, M. Hasegawa, M. G. Spillantini, M. J. Smith, and F. Hill, *PTL-1, a microtubule-associated protein with tau-like repeats from the nematode caenorhabditis elegans*, *J. Cell Sci.* **109 (Pt 11)** (Nov., 1996) 2661–2672.

[61] J. B. McDermott, S. Aamodt, and E. Aamodt, *ptl-1, a caenorhabditis elegans gene whose products are homologous to the tau microtubule-associated proteins*, *Biochemistry* **35** (July, 1996) 9415–9423.

[62] Y. L. Chew, X. Fan, J. Götz, and H. R. Nicholas, *PTL-1 regulates neuronal integrity and lifespan in c. elegans*, *J. Cell Sci.* **126** (May, 2013) 2079–2091.

[63] H. Kadavath, R. V. Hofele, J. Biernat, S. Kumar, K. Tepper, H. Urlaub, E. Mandelkow, and M. Zweckstetter, *Tau stabilizes microtubules by binding at the interface between tubulin heterodimers*, *Proc. Natl. Acad. Sci. U. S. A.* **112** (June, 2015) 7501–7506.

[64] K. Bhaskar, S.-H. Yen, and G. Lee, *Disease-related modifications in tau affect the interaction between fyn and tau**, *J. Biol. Chem.* **280** (Oct., 2005) 35119–35125.

[65] G. Lee, R. Thangavel, V. M. Sharma, J. M. Litersky, K. Bhaskar, S. M. Fang, L. H. Do, A. Andreadis, G. Van Hoesen, and H. Ksiezak-Reding, *Phosphorylation of tau by fyn: implications for alzheimer's disease*, *J. Neurosci.* **24** (Mar., 2004) 2304–2312.

[66] A. Abraha, N. Ghoshal, T. C. Gamblin, V. Cryns, R. W. Berry, J. Kuret, and L. I. Binder, *C-terminal inhibition of tau assembly in vitro and in alzheimer's disease*, *J. Cell Sci.* **113 Pt 21** (Nov., 2000) 3737–3745.

[67] P. Flores-Rodríguez, M. A. Ontiveros-Torres, M. C. Cárdenas-Aguayo, J. P. Luna-Arias, M. A. Meraz-Ríos, A. Viramontes-Pintos, C. R. Harrington, C. M. Wischik, R. Mena, B. Florán-Garduño, and J. Luna-Muñoz, *The relationship between truncation and phosphorylation at the c-terminus of tau protein in the paired helical filaments of alzheimer's disease*, *Front. Neurosci.* **9** (Feb., 2015) 33.

[68] C. Liu, X. Song, R. Nisbet, and J. Götz, *Co-immunoprecipitation with tau isoform-specific antibodies reveals distinct protein interactions and highlights a putative role for 2N tau in disease*, *J. Biol. Chem.* **291** (Apr., 2016) 8173–8188.

[69] M. Morris, G. M. Knudsen, S. Maeda, J. C. Trinidad, A. Ioanoviciu, A. L. Burlingame, and L. Mucke, *Tau post-translational modifications in wild-type and human amyloid precursor protein transgenic mice*, *Nat. Neurosci.* **18** (Aug., 2015) 1183–1189.

[70] C. Li and J. Götz, *Tau-based therapies in neurodegeneration: opportunities and challenges*, *Nat. Rev. Drug Discov.* **16** (Dec., 2017) 863–883.

[71] A. Alonso, T. Zaidi, M. Novak, I. Grundke-Iqbal, and K. Iqbal, *Hyperphosphorylation induces self-assembly of tau into tangles of paired helical filaments/straight filaments*, *Proc. Natl. Acad. Sci. U. S. A.* **98** (June, 2001) 6923–6928.

[72] S.-W. Min, S.-H. Cho, Y. Zhou, S. Schroeder, V. Haroutunian, W. W. Seeley, E. J. Huang, Y. Shen, E. Masliah, C. Mukherjee, D. Meyers, P. A. Cole, M. Ott, and L. Gan, *Acetylation of tau inhibits its degradation and contributes to tauopathy*, *Neuron* **67** (Sept., 2010) 953–966.

[73] T. J. Cohen, J. L. Guo, D. E. Hurtado, L. K. Kwong, I. P. Mills, J. Q. Trojanowski, and V. M. Y. Lee, *The acetylation of tau inhibits its function and promotes pathological tau aggregation*, *Nat. Commun.* **2** (2011) 252.

[74] I. R. A. Mackenzie and M. Neumann, *Molecular neuropathology of frontotemporal dementia: insights into disease mechanisms from postmortem studies*, *J. Neurochem.* **138 Suppl 1** (Aug., 2016) 54–70.

[75] T. Odawara, E. Iseki, K. Kosaka, H. Akiyama, K. Ikeda, and T. Yamamoto, *Investigation of tau-2 positive microglia-like cells in the subcortical nuclei of human neurodegenerative disorders*, *Neurosci. Lett.* **192** (June, 1995) 145–148.

[76] T. Komori, *Tau-positive glial inclusions in progressive supranuclear palsy, corticobasal degeneration and pick's disease*, *Brain Pathol.* **9** (Oct., 1999) 663–679.

[77] J. Götz, G. Halliday, and R. M. Nisbet, *Molecular pathogenesis of the tauopathies*, *Annu. Rev. Pathol.* **14** (Jan., 2019) 239–261.

[78] A. Pick, *Uber die beziehungen der senilen hirnatrophie zur aphasie*, *Prag Med Wochenschr* **17** (1892) 165–167.

[79] A. Alzheimer, *über eigenartige krankheitsfälle des späteren alters*, *Arch. Psychiatr. Nervenkr. Z. Gesamte Neurol. Psychiatr.* **4** (Dec., 1911) 356.

[80] C. L. Joachim, J. H. Morris, K. S. Kosik, and D. J. Selkoe, *Tau antisera recognize neurofibrillary tangles in a range of neurodegenerative disorders*, *Ann. Neurol.* **22** (Oct., 1987) 514–520.

[81] S. Kato and H. Nakamura, *Presence of two different fibril subtypes in the pick body: an immunoelectron microscopic study*, *Acta Neuropathol.* **81** (1990), no. 2 125–129.

[82] S. Murayama, H. Mori, Y. Ihara, and M. Tomonaga, *Immunocytochemical and ultrastructural studies of pick's disease*, *Ann. Neurol.* **27** (Apr., 1990) 394–405.

[83] A. Probst, M. Tolnay, D. Langui, M. Goedert, and M. G. Spillantini, *Pick's disease: hyperphosphorylated tau protein segregates to the somatoaxonal compartment*, *Acta Neuropathol.* **92** (Dec., 1996) 588–596.

[84] M. Yamazaki, I. Nakano, O. Imazu, R. Kaieda, and A. Terashi, *Astrocytic straight tubules in the brain of a patient with pick's disease*, *Acta Neuropathol.* **88** (1994), no. 6 587–591.

[85] I. Ferrer, I. López-González, M. Carmona, L. Arregui, E. Dalfó, B. Torrejón-Escribano, R. Diehl, and G. G. Kovacs, *Glial and neuronal tau pathology in tauopathies: characterization of disease-specific phenotypes and tau pathology progression*, *J. Neuropathol. Exp. Neurol.* **73** (Jan., 2014) 81–97.

[86] J. C. Steele, J. C. Richardson, and J. Olszewski, *PROGRESSIVE SUPRANUCLEAR PALSY. a HETEROGENEOUS DEGENERATION INVOLVING THE BRAIN STEM, BASAL GANGLIA AND CEREBELLUM WITH VERTICAL GAZE AND PSEUDOBULBAR PALSY, NUCHAL DYSTONIA AND DEMENTIA*, *Arch. Neurol.* **10** (Apr., 1964) 333–359.

[87] A. Probst, D. Langui, C. Lautenschlager, J. Ulrich, J. P. Brion, and B. H. Anderton, *Progressive supranuclear palsy: extensive neuropil threads in addition to neurofibrillary tangles. very similar antigenicity of subcortical neuronal pathology in progressive supranuclear palsy and alzheimer's disease*, *Acta Neuropathol.* **77** (1988), no. 1 61–68.

[88] T. Yamada, P. L. McGeer, and E. G. McGeer, *Appearance of paired nucleated, tau-positive glia in patients with progressive supranuclear palsy brain tissue*, *Neurosci. Lett.* **135** (Jan., 1992) 99–102.

[89] J. J. Hauw, S. E. Daniel, D. Dickson, D. S. Horoupian, K. Jellinger, P. L. Lantos, A. McKee, M. Tabaton, and I. Litvan, *Preliminary NINDS neuropathologic criteria for Steele-Richardson-Olszewski syndrome (progressive supranuclear palsy)*, *Neurology* **44** (Nov., 1994) 2015–2019.

[90] T. Nishimura, K. Ikeda, H. Akiyama, H. Kondo, M. Kato, F. Li, E. Iseki, and K. Kosaka, *Immunohistochemical investigation of tau-positive structures in the cerebral cortex of patients with progressive supranuclear palsy*, *Neurosci. Lett.* **201** (Dec., 1995) 123–126.

[91] D. W. Dickson, S. H. Yen, K. I. Suzuki, P. Davies, J. H. Garcia, and A. Hirano, *Ballooned neurons in select neurodegenerative diseases contain phosphorylated neurofilament epitopes*, *Acta Neuropathol.* **71** (1986), no. 3-4 216–223.

[92] G. M. Halliday, L. Davies, D. A. McRitchie, H. Cartwright, R. Pamphlett, and J. G. Morris, *Ubiquitin-positive achromatic neurons in corticobasal degeneration*, *Acta Neuropathol.* **90** (1995), no. 1 68–75.

[93] T. Uchihara, K. Mitani, H. Mori, H. Kondo, M. Yamada, and K. Ikeda, *Abnormal cytoskeletal pathology peculiar to corticobasal degeneration is different from that of alzheimer's disease or progressive supranuclear palsy*, *Acta Neuropathol.* **88** (1994), no. 4 379–383.

[94] T. Komori, N. Arai, M. Oda, H. Nakayama, H. Mori, S. Yagishita, T. Takahashi, N. Amano, S. Murayama, S. Murakami, N. Shibata, M. Kobayashi, S. Sasaki, and M. Iwata, *Astrocytic plaques and tufts of abnormal fibers do not coexist in corticobasal degeneration and progressive supranuclear palsy*, *Acta Neuropathol.* **96** (Oct., 1998) 401–408.

[95] D. W. Dickson, *Neuropathologic differentiation of progressive supranuclear palsy and corticobasal degeneration*, *J. Neurol.* **246 Suppl 2** (Sept., 1999) II6–15.

[96] B. Dubois, H. Hampel, H. H. Feldman, P. Scheltens, P. Aisen, S. Andrieu, H. Bakardjian, H. Benali, L. Bertram, K. Blennow, K. Broich, E. Cavedo, S. Crutch, J.-F. Dartigues, C. Duyckaerts, S. Epelbaum, G. B. Frisoni,

S. Gauthier, R. Genthon, A. A. Gouw, M.-O. Habert, D. M. Holtzman, M. Kivipelto, S. Lista, J.-L. Molinuevo, S. E. O'Bryant, G. D. Rabinovici, C. Rowe, S. Salloway, L. S. Schneider, R. Sperling, M. Teichmann, M. C. Carrillo, J. Cummings, C. R. Jack, Jr, and Proceedings of the Meeting of the International Working Group (IWG) and the American Alzheimer's Association on "The Preclinical State of AD"; July 23, 2015; Washington DC, USA, *Preclinical alzheimer's disease: Definition, natural history, and diagnostic criteria*, *Alzheimers. Dement.* **12** (Mar., 2016) 292–323.

[97] H. Braak and E. Braak, *Staging of alzheimer's disease-related neurofibrillary changes*, *Neurobiol. Aging* **16** (May, 1995) 271–8; discussion 278–84.

[98] P. Ganguly, T. D. Do, L. Larini, N. E. LaPointe, A. J. Sercel, M. F. Shade, S. C. Feinstein, M. T. Bowers, and J.-E. Shea, *Tau assembly: the dominant role of PHF6 (VQIVYK) in microtubule binding region repeat R3*, *J. Phys. Chem. B* **119** (Apr., 2015) 4582–4593.

[99] M.-A. Wulf, A. Senatore, and A. Aguzzi, *The biological function of the cellular prion protein: an update*, *BMC Biol.* **15** (May, 2017) 34.

[100] B. B. Holmes, J. L. Furman, T. E. Mahan, T. R. Yamasaki, H. Mirbaha, W. C. Eades, L. Belaygorod, N. J. Cairns, D. M. Holtzman, and M. I. Diamond, *Proteopathic tau seeding predicts tauopathy in vivo*, *Proc. Natl. Acad. Sci. U. S. A.* **111** (2014), no. 41 E4376–E4385.

[101] D.-E. C. Chung, Y. Carlomagno, C. N. Cook, K. Jansen-West, L. Daughrity, L. J. Lewis-Tuffin, M. Castanedes-Casey, M. DeTure, D. W. Dickson, and L. Petrucelli, *Tau exhibits unique seeding properties in globular glial tauopathy*, *Acta Neuropathol Commun* **7** (Mar., 2019) 36.

[102] S. Kaniyappan, K. Tepper, J. Biernat, R. R. Chandupatla, S. Hübschmann, S. Irsen, S. Bicher, C. Klatt, E.-M. Mandelkow, and E. Mandelkow, *FRET-based tau seeding assay does not represent prion-like templated assembly of tau filaments*, *Mol. Neurodegener.* **15** (July, 2020) 39.

[103] S. Dujardin, C. Commins, A. Lathuiliere, P. Beerepoot, A. R. Fernandes, T. V. Kamath, M. B. De Los Santos, N. Klickstein, D. L. Corjuc, B. T. Corjuc, P. M. Dooley, A. Viode, D. H. Oakley, B. D. Moore, K. Mullin, D. Jean-Gilles, R. Clark, K. Atchison, R. Moore, L. B. Chibnik, R. E. Tanzi, M. P. Frosch, A. Serrano-Pozo, F. Elwood, J. A. Steen, M. E. Kennedy, and B. T. Hyman, *Tau molecular diversity contributes to clinical heterogeneity in alzheimer's disease*, *Nat. Med.* **26** (Aug., 2020) 1256–1263.

[104] O. A. Morozova, Z. M. March, A. S. Robinson, and D. W. Colby, *Conformational features of tau fibrils from alzheimer's disease brain are faithfully propagated by unmodified recombinant protein*, *Biochemistry* **52** (Oct., 2013) 6960–6967.

[105] B. Nizynski, H. Nieznanska, R. Dec, S. Boyko, W. Dzwolak, and K. Nieznanski, *Amyloidogenic cross-seeding of tau protein: Transient emergence of structural variants of fibrils*, *PLoS One* **13** (July, 2018) e0201182.

[106] H. Mirbaha, D. Chen, O. A. Morazova, K. M. Ruff, A. M. Sharma, X. Liu, M. Goodarzi, R. V. Pappu, D. W. Colby, H. Mirzaei, L. A. Joachimiak, and M. I. Diamond, *Inert and seed-competent tau monomers suggest structural origins of aggregation*, *Elife* **7** (July, 2018).

[107] V. Meyer, P. D. Dinkel, E. Rickman Hager, and M. Margittai, *Amplification of tau fibrils from minute quantities of seeds*, *Biochemistry* **53** (Sept., 2014) 5804–5809.

[108] H. Xu, M. O'Reilly, G. S. Gibbons, L. Changolkar, J. D. McBride, D. M. Riddle, B. Zhang, A. Stieber, J. Nirschl, S.-J. Kim, K.-H. Hoxha, K. R. Brunden, G. D. Schellenberg, J. Q. Trojanowski, and V. M.-Y. Lee, *In vitro amplification of pathogenic tau conserves disease-specific bioactive characteristics*, *Acta Neuropathol.* **141** (Feb., 2021) 193–215.

[109] M. R. Sawaya, S. Sambashivan, R. Nelson, M. I. Ivanova, S. A. Sievers, M. I. Apostol, M. J. Thompson, M. Balbirnie, J. J. W. Wiltzius, H. T. McFarlane, A. Ø. Madsen, C. Riekel, and D. Eisenberg, *Atomic structures of amyloid cross-beta spines reveal varied steric zippers*, *Nature* **447** (May, 2007) 453–457.

[110] P. M. Seidler, D. R. Boyer, J. A. Rodriguez, M. R. Sawaya, D. Cascio, K. Murray, T. Gonen, and D. S. Eisenberg, *Structure-based inhibitors of tau aggregation*, *Nat. Chem.* **10** (Feb., 2018) 170–176.

[111] M. von Bergen, S. Barghorn, S. Jeganathan, E.-M. Mandelkow, and E. Mandelkow, *Spectroscopic approaches to the conformation of tau protein in solution and in paired helical filaments*, *Neurodegener. Dis.* **3** (2006), no. 4-5 197–206.

[112] O. C. Andronesi, M. von Bergen, J. Biernat, K. Seidel, C. Griesinger, E. Mandelkow, and M. Baldus, *Characterization of alzheimer's-like paired helical filaments from the core domain of tau protein using Solid-State NMR spectroscopy*, 2008.

[113] V. Daebel, S. Chinnathambi, J. Biernat, M. Schwalbe, B. Habenstein, A. Loquet, E. Akoury, K. Tepper, H. Müller, M. Baldus, C. Griesinger, M. Zweckstetter, E. Mandelkow, V. Vijayan, and A. Lange, *β-Sheet core of tau paired helical filaments revealed by solid-state NMR*, *J. Am. Chem. Soc.* **134** (Aug., 2012) 13982–13989.

[114] G. Jeschke, *DEER distance measurements on proteins*, *Annu. Rev. Phys. Chem.* **63** (Jan., 2012) 419–446.

[115] R. Kaminker, I. Kaminker, W. R. Gutekunst, Y. Luo, S. Lee, J. Niu, S. Han, and C. J. Hawker, *Tuning conformation and properties of peptidomimetic backbones through dual N/Cα-substitution*, *Chem. Commun.* **54** (May, 2018) 5237–5240.

[116] D. Bücker, A. Sickinger, J. D. Ruiz Perez, M. Oestringer, S. Mecking, and M. Drescher, *Direct observation of chain lengths and conformations in oligofluorene distributions from controlled polymerization by double Electron-Electron resonance*, *J. Am. Chem. Soc.* **142** (Jan., 2020) 1952–1956.

[117] Y.-W. Chiang, P. P. Borbat, and J. H. Freed, *The determination of pair distance distributions by pulsed ESR using tikhonov regularization*, *J. Magn. Reson.* **172** (Feb., 2005) 279–295.

[118] M. Srivastava and J. H. Freed, *Singular value decomposition method to determine distance distributions in pulsed dipolar electron spin resonance: II. estimating uncertainty*, *J. Phys. Chem. A* **123** (Jan., 2019) 359–370.

[119] L. F. Ibáñez and G. Jeschke, *Optimal background treatment in dipolar spectroscopy*, *Phys. Chem. Chem. Phys.* **22** (2020), no. 4 1855–1868.

[120] M. Srivastava, E. R. Georgieva, and J. H. Freed, *A new wavelet denoising method for experimental Time-Domain signals: Pulsed dipolar electron spin resonance*, *J. Phys. Chem. A* **121** (Mar., 2017) 2452–2465.

[121] T. Schmidt, J. Jeon, Y. Okuno, S. C. Chiliveri, and G. M. Clore, *Submillisecond freezing permits cryoprotectant-free EPR double electron-electron resonance spectroscopy*, *Chemphyschem* **21** (June, 2020) 1224–1229.

[122] M. T. Lerch, Z. Yang, E. K. Brooks, and W. L. Hubbell, *Mapping protein conformational heterogeneity under pressure with site-directed spin labeling and double electron-electron resonance*, *Proc. Natl. Acad. Sci. U. S. A.* **111** (Apr., 2014) E1201–10.

[123] B. M. Stadtmueller, M. D. Bridges, K.-M. Dam, M. T. Lerch, K. E. Huey-Tubman, W. L. Hubbell, and P. J. Bjorkman, *DEER spectroscopy measurements reveal multiple conformations of HIV-1 SOSIP envelopes that show similarities with envelopes on native virions*, *Immunity* **49** (Aug., 2018) 235–246.e4.

[124] M. C. Puljung, H. A. DeBerg, W. N. Zagotta, and S. Stoll, *Double electron-electron resonance reveals cAMP-induced conformational change in HCN channels*, *Proc. Natl. Acad. Sci. U. S. A.* **111** (July, 2014) 9816–9821.

[125] N. Sherck, T. Webber, D. R. Brown, T. Keller, M. Barry, A. DeStefano, S. Jiao, R. A. Segalman, G. H. Fredrickson, M. S. Shell, and S. Han, *End-to-End distance*

probability distributions of dilute poly(ethylene oxide) in aqueous solution, *J. Am. Chem. Soc.* **142** (Nov., 2020) 19631–19641.

[126] C. S. R. Gruning, E. A. Mirecka, A. N. Klein, E. Mandelkow, D. Willbold, S. F. Marino, M. Stoldt, and W. Hoyer, *Alternative conformations of the tau repeat domain in complex with an engineered binding protein*, *J. Biol. Chem.* **289** (2014), no. 33 23209–23218.

[127] T. K. Karikari, S. Keeling, E. Hill, J. L. Rodriguez, D. A. Nagel, B. Becker, K. Höglund, H. Zetterberg, K. Blennow, E. J. Hill, and K. G. Moffat, *Extensive plasmid library to prepare tau protein variants and study their functional biochemistry*, 2020.

[128] A. Sandberg, H. Ling, M. Gearing, B. Dombroski, L. Cantwell, L. R'Bibo, A. Levey, G. D. Schellenberg, J. Hardy, N. Wood, J. Fernius, S. Nyström, S. Svensson, S. Thor, P. Hammarström, T. Revesz, and K. Y. Mok, *Fibrillation and molecular characteristics are coherent with clinical and pathological features of 4-repeat tauopathy caused by MAPT variant G273R*, *Neurobiol. Dis.* **146** (Dec., 2020) 105079.

[129] A. Siddiqua, Y. Luo, V. Meyer, M. A. Swanson, X. Yu, G. Wei, J. Zheng, G. R. Eaton, B. Ma, R. Nussinov, S. S. Eaton, and M. Margittai, *Conformational basis for asymmetric seeding barrier in filaments of three- and four-repeat tau*, *J. Am. Chem. Soc.* **134** (June, 2012) 10271–10278.

[130] S. Weickert, M. Wawrzyniuk, L. H. John, S. G. D. Rüdiger, and M. Drescher, *The mechanism of hsp90-induced oligomerizaton of tau*, *Sci Adv* **6** (Mar., 2020) eaax6999.

[131] L. S. Stelzl, P. W. Fowler, M. S. P. Sansom, and O. Beckstein, *Flexible gates generate occluded intermediates in the transport cycle of LacY*, *J. Mol. Biol.* **426** (Feb., 2014) 735–751.

[132] A. J. Dregni, V. S. Mandala, H. Wu, M. R. Elkins, H. K. Wang, I. Hung, W. F. DeGrado, and M. Hong, *In vitro 0N4R tau fibrils contain a monomorphic β-sheet core enclosed by dynamically heterogeneous fuzzy coat segments*, *Proc. Natl. Acad. Sci. U. S. A.* **116** (Aug., 2019) 16357–16366.

[133] A. J. Dregni, H. K. Wang, H. Wu, P. Duan, J. Jin, W. F. DeGrado, and M. Hong, *Inclusion of the C-Terminal domain in the β-Sheet core of Heparin-Fibrillized Three-Repeat tau protein revealed by Solid-State nuclear magnetic resonance spectroscopy*, *J. Am. Chem. Soc.* **143** (May, 2021) 7839–7851.

[134] N. A. Eschmann, T. D. Do, N. E. LaPointe, J.-E. Shea, S. C. Feinstein, M. T. Bowers, and S. Han, *Tau aggregation propensity engrained in its solution state*, *J. Phys. Chem. B* **119** (Nov., 2015) 14421–14432.

[135] V. Meyer, M. A. Swanson, L. J. Clouston, P. J. Boratyński, R. A. Stein, H. S. Mchaourab, A. Rajca, S. S. Eaton, and G. R. Eaton, *Room-temperature distance measurements of immobilized spin-labeled protein by DEER/PELDOR*, *Biophys. J.* **108** (Mar., 2015) 1213–1219.

[136] T. H. Edwards and S. Stoll, *Optimal tikhonov regularization for DEER spectroscopy*, *J. Magn. Reson.* **288** (Mar., 2018) 58–68.

[137] M. Srivastava and J. H. Freed, *Singular value decomposition method to determine distance distributions in pulsed dipolar electron spin resonance*, *J. Phys. Chem. Lett.* **8** (2017), no. 22 5648–5655.

[138] G. Jeschke, V. Chechik, P. Ionita, A. Godt, H. Zimmermann, J. Banham, C. R. Timmel, D. Hilger, and H. Jung, *DeerAnalysis2006—a comprehensive software package for analyzing pulsed ELDOR data*, *Appl. Magn. Reson.* **30** (June, 2006) 473–498.

[139] M. Pannier, V. Schädler, M. Schöps, U. Wiesner, G. Jeschke, and H. W. Spiess, *Determination of ion cluster sizes and Cluster-to-Cluster distances in ionomers by Four-Pulse double electron electron resonance spectroscopy*, *Macromolecules* **33** (Oct., 2000) 7812–7818.

[140] S. Lövestam, F. A. Koh, B. van Knippenberg, A. Kotecha, A. G. Murzin, M. Goedert, and S. H. W. Scheres, *Assembly of recombinant tau into filaments identical to those of alzheimer's disease and chronic traumatic encephalopathy*, *Elife* **11** (Mar., 2022).

[141] A. J. Dregni, P. Duan, H. Xu, L. Changolkar, N. El Mammeri, V. M.-Y. Lee, and M. Hong, *Fluent molecular mixing of tau isoforms in alzheimer's disease neurofibrillary tangles*, *Nat. Commun.* **13** (May, 2022) 2967.

[142] J. L. Furman, J. Vaquer-Alicea, C. L. White, 3rd, N. J. Cairns, P. T. Nelson, and M. I. Diamond, *Widespread tau seeding activity at early braak stages*, *Acta Neuropathol.* **133** (Jan., 2017) 91–100.

[143] M. Usenovic, S. Niroomand, R. E. Drolet, L. Yao, R. C. Gaspar, N. G. Hatcher, J. Schachter, J. J. Renger, and S. Parmentier-Batteur, *Internalized tau oligomers cause neurodegeneration by inducing accumulation of pathogenic tau in human neurons derived from induced pluripotent stem cells*, *J. Neurosci.* **35** (Oct., 2015) 14234–14250.

[144] J.-P. Courade, R. Angers, G. Mairet-Coello, N. Pacico, K. Tyson, D. Lightwood, R. Munro, D. McMillan, R. Griffin, T. Baker, D. Starkie, R. Nan, M. Westwood, M.-L. Mushikiwabo, S. Jung, G. Odede, B. Sweeney, A. Popplewell, G. Burgess, P. Downey, and M. Citron, *Epitope determines efficacy of therapeutic anti-tau*

antibodies in a functional assay with human alzheimer tau, *Acta Neuropathol.* **136** (Nov., 2018) 729–745.

[145] E. Barini, G. Plotzky, Y. Mordashova, J. Hoppe, E. Rodriguez-Correa, S. Julier, F. LePrieult, I. Mairhofer, M. Mezler, S. Biesinger, M. Cik, M. W. Meinhardt, E. Ercan-Herbst, D. E. Ehrnhoefer, A. Striebinger, K. Bodie, C. Klein, L. Gasparini, and K. Schlegel, *Tau in the brain interstitial fluid is fragmented and seeding-competent*, *Neurobiol. Aging* **109** (Jan., 2022) 64–77.

[146] S. Takeda, C. Commins, S. L. DeVos, C. K. Nobuhara, S. Wegmann, A. D. Roe, I. Costantino, Z. Fan, S. B. Nicholls, A. E. Sherman, A. T. Trisini Lipsanopoulos, C. R. Scherzer, G. A. Carlson, R. Pitstick, E. R. Peskind, M. A. Raskind, G. Li, T. J. Montine, M. P. Frosch, and B. T. Hyman, *Seed-competent high-molecular-weight tau species accumulates in the cerebrospinal fluid of alzheimer's disease mouse model and human patients*, *Ann. Neurol.* **80** (Sept., 2016) 355–367.

[147] B. D. Hitt, J. Vaquer-Alicea, V. A. Manon, J. D. Beaver, O. M. Kashmer, J. N. Garcia, and M. I. Diamond, *Ultrasensitive tau biosensor cells detect no seeding in alzheimer's disease CSF*, *Acta Neuropathol Commun* **9** (May, 2021) 99.

[148] P. M. Seidler, D. R. Boyer, K. A. Murray, T. P. Yang, M. Bentzel, M. R. Sawaya, G. Rosenberg, D. Cascio, C. K. Williams, K. L. Newell, B. Ghetti, M. A. DeTure, D. W. Dickson, H. V. Vinters, and D. S. Eisenberg, *Structure-based inhibitors halt prion-like seeding by alzheimer's disease-and tauopathy-derived brain tissue samples*, *J. Biol. Chem.* **294** (Nov., 2019) 16451–16464.

[149] S. L. DeVos, B. T. Corjuc, D. H. Oakley, C. K. Nobuhara, R. N. Bannon, A. Chase, C. Commins, J. A. Gonzalez, P. M. Dooley, M. P. Frosch, and B. T. Hyman, *Synaptic tau seeding precedes tau pathology in human alzheimer's disease brain*, *Front. Neurosci.* **12** (Apr., 2018) 267.

[150] T. K. Karikari, D. A. Nagel, A. Grainger, C. Clarke-Bland, J. Crowe, E. J. Hill, and K. G. Moffat, *Distinct conformations, aggregation and cellular internalization of different tau strains*, *Front. Cell. Neurosci.* **13** (July, 2019) 296.

[151] I. Santa-Maria, M. Varghese, H. Ksiezak-Reding, A. Dzhun, J. Wang, and G. M. Pasinetti, *Paired helical filaments from alzheimer disease brain induce intracellular accumulation of tau protein in aggresomes*, *J. Biol. Chem.* **287** (June, 2012) 20522–20533.

[152] K. Rajasekhar, H. Mirbaha, M. I. Diamond, and others, *Site-specific hyperphosphorylation inhibits, rather than promotes, tau fibrillization, seeding capacity and its microtubule binding*, *Angewandte* (2019).

[153] J. L. Guo and V. M. Y. Lee, *Neurofibrillary tangle-like tau pathology induced by synthetic tau fibrils in primary neurons over-expressing mutant tau*, *FEBS Lett.* **587** (2013), no. 6 717–723.

[154] B. Falcon, A. Cavallini, R. Angers, S. Glover, T. K. Murray, L. Barnham, S. Jackson, M. J. O'Neill, A. M. Isaacs, M. L. Hutton, P. G. Szekeres, M. Goedert, and S. Bose, *Conformation determines the seeding potencies of native and recombinant tau aggregates*, *J. Biol. Chem.* **290** (2014), no. 2 1049–1065.

[155] K. H. Strang, C. L. Croft, Z. A. Sorrentino, P. Chakrabarty, T. E. Golde, and B. I. Giasson, *Distinct differences in prion-like seeding and aggregation between tau protein variants provide mechanistic insights into tauopathies*, *J. Biol. Chem.* **293** (Feb., 2018) 2408–2421.

[156] O. A. Morozova, Z. M. March, A. S. Robinson, and D. W. Colby, *Conformational features of tau fibrils from alzheimer's disease brain are faithfully propagated by unmodified recombinant protein*, *Biochemistry* **52** (Oct., 2013) 6960–6967.

[157] S. K. Kaufman, T. L. Thomas, K. Del Tredici, H. Braak, and M. I. Diamond, *Characterization of tau prion seeding activity and strains from formaldehyde-fixed tissue*, *Acta Neuropathol Commun* **5** (June, 2017) 41.

[158] Z. Skachokova, A. Martinisi, M. Flach, F. Sprenger, Y. Naegelin, V. Steiner-Monard, M. Sollberger, A. U. Monsch, M. Goedert, M. Tolnay, and D. T. Winkler, *Cerebrospinal fluid from alzheimer's disease patients promotes tau aggregation in transgenic mice*, *Acta Neuropathol Commun* **7** (May, 2019) 72.

[159] M. Albert, G. Mairet-Coello, C. Danis, S. Lieger, R. Caillierez, S. Carrier, E. Skrobala, I. Landrieu, A. Michel, M. Schmitt, M. Citron, P. Downey, J.-P. Courade, L. Buée, and M. Colin, *Prevention of tau seeding and propagation by immunotherapy with a central tau epitope antibody*, *Brain* **142** (June, 2019) 1736–1750.

[160] J. R. Detrez, H. Maurin, K. Van Kolen, R. Willems, J. Colombelli, B. Lechat, B. Roucourt, F. Van Leuven, S. Baatout, P. Larsen, R. Nuydens, J.-P. Timmermans, and W. H. De Vos, *Regional vulnerability and spreading of hyperphosphorylated tau in seeded mouse brain*, *Neurobiol. Dis.* **127** (July, 2019) 398–409.

[161] Z. He, J. D. McBride, H. Xu, L. Changolkar, S.-J. Kim, B. Zhang, S. Narasimhan, G. S. Gibbons, J. L. Guo, M. Kozak, G. D. Schellenberg, J. Q. Trojanowski, and V. M.-Y. Lee, *Transmission of tauopathy strains is independent of their isoform composition*, *Nat. Commun.* **11** (Jan., 2020) 7.

[162] F. Clavaguera, H. Akatsu, G. Fraser, R. A. Crowther, S. Frank, J. Hench, A. Probst, D. T. Winkler, J. Reichwald, M. Staufenbiel, B. Ghetti, M. Goedert, and M. Tolnay, *Brain homogenates from human tauopathies induce tau inclusions in mouse brain*, *Proc. Natl. Acad. Sci. U. S. A.* **110** (June, 2013) 9535–9540.

[163] S. Narasimhan, L. Changolkar, D. M. Riddle, A. Kats, A. Stieber, S. A. Weitzman, B. Zhang, Z. Li, E. D. Roberson, J. Q. Trojanowski, and Others, *Human tau pathology transmits glial tau aggregates in the absence of neuronal tau*, *J. Exp. Med.* **217** (2020), no. 2.

[164] S. Narasimhan, J. L. Guo, L. Changolkar, A. Stieber, J. D. McBride, L. V. Silva, Z. He, B. Zhang, R. J. Gathagan, J. Q. Trojanowski, and V. M. Y. Lee, *Pathological tau strains from human brains recapitulate the diversity of tauopathies in nontransgenic mouse brain*, *Journal of Neuroscience* **37** (Nov., 2017) 11406–11423.

[165] A. de Calignon, M. Polydoro, M. Suarez-Calvet, C. William, D. H. Adamowicz, K. J. Kopeikina, R. Pitstick, N. Sahara, K. H. Ashe, G. A. Carlson, T. L. Spires-Jones, and B. T. Hyman, *Propagation of tau pathology in a model of early alzheimer's disease*, *Neuron* **73** (2012), no. 4 685–697.

[166] M. D. Weingarten, A. H. Lockwood, S. Y. Hwo, and M. W. Kirschner, *A protein factor essential for microtubule assembly*, *Proc. Natl. Acad. Sci. U. S. A.* **72** (May, 1975) 1858–1862.

[167] I. Grundke-Iqbal, K. Iqbal, Y. C. Tung, M. Quinlan, H. M. Wisniewski, and L. I. Binder, *Abnormal phosphorylation of the Microtubule-Associated Protein-Tau (tau) in alzheimer cytoskeletal pathology*, *Proc. Natl. Acad. Sci. U. S. A.* **83** (July, 1986) 4913–4917.

[168] M. Goedert, *Tau protein and the neurofibrillary pathology of alzheimer's disease*, *Ann. N. Y. Acad. Sci.* **777** (Jan., 1996) 121–131.

[169] M. von Bergen, S. Barghorn, S. A. Muller, M. Pickhardt, J. Biernat, E. M. Mandelkow, P. Davies, U. Aebi, and E. Mandelkow, *The core of tau-paired helical filaments studied by scanning transmission electron microscopy and limited proteolysis*, *Biochemistry* **45** (2006), no. 20 6446–6457.

[170] T. Gómez-Isla, R. Hollister, H. West, S. Mui, J. H. Growdon, R. C. Petersen, J. E. Parisi, and B. T. Hyman, *Neuronal loss correlates with but exceeds neurofibrillary tangles in alzheimer's disease*, *Ann. Neurol.* **41** (Jan., 1997) 17–24.

[171] R. D. Terry, *The pathogenesis of alzheimer disease: An alternative to the amyloid hypothesis*, *J. Neuropathol. Exp. Neurol.* **55** (Oct., 1996) 1023–1025.

[172] P. Giannakopoulos, F. R. Herrmann, T. Bussière, C. Bouras, E. Kövari, D. P. Perl, J. H. Morrison, G. Gold, and P. R. Hof, *Tangle and neuron numbers, but not amyloid load, predict cognitive status in alzheimer's disease*, *Neurology* **60** (May, 2003) 1495–1500.

[173] T. Kampers, P. Friedhoff, J. Biernat, E. M. Mandelkow, and E. Mandelkow, *RNA stimulates aggregation of microtubule-associated protein tau into alzheimer-like paired helical filaments*, *FEBS Lett.* **399** (Dec., 1996) 344–349.

[174] M. Goedert, R. Jakes, M. G. Spillantini, M. Hasegawa, M. J. Smith, and R. A. Crowther, *Assembly of microtubule-associated protein tau into alzheimer-like filaments induced by sulphated glycosaminoglycans*, *Nature* **383** (Oct., 1996) 550–553.

[175] M. Pérez, J. M. Valpuesta, M. Medina, E. Montejo de Garcini, and J. Avila, *Polymerization of tau into filaments in the presence of heparin: the minimal sequence required for tau-tau interaction*, *J. Neurochem.* **67** (Sept., 1996) 1183–1190.

[176] M. Pérez, M. Arrasate, E. Montejo De Garcini, V. Muñoz, and J. Avila, *In vitro assembly of tau protein: mapping the regions involved in filament formation*, *Biochemistry* **40** (May, 2001) 5983–5991.

[177] M. Margittai and R. Langen, *Template-assisted filament growth by parallel stacking of tau*, *Proc. Natl. Acad. Sci. U. S. A.* **101** (2004), no. 28 10278–10283.

[178] J. Berriman, L. C. Serpell, K. A. Oberg, A. L. Fink, M. Goedert, and R. A. Crowther, *Tau filaments from human brain and from in vitro assembly of recombinant protein show cross-beta structure*, *Proc. Natl. Acad. Sci. U. S. A.* **100** (2003), no. 15 9034–9038.

[179] A. Pavlova, C. Y. Cheng, M. Kinnebrew, J. Lew, F. W. Dahlquist, and S. Han, *Protein structural and surface water rearrangement constitute major events in the earliest aggregation stages of tau*, *Proc. Natl. Acad. Sci. U. S. A.* **113** (2016), no. 2 E127–E136.

[180] D. W. Li, S. Mohanty, A. Irback, and S. H. Huo, *Formation and growth of oligomers: A monte carlo study of an amyloid tau fragment*, *PLoS Comput. Biol.* **4** (Dec., 2008).

[181] N. Sibille, A. Sillen, A. Leroy, J.-M. Wieruszeski, B. Mulloy, I. Landrieu, and G. Lippens, *Structural impact of heparin binding to full-length tau as studied by NMR spectroscopy*, *Biochemistry* **45** (Oct., 2006) 12560–12572.

[182] S. Jeganathan, M. von Bergen, E. M. Mandelkow, and E. Mandelkow, *The natively unfolded character of tau and its aggregation to alzheimer-like paired helical filaments*, *Biochemistry* **47** (2008), no. 40 10526–10539.

[183] M. F. Mossuto, *Disulfide bonding in neurodegenerative misfolding diseases*, *Int. J. Cell Biol.* **2013** (2013) 7.

[184] M. von Bergen, S. Barghorn, L. Li, A. Marx, J. Biernat, E. M. Mandelkow, and E. Mandelkow, *Mutations of tau protein in frontotemporal dementia promote aggregation of paired helical filaments by enhancing local beta-structure*, *J. Biol. Chem.* **276** (Dec., 2001) 48165–48174.

[185] F. Scaramozzino, D. W. Peterson, P. Farmer, J. T. Gerig, D. J. Graves, and J. Lew, *TMAO promotes fibrillization and microtubule assembly activity in the c-terminal repeat region of tau*, *Biochemistry* **45** (2006), no. 11 3684–3691.

[186] S. Bibow, M. D. Mukrasch, S. Chinnathambi, J. Biernat, C. Griesinger, E. Mandelkow, and M. Zweckstetter, *The dynamic structure of filamentous tau*, *Angewandte Chemie-International Edition* **50** (2011), no. 48 11520–11524.

[187] N. Sahara, S. Maeda, M. Murayama, T. Suzuki, N. Dohmae, S. H. Yen, and A. Takashima, *Assembly of two distinct dimers and higher-order oligomers from full-length tau*, *Eur. J. Neurosci.* **25** (May, 2007) 3020–3029.

[188] J. Greenwald and R. Riek, *Biology of amyloid: structure, function, and regulation*, *Structure* **18** (Oct., 2010) 1244–1260.

[189] T. R. Jahn and S. E. Radford, *The yin and yang of protein folding*, *FEBS J.* **272** (Dec., 2005) 5962–5970.

[190] T. P. Knowles, A. W. Fitzpatrick, S. Meehan, H. R. Mott, M. Vendruscolo, C. M. Dobson, and M. E. Welland, *Role of intermolecular forces in defining material properties of protein nanofibrils*, *Science* **318** (Dec., 2007) 1900–1903.

[191] E.-M. Mandelkow and E. Mandelkow, *Biochemistry and cell biology of tau protein in neurofibrillary degeneration*, *Cold Spring Harb. Perspect. Med.* **2** (July, 2012) a006247.

[192] M. Goedert, R. Jakes, M. G. Spillantini, M. Hasegawa, M. J. Smith, and R. A. Crowther, *Assembly of microtubule-associated protein tau into alzheimer-like filaments induced by sulphated glycosaminoglycans*, *Nature* **383** (Oct., 1996) 550–553.

[193] T. Kampers, P. Friedhoff, J. Biernat, E. M. Mandelkow, and E. Mandelkow, *RNA stimulates aggregation of microtubule-associated protein tau into alzheimer-like paired helical filaments*, *FEBS Lett.* **399** (Dec., 1996) 344–349.

[194] D. M. Wilson and L. I. Binder, *Free fatty acids stimulate the polymerization of tau and amyloid beta peptides. in vitro evidence for a common effector of pathogenesis in alzheimer's disease*, *Am. J. Pathol.* **150** (June, 1997) 2181–2195.

[195] P. D. Dinkel, M. R. Holden, N. Matin, and M. Margittai, *RNA binds to tau fibrils and sustains Template-Assisted growth*, *Biochemistry* **54** (Aug., 2015) 4731–4740.

[196] V. Meyer, P. D. Dinkel, E. Rickman Hager, and M. Margittai, *Amplification of tau fibrils from minute quantities of seeds*, *Biochemistry* **53** (Sept., 2014) 5804–5809.

[197] G. Ramachandran and J. B. Udgaonkar, *Understanding the kinetic roles of the inducer heparin and of rod-like protofibrils during amyloid fibril formation by tau protein**, *J. Biol. Chem.* **286** (Nov., 2011) 38948–38959.

[198] S. W. Carlson, M. Branden, K. Voss, Q. Sun, C. A. Rankin, and T. C. Gamblin, *A complex mechanism for inducer mediated tau polymerization*, *Biochemistry* **46** (July, 2007) 8838–8849.

[199] N. Sibille, A. Sillen, A. Leroy, J.-M. Wieruszeski, B. Mulloy, I. Landrieu, and G. Lippens, *Structural impact of heparin binding to full-length tau as studied by NMR spectroscopy*, *Biochemistry* **45** (Oct., 2006) 12560–12572.

[200] B. Falcon, A. Cavallini, R. Angers, S. Glover, T. K. Murray, L. Barnham, S. Jackson, M. J. O'Neill, A. M. Isaacs, M. L. Hutton, P. G. Szekeres, M. Goedert, and S. Bose, *Conformation determines the seeding potencies of native and recombinant tau aggregates*, *J. Biol. Chem.* **290** (Jan., 2015) 1049–1065.

[201] W. L. Hubbell and C. Altenbach, *Investigation of structure and dynamics in membrane proteins using site-directed spin labeling*, *Curr. Opin. Struct. Biol.* **4** (Jan., 1994) 566–573.

[202] S. S. Mirra, J. R. Murrell, M. Gearing, M. G. Spillantini, M. Goedert, R. A. Crowther, A. I. Levey, R. Jones, J. Green, J. M. Shoffner, B. H. Wainer, M. L. Schmidt, J. Q. Trojanowski, and B. Ghetti, *Tau pathology in a family with dementia and a P301L mutation in tau*, *J. Neuropathol. Exp. Neurol.* **58** (Apr., 1999) 335–345.

[203] N. A. Eschmann, E. R. Georgieva, P. Ganguly, P. P. Borbat, M. D. Rappaport, Y. Akdogan, J. H. Freed, J. E. Shea, and S. Han, *Signature of an aggregation-prone conformation of tau*, *Sci. Rep.* **7** (2017).

[204] D. W. Sanders, S. K. Kaufman, S. L. DeVos, A. M. Sharma, H. Mirbaha, A. Li, S. J. Barker, A. C. Foley, J. R. Thorpe, L. C. Serpell, T. M. Miller, L. T. Grinberg, W. W. Seeley, and M. I. Diamond, *Distinct tau prion strains propagate in cells and mice and define different tauopathies*, *Neuron* **82** (June, 2014) 1271–1288.

[205] B. Falcon, A. Cavallini, R. Angers, S. Glover, T. K. Murray, L. Barnham, S. Jackson, M. J. O'Neill, A. M. Isaacs, M. L. Hutton, P. G. Szekeres, M. Goedert, and S. Bose, *Conformation determines the seeding potencies of native and recombinant tau aggregates*, *J. Biol. Chem.* **290** (Jan., 2015) 1049–1065.

[206] D. Xia, J. M. Gutmann, and J. Götz, *Mobility and subcellular localization of endogenous, gene-edited tau differs from that of over-expressed human wild-type and P301L mutant tau*, *Sci. Rep.* **6** (July, 2016) 29074.

[207] K. Yamada, *Extracellular tau and its potential role in the propagation of tau pathology*, *Front. Neurosci.* **11** (Nov., 2017) 667.

[208] A. Maïza, S. Chantepie, C. Vera, A. Fifre, M. B. Huynh, O. Stettler, M. O. Ouidja, and D. Papy-Garcia, *The role of heparan sulfates in protein aggregation and their potential impact on neurodegeneration*, *FEBS Lett.* **592** (Dec., 2018) 3806–3818.

[209] X. Zhang, Y. Lin, N. A. Eschmann, H. Zhou, J. N. Rauch, I. Hernandez, E. Guzman, K. S. Kosik, and S. Han, *RNA stores tau reversibly in complex coacervates*, *PLoS Biol.* **15** (July, 2017) e2002183.

[210] S. D. Ginsberg, J. E. Galvin, T. S. Chiu, V. M. Lee, E. Masliah, and J. Q. Trojanowski, *RNA sequestration to pathological lesions of neurodegenerative diseases*, *Acta Neuropathol.* **96** (Nov., 1998) 487–494.

[211] B. Frost, J. Ollesch, H. Wille, and M. I. Diamond, *Conformational diversity of wild-type tau fibrils specified by templated conformation change*, *J. Biol. Chem.* **284** (Feb., 2009) 3546–3551.

[212] B. B. Holmes, S. L. DeVos, N. Kfoury, M. Li, R. Jacks, K. Yanamandra, M. O. Ouidja, F. M. Brodsky, J. Marasa, D. P. Bagchi, P. T. Kotzbauer, T. M. Miller, D. Papy-Garcia, and M. I. Diamond, *Heparan sulfate proteoglycans mediate internalization and propagation of specific proteopathic seeds*, *Proc. Natl. Acad. Sci. U. S. A.* **110** (Aug., 2013) E3138–47.

[213] B. Falcon, A. Cavallini, R. Angers, S. Glover, T. K. Murray, L. Barnham, S. Jackson, M. J. O'Neill, A. M. Isaacs, M. L. Hutton, P. G. Szekeres, M. Goedert, and S. Bose, *Conformation determines the seeding potencies of native and recombinant tau aggregates*, *J. Biol. Chem.* **290** (Jan., 2015) 1049–1065.

[214] S. J. Jackson, C. Kerridge, J. Cooper, A. Cavallini, B. Falcon, C. V. Cella, A. Landi, P. G. Szekeres, T. K. Murray, Z. Ahmed, M. Goedert, M. Hutton, M. J. O'Neill, and S. Bose, *Short fibrils constitute the major species of Seed-Competent tau in the brains of mice transgenic for human P301S tau*, *J. Neurosci.* **36** (Jan., 2016) 762–772.

[215] S. Narasimhan, J. L. Guo, L. Changolkar, A. Stieber, J. D. McBride, L. V. Silva, Z. He, B. Zhang, R. J. Gathagan, J. Q. Trojanowski, and V. M. Y. Lee, *Pathological tau strains from human brains recapitulate the diversity of tauopathies in nontransgenic mouse brain*, *J. Neurosci.* **37** (Nov., 2017) 11406–11423.

[216] H. Mirbaha, B. B. Holmes, D. W. Sanders, J. Bieschke, and M. I. Diamond, *Tau trimers are the minimal propagation unit spontaneously internalized to seed intracellular aggregation*, *J. Biol. Chem.* **290** (2015), no. 24 14893–14903.

[217] T. P. J. Knowles, M. Vendruscolo, and C. M. Dobson, *The amyloid state and its association with protein misfolding diseases*, *Nat. Rev. Mol. Cell Biol.* **15** (June, 2014) 384–396.

[218] F. Kundel, L. Hong, B. Falcon, W. A. McEwan, T. C. T. Michaels, G. Meisl, N. Esteras, A. Y. Abramov, T. J. P. Knowles, M. Goedert, and D. Klenerman, *Measurement of tau filament fragmentation provides insights into prion-like spreading*, *ACS Chem. Neurosci.* **9** (June, 2018) 1276–1282.

[219] M. F. Bishop and F. A. Ferrone, *Kinetics of nucleation-controlled polymerization. a perturbation treatment for use with a secondary pathway*, *Biophys. J.* **46** (Nov., 1984) 631–644.

[220] F. Ferrone, *[17] analysis of protein aggregation kinetics*, in *Methods in Enzymology*, vol. 309, pp. 256–274. Academic Press, Jan., 1999.

[221] C. B. Andersen, H. Yagi, M. Manno, V. Martorana, T. Ban, G. Christiansen, D. E. Otzen, Y. Goto, and C. Rischel, *Branching in amyloid fibril growth*, *Biophys. J.* **96** (Feb., 2009) 1529–1536.

[222] S. I. A. Cohen, S. Linse, L. M. Luheshi, E. Hellstrand, D. A. White, L. Rajah, D. E. Otzen, M. Vendruscolo, C. M. Dobson, and T. P. J. Knowles, *Proliferation of amyloid-β42 aggregates occurs through a secondary nucleation mechanism*, *Proc. Natl. Acad. Sci. U. S. A.* **110** (June, 2013) 9758–9763.

[223] A. K. Buell, C. Galvagnion, R. Gaspar, E. Sparr, M. Vendruscolo, T. P. J. Knowles, S. Linse, and C. M. Dobson, *Solution conditions determine the relative importance of nucleation and growth processes in α-synuclein aggregation*, *Proc. Natl. Acad. Sci. U. S. A.* **111** (May, 2014) 7671–7676.

[224] J. W. Wu, M. Herman, L. Liu, S. Simoes, C. M. Acker, H. Figueroa, J. I. Steinberg, M. Margittai, R. Kayed, C. Zurzolo, G. Di Paolo, and K. E. Duff, *Small misfolded tau species are internalized via bulk endocytosis and anterogradely and retrogradely transported in neurons*, *J. Biol. Chem.* **288** (2013), no. 3 1856–1870.

[225] H. A. Weismiller, R. Murphy, G. Wei, B. Ma, R. Nussinov, and M. Margittai, *Structural disorder in four-repeat tau fibrils reveals a new mechanism for barriers to cross-seeding of tau isoforms*, *J. Biol. Chem.* **293** (Nov., 2018) 17336–17348.

[226] S. Takeda, S. Wegmann, H. S. Cho, S. L. Devos, C. Commins, A. D. Roe, S. B. Nicholls, G. A. Carlson, R. Pitstick, C. K. Nobuhara, I. Costantino, M. P. Frosch, D. J. Muller, D. Irimia, and B. T. Hyman, *Neuronal uptake and propagation of a rare phosphorylated high-molecular-weight tau derived from alzheimer's disease brain*, *Nat. Commun.* **6** (Oct., 2015).

[227] N. Kfoury, B. B. Holmes, H. Jiang, D. M. Holtzman, and M. I. Diamond, *Trans-cellular propagation of tau aggregation by fibrillar species*, *J. Biol. Chem.* **287** (2012), no. 23 19440–19451.

[228] M. Tanaka, S. R. Collins, B. H. Toyama, and J. S. Weissman, *The physical basis of how prion conformations determine strain phenotypes*, *Nature* **442** (Aug., 2006) 585–589.

[229] S. M. Doyle, O. Genest, and S. Wickner, *Protein rescue from aggregates by powerful molecular chaperone machines*, *Nat. Rev. Mol. Cell Biol.* **14** (Oct., 2013) 617–629.

[230] P. T. Nelson, I. Alafuzoff, E. H. Bigio, C. Bouras, H. Braak, N. J. Cairns, R. J. Castellani, B. J. Crain, P. Davies, K. Del Tredici, C. Duyckaerts, M. P. Frosch, V. Haroutunian, P. R. Hof, C. M. Hulette, B. T. Hyman, T. Iwatsubo, K. A. Jellinger, G. A. Jicha, E. Kövari, W. A. Kukull, J. B. Leverenz, S. Love, I. R. Mackenzie, D. M. Mann, E. Masliah, A. C. McKee, T. J. Montine, J. C. Morris, J. A. Schneider, J. A. Sonnen, D. R. Thal, J. Q. Trojanowski, J. C. Troncoso, T. Wisniewski, R. L. Woltjer, and T. G. Beach, *Correlation of alzheimer disease neuropathologic changes with cognitive status: a review of the literature*, *J. Neuropathol. Exp. Neurol.* **71** (May, 2012) 362–381.

[231] P. V. Arriagada, K. Marzloff, and B. T. Hyman, *Distribution of alzheimer-type pathologic changes in nondemented elderly individuals matches the pattern in alzheimer's disease*, *Neurology* **42** (Sept., 1992) 1681–1688.

[232] B. Frost, R. L. Jacks, and M. I. Diamond, *Propagation of tau misfolding from the outside to the inside of a cell**, *J. Biol. Chem.* **284** (May, 2009) 12845–12852.

[233] B. Frost, R. L. Jacks, and M. I. Diamond, *Propagation of tau misfolding from the outside to the inside of a cell*, *J. Biol. Chem.* **284** (2009), no. 19 12845–12852.

[234] A. L. Woerman, J. Stöhr, A. Aoyagi, R. Rampersaud, Z. Krejciova, J. C. Watts, T. Ohyama, S. Patel, K. Widjaja, A. Oehler, D. W. Sanders, M. I. Diamond, W. W. Seeley, L. T. Middleton, S. M. Gentleman, D. A. Mordes, T. C. Südhof,

K. Giles, and S. B. Prusiner, *Propagation of prions causing synucleinopathies in cultured cells*, *Proc. Natl. Acad. Sci. U. S. A.* **112** (Sept., 2015) E4949–58.

[235] J. Safar, H. Wille, V. Itri, D. Groth, H. Serban, M. Torchia, F. E. Cohen, and S. B. Prusiner, *Eight prion strains have PrP(Sc) molecules with different conformations*, *Nat. Med.* **4** (Oct., 1998) 1157–1165.

[236] M. R. Nilsson, *Techniques to study amyloid fibril formation in vitro*, *Methods* **34** (Sept., 2004) 151–160.

[237] M. L. Schmidt, V. Zhukareva, K. L. Newell, V. M. Lee, and J. Q. Trojanowski, *Tau isoform profile and phosphorylation state in dementia pugilistica recapitulate alzheimer's disease*, *Acta Neuropathol.* **101** (May, 2001) 518–524.

[238] A. Leuzy, K. Chiotis, L. Lemoine, P.-G. Gillberg, O. Almkvist, E. Rodriguez-Vieitez, and A. Nordberg, *Tau PET imaging in neurodegenerative tauopathies-still a challenge*, *Mol. Psychiatry* **24** (Aug., 2019) 1112–1134.

[239] P. Poorkaj, T. D. Bird, E. Wijsman, E. Nemens, R. M. Garruto, L. Anderson, A. Andreadis, W. C. Wiederholt, M. Raskind, and G. D. Schellenberg, *Tau is a candidate gene for chromosome 17 frontotemporal dementia*, *Ann. Neurol.* **43** (June, 1998) 815–825.

[240] S. Spina, D. R. Schonhaut, B. F. Boeve, W. W. Seeley, R. Ossenkoppele, J. P. O'Neil, A. Lazaris, H. J. Rosen, A. L. Boxer, D. C. Perry, B. L. Miller, D. W. Dickson, J. E. Parisi, W. J. Jagust, M. E. Murray, and G. D. Rabinovici, *Frontotemporal dementia with the V337M MAPT mutation: Tau-PET and pathology correlations*, *Neurology* **88** (Feb., 2017) 758–766.